

# Rashin Khera

## Thesis final \_Rashin Khera.pdf



Delhi Technological University

### Document Details

Submission ID

trn:oid:::27535:124237181

Submission Date

Dec 11, 2025, 12:37 PM GMT+5:30

Download Date

Dec 11, 2025, 12:44 PM GMT+5:30

File Name

Thesis final \_Rashin Khera.pdf

File Size

4.6 MB

149 Pages

39,113 Words

213,486 Characters

# 8% Overall Similarity

The combined total of all matches, including overlapping sources, for each database.





## Filtered from the Report

- Bibliography
- Quoted Text
- Cited Text
- Small Matches (less than 14 words)




## Exclusions

- 4 Excluded Sources

## Match Groups


-  **97 Not Cited or Quoted 8%**  
Matches with neither in-text citation nor quotation marks
-  **0 Missing Quotations 0%**  
Matches that are still very similar to source material
-  **0 Missing Citation 0%**  
Matches that have quotation marks, but no in-text citation
-  **0 Cited and Quoted 0%**  
Matches with in-text citation present, but no quotation marks

## Top Sources

- 6%  Internet sources
- 5%  Publications
- 2%  Submitted works (Student Papers)

## Integrity Flags

### 1 Integrity Flag for Review

-  **Replaced Characters**  
9 suspect characters on 5 pages  
Letters are swapped with similar characters from another alphabet.

Our system's algorithms look deeply at a document for any inconsistencies that would set it apart from a normal submission. If we notice something strange, we flag it for you to review.

A Flag is not necessarily an indicator of a problem. However, we'd recommend you focus your attention there for further review.

## Match Groups

- 97 Not Cited or Quoted 8%**  
Matches with neither in-text citation nor quotation marks
- 0 Missing Quotations 0%**  
Matches that are still very similar to source material
- 0 Missing Citation 0%**  
Matches that have quotation marks, but no in-text citation
- 0 Cited and Quoted 0%**  
Matches with in-text citation present, but no quotation marks

## Top Sources

- 6% Internet sources
- 5% Publications
- 2% Submitted works (Student Papers)

## Top Sources

The sources with the highest number of matches within the submission. Overlapping sources will not be displayed.

1	Internet	iifir.org	2%
2	Internet	www.ijert.org	<1%
3	Publication	Xue, Y.. "A critical review of temperature separation in a vortex tube", Experimen...	<1%
4	Internet	www.researchgate.net	<1%
5	Internet	dspace.dtu.ac.in:8080	<1%
6	Publication	Sandeep Kumar, B.B. Arora, Akhilesh Arora. "Thermodynamic assessment and op...	<1%
7	Submitted works	Delhi Technological University on 2025-01-23	<1%
8	Publication	Yunpeng Xue, Maziar Arjomandi, Richard Kelso. "A critical review of temperature ...	<1%
9	Publication	Seyed Ehsan Rafiee, M.M. Sadeghiyazad. "Three-dimensional and experimental inv...	<1%
10	Internet	iieta.org	<1%

11	Submitted works	Delhi Technological University on 2020-07-23	<1%
12	Publication	Yuke Wan, Chuang Wu, Chao Liu, Liyong Xin, Xuhui Jiang, Xiao Xue, Jiajun He. "A n...	<1%
13	Publication	Adem Celik, Mehmet Yilmaz, Omer Faruk Yildiz. "EFFECTS OF VORTEX TUBE ON EX...	<1%
14	Internet	www.eprint.iitd.ac.in	<1%
15	Publication	Pan Zhao, Wenpan Xu, Feifei Gou, Gang Fan, Jiangfeng Wang. "Performance analy...	<1%
16	Internet	www.dspace.dtu.ac.in:8080	<1%
17	Publication	Ahmadi, Pouria. "Modeling, Analysis and Optimization of Integrated Energy Syste...	<1%
18	Internet	bura.brunel.ac.uk	<1%
19	Internet	www.sciencegate.app	<1%
20	Submitted works	Higher Education Commission Pakistan on 2017-12-19	<1%
21	Internet	www.tandfonline.com	<1%
22	Submitted works	Higher Education Commission Pakistan on 2021-08-25	<1%
23	Publication	Ashutosh Mishra, B. B. Arora, Akhilesh Arora. "Exergy-based sustainability analysi...	<1%
24	Publication	"Recent Advances in Mechanical Engineering, Volume 2", Springer Science and Bu...	<1%

25	Publication	Bo Zhang, Xiangji Guo. "Prospective applications of Ranque–Hilsch vortex tubes t...	<1%
26	Internet	dspaces.uok.edu.in	<1%
27	Internet	s3.wp.wsu.edu	<1%
28	Publication	Gaurav Jain, Akhilesh Arora, S. N. Gupta. " Exergy analysis of a vortex tube expan...	<1%
29	Publication	Brian T. Austin, K. Sumathy. "Transcritical carbon dioxide heat pump systems: A r...	<1%
30	Submitted works	Graphic Era University on 2018-07-25	<1%
31	Publication	Warusevitane, Achinie. "Numerical Investigation of Intershaft Hydraulic Seals in ...	<1%
32	Internet	www.journal-aquaticscience.com	<1%
33	Internet	arc.aiaa.org	<1%
34	Publication	Park, Chasik, Hoseong Lee, Yunho Hwang, and Reinhard Radermacher. "Recent a...	<1%
35	Internet	fleek.ipfs.io	<1%
36	Publication	Adib Bazgir, Ali Heydari. "CFD optimization of injection nozzles geometric dimensi...	<1%
37	Publication	Haghighat Mamaghani, Alireza, Behzad Najafi, Ali Shirazi, and Fabio Rinaldi. "4E a...	<1%
38	Publication	Vakiloroaya, Vahid. "Toward Green Buildings: Design, Development and Performa...	<1%

39	Internet	theses.hal.science	<1%
40	Submitted works	Arizona State University	<1%
41	Publication	Gaurav Jain, Akhilesh Arora, S. N. Gupta. " Performance characteristics of a Two- s...	<1%
42	Publication	Seyed Ehsan Rafiee, Masoud Rahimi. "Experimental study and three-dimensional ...	<1%
43	Submitted works	Central Queensland University on 2014-11-24	<1%
44	Submitted works	Karabük Üniversitesi on 2018-05-18	<1%
45	Publication	Zibing Luo, Weiwei Chen, Xinjun Li, Shihua Lu, Feihong Guo. "Performance impro...	<1%
46	Internet	dspace.aus.edu	<1%
47	Publication	H Kursad Ersoy, Nagihan Bilir. " Performance characteristics of ejector expander t...	<1%
48	Submitted works	Plainfield East High School on 2017-10-04	<1%
49	Publication	Vaibhav Jain, Gulshan Sachdeva, Surendra Singh Kachhwaha. "Energy, exergy, ec...	<1%
50	Publication	Weiwei Xu, Zhihong Yu, Qingkai Mu, Bingyang Peng, Qiang Li. "Study of an integr...	<1%
51	Internet	idoc.pub	<1%
52	Internet	www.arpapress.com	<1%

53

Internet

www.grafiati.com

<1%

16

# **THERMAL OPTIMIZATION OF REFRIGERATION SYSTEMS**

**Thesis Submitted**

**in Partial Fulfilment of the Requirements for the**

**Degree of**

**DOCTOR OF PHILOSOPHY**

**in**

**Mechanical Engineering**

**by**

**RASHIN KHERA**

**(2K18/PHDME/02)**

**Under the Supervision of**

**Prof. B. B. Arora**

**Professor**

**Mechanical Engineering**

**Prof. Akhilesh Arora**

**Professor**

**Mechanical Engineering**



16

**Department of Mechanical Engineering**

**DELHI TECHNOLOGICAL UNIVERSITY**

**(Formerly Delhi College of Engineering)**

**Shahbad Daulatpur, Main Bawana Road, Delhi-110042, India**

**October, 2025**



## CERTIFICATE

Certified that **Rashin Khera (2K18/PHD/ME/02)** has carried out his research work presented in this thesis entitled “**Thermal Optimization of Refrigeration Systems**” for the award of **Doctor of Philosophy** from Delhi Technological University, New Delhi, under our supervision. The thesis embodies results of original work, and studies are carried out by the student himself and the contents of the thesis do not form the basis for the award of any other degree to the candidate or to anybody else from this or any other University/Institution.

**Prof. B. B. Arora**

Professor

Department of Mechanical Engg.

DTU, New Delhi

**Prof. Akhilesh Arora**

Professor

Department of Mechanical Engg.

DTU, New Delhi

Date:

## CANDIDATE'S DECLARATION

I hereby declare that the thesis entitled “**Thermal Optimization of Refrigeration Systems**” submitted by me, for the award of the degree of Doctor of Philosophy to the Delhi Technological University (Formerly Delhi College of Engineering) is a record of bonafide work carried out by me under the guidance of **Prof. B. B. Arora & Prof. Akhilesh Arora**.

I further declare that the work reported in this thesis has not been submitted and will not be submitted, either in part or in full, for the award of any other degree or diploma in this Institute or any other Institute or University.

Place:

**RASHIN KHERA**

Date:

Roll No.:2K18/PHDME/02

Department of Mechanical Engineering,  
Delhi Technological University

## ACKNOWLEDGEMENTS

First and foremost, I would like to express my deep and sincere gratitude to my supervisors, **Prof. B. B. Arora**, and **Prof. Akhilesh Arora**, for their valuable guidance and never-ending support. Their enthusiasm and passion have been constant sources of inspiration and encouragement.

I would like to express my gratitude to Prof. Prateek Sharma, Honourable Vice Chancellor, Delhi Technological University, Delhi, for providing this opportunity to work in this prestigious Institute.

I would like to express my gratitude to Prof. B.B Arora, Head of the Department of Mechanical Engineering, and Prof. Atul Kumar Agarwal, DRC Chairperson of the Mechanical Engineering Department for his kind support in accomplishing this work.

I wish to record my thanks and gratitude to Prof. Subhasis Maji, Prof. Sagar Maji, Prof. Vipin, and for their invaluable suggestions and constructive discussion during this research work.

Moreover, I would like to thank my friends and colleagues, Dr. Ashutosh Mishra, Dr. Gulam Mustafa, Dr. Naveen Solanki, Dr. Vinay Kumar Yadav, Dr. Siddharth Arora, Mr. Pankaj Kumar Sagar for their support throughout my time at the University. Also, I am thankful to lab technician Sh. Gagan Ram of Refrigeration and Air-conditioning lab, for his support in my research work.

I would like to thank my parents, Sh. Harish Khera & Smt. Beena Khera; and my brothers, Anupam Khera and Saharsh Khera for their understanding and encouragement throughout my education.

At the last but not least, I am extremely thankful to the Almighty with whose grace I am able to pursue and finish this task.

## ABSTRACT

This study examines the thermodynamic assessment and multi-objective optimisation of a modified vapour compression refrigeration cycle (VCR) in both subcritical and transcritical modes. The cycle modification is achieved through the use of a vortex tube in the VCR, with the objective of enhancing system performance. The efficiency of a standalone vortex tube is low; however, its integration into a thermodynamic cycle or VCR system enhances the coefficient of performance (COP) and reduces exergy losses, particularly when the cycle operates within the transcritical zone. An economic analysis of the modified VCR cycle with a vortex tube has been conducted to compare it with the base case. Moreover, this research conducted a computational fluid dynamics (CFD) study of a standalone vortex tube to enhance its temperature separation phenomenon.

In this research, thermodynamic performance of a vortex tube integrated single-stage vapour compression refrigeration cycle (VTC) has been evaluated in a subcritical region. The thermodynamic evaluation consists of an energy and exergy analyses for VTC in order to determine the effect of various design and operating parameters on its performance. Moreover, the results of VTC are compared with those of simple VCR for the considered range of evaporator and condenser temperatures using R1234yf as the refrigerant. The analysis reveals that the cooling capacity of VTC is 14.5% to 49.7% higher than that of VCR for the considered range of condenser temperature. Also, the maximum COP of VTC is 5.6% to 27.3% higher than that of VCR. The exergetic efficiency of VTC is 5.6% to 27.3% higher than that of VCR. A multi-objective optimization using a genetic algorithm has been conducted, which suggests that evaporator temperature is the major decisive parameter to find the suitability of various applications of the system based on VTC.

Further, this research deals with the thermodynamic investigation of vortex tube coupled with trans-critical vapour compression refrigeration cycle (TVTC) using Carbon-Dioxide, followed by environmental analysis and multi-objective optimization. In this study, effect of various operating and design parameters is studied on the performance of TVTC. Furthermore, a comparison is made between the outcomes of TVTC and simple trans-critical vapour compression refrigeration cycle

(TVCR). Results show that the optimum gascooler pressure for TVTC is observed to be lower than that of TVCR. Also, the cooling capacity and COP of TVTC are observed to be 10.1% to 21.1% and 2.3% to 11.3%, respectively, greater than those of TVCR. Moreover, the exergetic efficiency of TVTC is 2.3% to 11.3% higher than that of TVCR for the investigated range of evaporator and gascooler exit temperatures. The environmental penalty cost (per unit cooling capacity) of TVTC is 3.5% to 12.2% lower than that of TVCR. Furthermore, the coefficient of structural bond is calculated in order to choose the most sensitive parameters for system's performance. Additionally, genetic algorithm-based multi-objective optimization has been performed, with the evaporator temperature serving as the primary determining factor in establishing the optimal solution. This finding can guide the development of TVTC-based systems for a wide range of applications.

Nevertheless, this study conducts an economic analysis of TVTC and compares it with the base case, TVCR. For the economic analysis, three cost components have been considered: capital and maintenance cost, operational cost, and environmental penalty cost. The sum of all three components constitutes the total plant cost. The influence of parameters including evaporator temperature, gas cooler exit temperature, and cooling load on the individual components of cost and the overall plant cost rate has been analysed. Results indicate that the plant cost rate of TVCR is 6.8% to 7.3% higher than that of TVTC and plant cost rate of VCR is 7.5% to 17% higher than that of VTC. This supports the use of vortex tube in transcritical vapour compression refrigeration cycles from an economic standpoint.

While the application of vortex tubes in refrigeration cycles shows benefits in thermal performance, standalone vortex tubes are noted for their low efficiency in temperature separation. Therefore, efforts have been undertaken to analyse the thermal performance of a standalone vortex tube through a CFD study utilising compressed air as the working fluid. This study examines the impact of geometrical modifications on the temperature drop at the cold exit of a vortex tube. The influence of varying air entry angles (ranging from 0° to 5°) on the cold exit temperature of the vortex tube has been examined. A three-dimensional solid model of a vortex tube has been created, and the

standard k-epsilon model is employed to conduct the simulation in ANSYS FLUENT 2022 R1. The maximum temperature reduction occurs at the cold exit when air enters the VT at angles of  $2^\circ$  and  $3^\circ$ . The minimum cold end temperature achieved is approximately 262 K, representing an improvement of 2 K to 3 K compared to the base case (i.e., air entry angle at  $0^\circ$ ).

**Keywords:** vortex tube, COP, energy, exergy, multi-objective optimization, R1234yf, CO<sub>2</sub>, structural bond method, CFD, compressed air, standard k-epsilon, temperature separation.

## TABLE OF CONTENTS

<b>Certificate.....</b>	<b>(ii)</b>
<b>Candidate's Declaration.....</b>	<b>(iii)</b>
<b>Acknowledgements.....</b>	<b>(iv)</b>
<b>Abstract.....</b>	<b>(v)</b>
<b>List of Figures.....</b>	<b>(xiii)</b>
<b>List of Tables.....</b>	<b>(xvi)</b>
<b>List of Symbols.....</b>	<b>(xviii)</b>
<b>CHAPTER 1: INTRODUCTION .....</b>	<b>1</b>
1.1 Motivation .....	1
1.2 Vapour Compression Refrigeration Cycle.....	2
1.2.1 Subcritical Vapour Compression Cycle .....	3
1.2.2 Transcritical Vapour Compression Cycle.....	3
1.3 Modifications in Vapour Compression Systems.....	4
1.4 Vortex Tube .....	5
1.5 Refrigerant Used in this Work .....	6
1.5.1 Refrigerant R1234yf.....	6
1.5.2 Refrigerant CO <sub>2</sub> .....	7
1.6 Thesis Organization.....	8
<b>CHAPTER 2: LITERATURE REVIEW .....</b>	<b>11</b>
2.1 Historical Background of Vortex Tube .....	11
2.2 Working Principles of Vortex Tube .....	12
2.2.1 Pressure Gradient .....	12
2.2.2 Viscosity and Turbulence .....	13
2.2.3 Secondary Circulation.....	14
2.2.4 Acoustic Streaming .....	15

2.3	Use Of Vortex Tube in Conventional Refrigeration, Air Conditioning and Heat Pump Systems.....	16
2.3.1	Use of Vortex Tube in Transcritical Refrigeration Cycle.....	16
2.3.2	Use of Vortex Tube in Subcritical Refrigeration Cycle.....	20
2.3.3	Use of Vortex Tube in Power Cycle, Gas Liquification Cycles and other Thermodynamic Cycles .....	20
2.3.4	Self-Condensing Vortex Tube Cycle .....	23
2.3.5	Other Thermodynamic Cycle Based on Vortex Tube.....	24
2.3.6	Application of Vortex Tube In IC Engines.....	25
2.3.7	Vortex Tube in Liquefaction Process .....	25
2.3.8	CFD Study of Vortex Tube.....	26
2.3.9	Economic Analysis of Vortex Tube.....	28
2.3.10	Optimisation of Vortex Tube Integrated Refrigeration Cycle .....	29
2.4	Research Gaps and Objectives .....	29
2.4.1	Research Gaps from Literature .....	29
2.4.2	Research Objectives of Thesis .....	30
<b>CHAPTER 3: ENERGY, EXERGY AND MULTI-OBJECTIVE OPTIMIZATION OF VORTEX TUBE INTEGRATED SUBCRITICAL VAPOUR COMPRESSION REFRIGERATION CYCLE .....</b>		<b>31</b>
3.1	Introduction .....	31
3.2	System Description.....	31
3.3	Thermodynamic Analysis and Mathematical Modelling of VTC and VCR	33
3.3.1	Conservation of Mass.....	34
3.3.2	Energy Analysis .....	34
3.3.3	Exergy Analysis .....	37
3.3.4	Efficiency Defect for VTC And VCR .....	39



3.4	Results and Discussion .....	40
3.4.1	Model Validation .....	40
3.4.2	Results Based on Energy Analysis .....	41
3.4.3	Results Based on Exergy Analysis .....	49
3.4.4	Multi-Objective Optimization .....	58

## **CHAPTER 4: ENERGY, EXERGY, ENVIRONMENTAL (3E) ANALYSES AND MULTI-OBJECTIVE OPTIMIZATION OF VORTEX TUBE COUPLED WITH TRANS-CRITICAL VAPOUR COMPRESSION REFRIGERATION CYCLE**

4.1	Introduction .....	62
4.2	Vortex Tube Coupled With Transcritical Vapour Compression Refrigeration Cycle (TVTC).....	62
4.3	Mathematical Modelling Of TVTC .....	65
4.3.1	Mass Conservation .....	65
4.3.2	Energy Conservation .....	65
4.3.3	Exergy Balance .....	65
4.3.4	Environmental Analysis .....	68
4.3.5	Structural Bond Analysis .....	69
4.4	Model Validation .....	70
4.5	Results and Discussion .....	71
4.5.1	Results of Energy Analysis .....	72
4.5.2	Results of Exergy Analysis .....	84
4.5.3	Results of Environment Analysis .....	91
4.5.4	Results of Structural Bond Method.....	92
4.5.5	Multi-Objective Optimization.....	93

## **CHAPTER 5: ECONOMIC ANALYSIS OF VORTEX TUBE COUPLED WITH TRANSCRITICAL AND SUBCRITICAL VAPOUR COMPRESSION REFRIGERATION SYSTEMS .....**

96

5.1	Introduction .....	96
5.2	Methodology .....	96
5.2.1	Assumptions.....	96
5.3	Results and Discussion.....	98
5.3.1	Economic Analysis of TVTC .....	100
5.3.2	Economic Analysis of VTC .....	103
<b>CHAPTER 6: COMPUTATIONAL FLUID DYNAMICS (CFD) STUDY OF VORTEX TUBE .....</b>		<b>107</b>
6.1	Introduction .....	107
6.2	Geometrical Description.....	107
6.3	Numerical Modelling .....	109
6.3.1	Governing Equations.....	109
6.3.2	Mesh Information.....	110
6.3.3	Boundary Conditions .....	111
6.3.4	Grid Independence .....	112
6.4	Results and Discussion.....	113
<b>CHAPTER 7: CONCLUSION .....</b>		<b>116</b>
7.1	Vortex Tube Coupled with Subcritical Vapour Compression Refrigeration Cycle (VTC).....	116
7.2	Vortex Tube Coupled With Transcritical Vapour Compression Refrigeration Cycle (TVTC).....	117
7.3	Economic Analysis of Vortex Tube Coupled with Transcritical and Subcritical Vapour Compression Refrigeration Systems .....	118
7.4	Computational Fluid Dynamic Analysis of Vortex Tube.....	118
7.5	Future Scope.....	119
<b>REFERENCES.....</b>		<b>120</b>

<b>LIST OF PUBLICATIONS .....</b>	<b>128</b>
-----------------------------------	------------

## LIST OF FIGURES

Fig. 1.1 P–h diagram of subcritical VCR cycle .....	3
Fig. 1.2 P–h diagram of transcritical VCR system.....	4
Fig. 1.3 Flow structure in a counter-flow vortex tube[1] .....	5
Fig. 3.1 Block diagrams of VTC and VCR (7-2b-3-3a).....	32
Fig. 3.2 P-h diagram of VTC and VCR (7-2b-3-3a) .....	33
Fig. 3.3 Effect of intermediate temperature on COP of VTC and intermediate pressure .....	42
Fig. 3.4 Effect of evaporator temperature on cooling capacity, compression power, and COP for VCR and VTC.....	43
Fig. 3.5 Effect of condenser temperature on cooling capacity, compression power, and COP for VCR and VTC .....	44
Fig. 3.6 Effect of cold mass fraction on cooling capacity, compressor power and maximum COP of VTC.....	45
Fig. 3.7 Effect of effectiveness of subcooler and desuperheater on cooling capacity and compressor power of VTC .....	47
Fig. 3.8 Effect of effectiveness of subcooler and desuperheater on COP of VTC and its improvement over VCR .....	48
Fig. 3.9 Effect of VT-nozzle efficiency on cooling capacity and compressor power of VTC.....	49
Fig. 3.10 Effect of evaporator temperature on efficiency defect of VTC .....	51
Fig. 3.11 Effect of evaporator temperature on exergetic efficiency and total irreversibility of VTC and VCR.....	52
Fig. 3.12 Effect of condenser temperature on efficiency defect of VTC and VCR ...	55
Fig. 3.13 Effect of condenser temperature on exergetic efficiency and total irreversibility of VTC and VCR.....	56
Fig. 3.14 Effect of isentropic efficiency of compressor on exergetic efficiency of VTC and VCR.....	57
Fig. 3.15 Pareto front calculated using GA for compressor work and exergetic efficiency of VTC.....	60
Fig. 4.1 Schematic diagram of TVTC and TVCR (7-2b-3-3a) .....	63

Fig. 4.2 P-h diagram of TVTC and TVCR (7-2b-3-3a) .....	64
Fig. 4.3 Effect of gascooler pressure on COP of TVTC and TVCR .....	73
Fig. 4.4 Effect of evaporator and gascooler exit temperatures on optimum gascooler and intermediate pressures .....	74
Fig. 4.5 Effect of evaporator temperature on compressor power, cooling capacity, and COP .....	76
Fig. 4.6 Effect of gascooler exit temperature on compressor power, cooling capacity, and COP .....	78
Fig. 4.7 Effect of cold mass fraction and isentropic efficiency of VT-nozzle on cooling capacity, compressor power and COP of TVTC .....	79
Fig. 4.8 Effect of effectiveness of subcooler and desuperheater on cooling capacity, compressor power and COP of TVTC .....	83
Fig. 4.9 Effect of evaporator temperature on irreversibilities of various components of TVTC .....	85
Fig. 4.10 Effect of evaporator temperature on exergetic efficiency and total irreversibility of TVTC and TVCR .....	86
Fig. 4.11 Effect of gascooler exit temperature on irreversibility of various components of TVTC .....	88
Fig. 4.12 Effect of gascooler exit temperature on exergetic efficiency and total irreversibility of TVTC and TVCR .....	89
Fig. 4.13 Effect of isentropic efficiency of compressor on COP and exergetic efficiency of TVCR and TVTC .....	90
Fig. 4.14 Coefficient of structural bond (CSB) of various components of TVTC .....	93
Fig. 4.15 Pareto optimality obtained between compressor power and exergetic efficiency of TVTC .....	95
Fig. 5.1 Effect of evaporator temperature on various costs of TVTC .....	100
Fig. 5.2 Effect of gascooler exit temperature on various costs of TVTC .....	101
Fig. 5.3 Effect of cooling capacity on various costs of TVTC .....	102
Fig. 5.4 Effect of evaporator temperature on various costs of VTC .....	104
Fig. 5.5 Effect of condenser temperature on various costs of VTC .....	105
Fig. 5.6 Effect of cooling capacity on various costs of VTC .....	106

Fig. 6.1 Geometrical configuration of counter flow vortex tube (a) Front view (b) side view.....	108
Fig. 6.2 Various nozzle entry angles (a) 0° (b) 2° (c) 3° (d) 4° (e) 5°.....	109
Fig. 6.3 3D CFD Mesh Grid of Vortex Tube with 1870916 elements .....	111
Fig. 6.4 Grid Independence study for vortex tube .....	113
Fig. 6.5 Temperature contour in vortex tube.....	114
Fig. 6.6 Temperature contour at the cold exit for various air entry angles in VT (a)0° (b) 2° (c) 3° (d) 4° (e) 5° .....	115

## LIST OF TABLES

Table 1.1 Properties of Refrigerant R1234yf .....	7
Table 3.1 Comparison of results of present work with that of Sarkar.....	40
Table 3.2 Base values and range of Input Parameters for VTC .....	40
Table 3.3 Effect of evaporator temperature on efficiency defect in various components of VCR.....	50
Table 3.4 Comparison of irreversibility in various components of VTC and VCR...	53
Table 3.5 Effect of condenser temperature on efficiency defect in various components of VCR.....	54
Table 3.6 Effect of cold mass fraction on exergetic efficiency of VTC.....	57
Table 3.7 Statistical data for different Regression Models .....	59
Table 4.1 Various equations for Mass balance and Energy Balance in TVTC .....	66
Table 4.2 Various equations for Exergy Balance in TVTC .....	67
Table 4.3 Comparison of the present work with Sarkar .....	70
Table 4.4 Base values and range of Input Parameters for TVTC.....	71
Table 4.5 Comparison of present work's outcomes (2 DOF) to those of Sarkar (1 DOF) .....	72
Table 4.6 Effect of on the heat rejected by the desuperheater at different values of effectiveness of desuperheater .....	81
Table 4.7 Effect of water inlet temperature on cooling capacity, compressor power and COP of TVTC.....	82
Table 4.8 Effect of evaporator temperature on irreversibilities in various components of TVCR.....	84
Table 4.9 Effect of gascooler exit temperature on irreversibilities in various components of TVCR .....	88
Table 4.10 Yearly penalty cost of CO <sub>2</sub> emission for TVCR and TVTC .....	91
Table 5.1 Cost functions for various components of TVTC .....	97
Table 5.2 Input data for various parameters for economic analysis of TVTC and VTC .....	99
Table 5.3 Comparison of plant cost of TVTC and TVCR with variation of evaporator and gascooler temperature.....	103

Table 5.4 Comparison of plant cost of VTC and VCR with variation of evaporator and gascooler temperature.....	106
Table 6.1 Dimensions of vortex tube .....	108
Table 6.2 Boundary condition of the vortex tube.....	112



## **LIST OF SYMBOLS**

### **Abbreviations**

AP	Adequate Precision
C	Cost rate
CO <sub>2</sub>	Carbon Dioxide
CSB	Coefficient of Structural Bond
COP	Coefficient of performance
CV	Control Volume
DOF	Degree of Freedom (-)
EES	Engineering equation solver
EF	Exergy of Fuel (kW)
EP	Exergy of Product (kW)
EPR	Expansion pressure ratio
GA	Genetic Algorithm
GWP	Global Warming Potential
MOO	Multi Objective Optimisation
N <sub>2</sub> O	Nitrous oxide
ODP	Ozone Depletion Potential
TCEV	Transcritical cycle with expansion valve
TVTC	Vortex Tube coupled with Trans-critical vapour compression refrigeration cycle
TVCR	Trans-critical vapour compression refrigeration cycle

VCR	Vapour compression refrigeration cycle
VT	Vortex Tube
VTC	Vortex tube integrated single-stage vapour compression refrigeration cycle

## Nomenclature

$h$	Specific enthalpy (kJ kg <sup>-1</sup> )
$I$	Irreversibility (kW)
$P$	Pressure (kPa)
$Q$	Cooling capacity (kW)
$s$	Specific entropy (kJ kg <sup>-1</sup> K <sup>-1</sup> )
$T$	Temperature (°C)
$W$	Compressor power (kW)
$x$	Dryness fraction

## Greek Symbols

$\mu$	Cold mass fraction (-)
$\delta$	Efficiency defect (-)
$\varepsilon$	Effectiveness (-)
$\eta$	Efficiency (-)
$\lambda$	Emission conversion factor

## Subscripts

<i>1...11, 3a, 2b, 4d, 9C, 9H</i>	Various state points
<i>c</i>	Condenser
<i>comp</i>	Compressor
<i>ds</i>	Desuperheater
<i>e</i>	Evaporator
<i>ex</i>	Exergetic
<i>env</i>	environmental
<i>gc</i>	Gascooler
<i>imp</i>	Improvement
<i>int</i>	Intermediate
<i>max</i>	maximum
<i>mx</i>	mixing
<i>o</i>	Ambient condition or dead state
<i>op</i>	Operational time
<i>opt</i>	Optimum
<i>r</i>	Refrigerated space
<i>sc</i>	Subcooler
<i>sep</i>	Separator
<i>th</i>	Throttle valve
<i>t</i>	total
<i>tvc</i>	trans-critical vapour compression refrigeration cycle
<i>tvte</i>	vortex tube coupled with trans-critical vapour compression refrigeration cycle
<i>v</i>	Vortex tube nozzle

<i>vcr</i>	Vapour compression refrigeration cycle
<i>vt</i>	Vortex tube
<i>vtc</i>	Vortex tube integrated single-stage vapour compression refrigeration cycle
<i>w<sub>i</sub></i>	Water at the inlet to desuperheater
<i>w<sub>o</sub></i>	Water at the outlet to desuperheater

## CHAPTER 1: INTRODUCTION

### 1.1 MOTIVATION

In the present time society depends very highly on refrigeration and air conditioning. It covers a wide range of applications in residential, commercial and industrial sectors. The most widely system being used today in the world for refrigeration, air conditioning & heat pumps is vapour compression refrigeration system (VCR). The conventional refrigerants used in these systems were chlorofluorocarbons (CFCs) and hydrochlorofluorocarbons (HCFCs) due to their favourable thermo-physical and thermodynamic properties. However, these refrigerants contain chlorine, which causes ozone layer depletion. In the year 1987, 'Montreal Protocol' was established to prevent the consumption and production of ozone depleting substances such as R11, R12 etc. Subsequently, hydrofluorocarbons (HFCs) gradually replaced CFCs and HCFCs. However, HFCs were not found to be the permanent solution because of their high Global Warming Potential (GWP). The issue of 'Global Warming' was brought in front of the international community through the Kyoto Protocol in 1997.

To counter the problems of ozone depletion and global warming, a permanent solution was needed for refrigerant associated problems. It has inspired the researchers to develop the novel refrigeration systems with high energy efficiency and also use such refrigerants which are environment-friendly. The natural refrigerants (water, air, ammonia, nitrous oxide, carbon dioxide, hydrocarbons, etc.) along with hydrofluoroolefins (HFOs) such as R1234yf, R1234ze etc., are preferred now in VCR because of their low ozone depletion potential (ODP), low GWP and low toxicity.

The global demand of power consumption in HVAC sector is continuously increasing. In order to address this increased electricity consumption, thermal power plants have to emit more CO<sub>2</sub> into the environment which leads to increased carbon footprint. The increased CO<sub>2</sub> emissions can be reduced by increasing the performance of VCR systems. This can be done by suitably modifying the cycle structure, so that for a given amount of cooling capacity, power consumption can be reduced. The performance improvement not only reduces the consumption of electricity but also lowers the production of harmful gases from the thermal power plants. Many methods

have been reported in the literature for modification of the vapour compression systems which bring an increase in its COP such as the use of subcooler for subcooling, internal heat exchanger, multistage compression with an intercooler, expander in place of the expansion valve, ejector, dedicated subcooling or combination of these methods. A vortex tube (VT) can also be incorporated in a vapour compression refrigeration cycle to improve its thermodynamic performance.

The thermodynamic performance of a VCR system can be evaluated on the basis of first and second law of thermodynamics. The first law is mainly related with the conservation of energy. It does not provide any information about location of exergy destructions (irreversibility losses) occurring in various components of the refrigeration system. On the other hand, exergy analysis is based on second law of thermodynamics, a powerful method for the performance assessment and optimization of refrigeration systems.

Exergy analysis of a refrigeration system can be carried out by the analysis of all system components for exergy destruction (irreversibility). The evaluation of exergy destruction contributes towards identification of the sites of exergy destruction i.e. system component with maximum exergy destruction. Potential improvement in the system design can be achieved by identifying the main locations of exergy destruction. Thus, exergy analysis takes into account the irreversibility appearing in the refrigeration system, which could help in measuring the true performance of the system.

Thus, it can be summarized that the use of appropriate refrigerant in a modified vapour compression system is the need of the hour to reduce the Ozone layer depletion and global warming of the atmosphere. Furthermore, the modified vapour compression system must be analysed on the basis of both first and second laws of thermodynamics.

## 1.2 VAPOUR COMPRESSION REFRIGERATION CYCLE

The VCR system is a common method for refrigeration. In this system heat is transferred from a low temperature source to high temperature source by a refrigerant. In this system the phase change of refrigerant takes place. These systems are generally

used in domestic refrigerators, air-conditioning of buildings and automobiles. Vapour compression systems are of two types:

### 1.2.1 Subcritical Vapour Compression Cycle

In a conventional subcritical vapour compression refrigeration cycle, the complete cycle lies below the critical point of the used refrigerant. The refrigerant absorbs the heat from evaporator at low pressure and rejects the heat at high pressure through condensation inside a condenser. Fig. 1.1 shows the P-h diagram of subcritical VCR cycle.

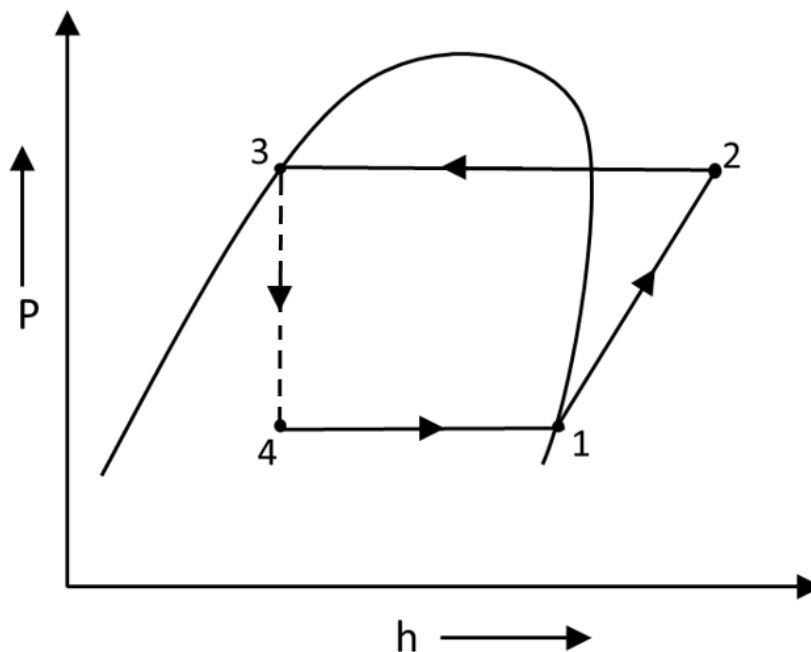


**Fig. 1.1** P-h diagram of subcritical VCR cycle

### 1.2.2 Transcritical Vapour Compression Cycle

In a transcritical vapour compression cycle a refrigerant absorbs the heat from the evaporator but heat is rejected through a gascooler instead of a condenser. In transcritical system the refrigerant pressure is increased above the critical pressure, and heat rejection takes place by single-phase sensible cooling (gas cooling) of the refrigerant. Fig. 1.2 shows the P-h diagram of transcritical VCR cycle.

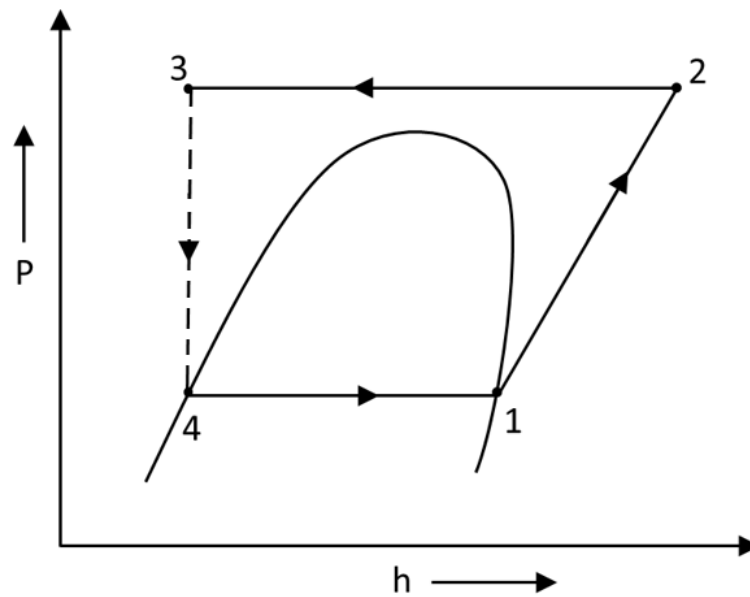


**Fig. 1.2** P–h diagram of transcritical VCR system

### 1.3 MODIFICATIONS IN VAPOUR COMPRESSION SYSTEMS

The vapour compression systems have significant thermodynamic losses than that of the ideal reverse Carnot cycle. These are thermodynamic losses due to gas compression and isenthalpic expansion. The first loss causes high discharge refrigerant temperature, high compression work, and high heat rejection in a condenser or gas cooler. The second loss causes low refrigeration capacity and large throttling losses. To reduce these thermodynamic losses, several researchers have suggested modifications in the subcritical and transcritical vapour compression systems by the incorporation of various performance enhancing devices such as mechanical subcooler, thermoelectric subcooler, heat exchanger, desuperheater, intercooler, ejector, expander and vortex tube etc.

The literature present number of ways to use this performance enhancing device in subcooling systems (Heat exchanger, mechanical subcooler, and thermoelectric subcooler), expansion loss recovery systems (expander, ejector and vortex tube) and multi-stage systems (Desuperheater, intercooler). The appropriate use of these devices usually enhances the COP and exergetic efficiency of subcritical and



transcritical vapour compression systems. In the present research, to reduce the exergy losses of both subcritical and transcritical refrigeration cycles, vortex tube has been employed in simple VCR cycle, along with other performance enhancing devices such as desuperheater and subcooler at appropriate places.

#### 1.4 VORTEX TUBE

A vortex tube is a thermo-fluidic device that utilizes compressed gas as its working medium. The invention of the vortex tube is attributed to the French physicist Georges J. Ranque in 1933, with subsequent advancements made by the German engineer Rudolf Hilsch in 1947 [2, 3]. As a result, the device is commonly referred to as the Ranque–Hilsch vortex tube (RHVT) [2, 4]. The vortex tube generates two low-pressure streams with significantly distinct temperatures when high-pressure gas flows through it. The compressed gas enters the tube tangentially, where it undergoes expansion and separation before exiting through separate outlets at high and low temperatures, respectively. These temperatures are notably higher and lower than the inlet temperature. This unique mechanism enables the vortex tube to produce both cold and hot streams without requiring additional components. The cold stream can be utilized for refrigeration and air conditioning purposes, while the hot stream is suitable for heating applications.

The geometrical construction of RHVT (utilized for delivering refrigerated gas) is simple with stationary parts only[5]. The RHVT comprises of the following components: inlet nozzles for introducing high pressure gas, control valve which is located at the hot exit for varying the flow rates of hot and cold streams, cold end orifice, vortex generator, and working tube [2, 5, 6].

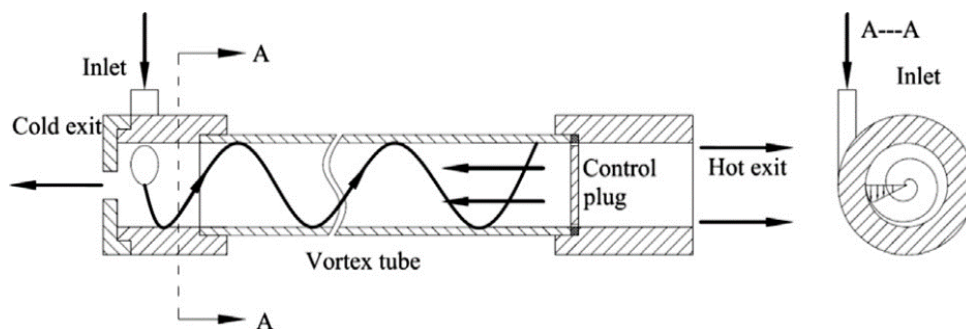


Fig. 1.3 Flow structure in a counter-flow vortex tube[1]

The vortex tubes are classified as counter-flow (CFVT) and uni-flow (UFVT) based upon the direction of flow. In the CFVT, the flow of forced and free vortices is in opposite directions thus cold and hot streams leave from opposite ends, as shown in Fig. 1.3. This makes the heat exchange very effective and efficient in CFVT as the heat exchange takes place between flows in opposite directions [7]. On the other hand, when both cold and hot flows leave from the hot end such a VT is known as “uni-flow”. Since both hot air and cold air flow in the same direction hence heat exchange becomes less effective or efficient as the temperature gradient between the two reduces in the direction of the flow thereby affecting the heat transfer rate [8]. Another classification is based on the number of exits; two- exit VT and three- exit VT. The double exit VT is used in the thermodynamic cycle based on the Keller model[9] whereas three-exit vortex tube, which is also referred as self- condensing vortex tube[10], is used in the thermodynamic cycle based on the Maurer model [11].

A vortex tube (VT) can be incorporated in a single stage vapour compression refrigeration cycle to improve its thermodynamic performance. Additionally, a vortex tube can approach isentropic expansion, which is preferable for enhancing the thermodynamic performance of the vapour compression refrigeration cycle [12]. VT has some benefits, like the absence of moving parts, no chemical or electrical elements, lightweight, low maintenance, and temperature adjustment facility [13, 14]. Several studies are available on the application of VT in various thermodynamic cycles like transcritical VCR, vapour absorption cycle [15], and CO<sub>2</sub> Rankine cycle [16].

## **1.5 REFRIGERANT USED IN THIS WORK**

### **1.5.1 Refrigerant R1234yf**

R1234yf is the refrigerant employed in the proposed research, as discussed further. R1234yf, also known as 2,3,3,3-tetrafluoropropene, is an HFO (hydrofluoroolifine) produced from alkenes) having zero ozone depletion potential (ODP) and global warming potential (GWP) less than one over 100-year span [17]. According to reports, R1234yf has minimal toxicity in terms of safety [18]. In addition, R1234yf shows high lower flammability, a high minimum ignition energy [19], and a low burning velocity of 1.5 cm/s, indicating a low ignition damage potential [20].

Moreover, its ignition temperature is high (405 °C) [20]. Consequently, R1234yf is classified by ASHRAE as A2L (lower flammability). According to the findings, without system modifications, the cooling capacity and energy efficiency of R1234yf differ by between 4 and 8% compared to R134a [21].

There are some drawbacks to R1234yf as specified further. The lubricants created for R134a or R410A are incompatible with R1234yf [22]. In addition, R1234yf has a lower solubility in the same lubricant as R134a, which may increase oil retention in the condenser and evaporator, thereby decreasing heat transfer efficiency [23]. It is noted in the literature that R1234yf is used in numerous applications, including mobile air conditioners [24], window air conditioners [25], split air conditioners [26], small capacity refrigerators [27], air space heating in buildings [28], and residential heat pump water heaters [29]. This research focuses on the application of R1234yf in refrigeration and mobile air conditioning (MAC) only. The thermodynamic properties of refrigerant R1234yf are given in Table 1.

**Table 1.1** Properties of Refrigerant R1234yf

Quantitative Parameter (Unit)	Value [30, 31]
Molar gas constant ( $\text{J mol}^{-1}\text{K}^{-1}$ )	8.314472
Molar mass ( $\text{kg kmol}^{-1}$ )	114.0415
Critical temperature ( $^{\circ}\text{C}$ )	94.7
Critical pressure (MPa)	3.3822
Triple point temperature ( $^{\circ}\text{C}$ )	-150.38
Normal boiling point temperature ( $^{\circ}\text{C}$ )	-29.49
GWP (100 years span)	<1
ODP	0

### 1.5.2 Refrigerant CO<sub>2</sub>

It is observed that the use of synthetic refrigerants like CFCs and HCFCs has amplified the environmental-related problems such as the greenhouse effect and ozone layer depletion [32]. Therefore, natural refrigerants like carbon dioxide, ammonia, butane, and isobutane have been chosen to replace synthetic refrigerants in

refrigeration, air-conditioning and heat pump systems [33, 34]. Among these natural refrigerants, CO<sub>2</sub> (R744) has zero ODP and GWP of one [35]. CO<sub>2</sub> is non-flammable, non-toxic and cheaper than that of HFC mixtures [36]. CO<sub>2</sub> has high critical pressure of 7.377 MPa [37] and low critical temperature of 31°C [38]. Due to its high operating pressure, CO<sub>2</sub> has a higher volumetric capacity than other refrigerants; consequently, size of compressor, pipelines, and other components involved in the trans-critical CO<sub>2</sub> cycle is significantly reduced[35-39].

## 1.6 THESIS ORGANIZATION

### Chapter 1: Introduction

This chapter presents the overview of vapour compression refrigeration cycle and ways to modify the cycle with vortex tube in order to improve its thermodynamic performance. Moreover, a brief discussion on the vortex tube has been conducted like, its types, working principle, application, etc. The energy and environmental issues associated with conventional vapour compression refrigeration technology are also discussed. The novel approach of investigated and evaluating refrigeration system coupled with vortex tube based on energy, exergy, environment, economic and optimisation are discussed. Further, chapter wise organisation of the thesis is presented in this chapter.

### Chapter 2: Literature Review

This chapter presents the up-to-date literature survey of vortex tube, use of vortex tube in conventional refrigeration systems, use of vortex tube in power cycles and other thermodynamic cycles. Also, the literature based on the CFD study has been done. The gaps from the literature survey have been identified. Furthermore, the objectives of the present work have been presented.

### Chapter 3: Energy, Exergy, Environment and Optimization of Vortex Tube Coupled with Subcritical Vapour Compression Refrigeration Cycle

This chapter evaluates the thermodynamic performance, environment analysis followed by multi-objective optimization of a vortex tube integrated single-stage vapour compression refrigeration cycle (VTC) in a subcritical region. The thermodynamic evaluation consists of an energy and exergy analysis for VTC in order

to determine the effect of various design and operating parameters on its performance. Moreover, the results of VTC are compared with those of a simple vapour compression refrigeration cycle (i.e., VCR) for the considered range of evaporator and condenser temperatures using R1234yf as the refrigerant. A multi-objective optimization using a genetic algorithm has been conducted to know about major decisive parameter to find the suitability for various applications of the system based on VTC.

#### **Chapter 4: Energy, Exergy, Environment and Optimization of Vortex Tube Coupled with Transcritical Vapour Compression Refrigeration Cycle**

This chapter deals with the thermodynamic investigation of vortex tube coupled with trans-critical vapour compression refrigeration cycle (TVTC), followed by environmental analysis and multi-objective optimization. In this research, effect of various operating and design parameters is studied on the performance of TVTC. Furthermore, a comparison is made between the outcomes of TVTC and simple trans-critical vapour compression refrigeration cycle (TVCR) for refrigerant CO<sub>2</sub>. The environmental penalty cost (per unit cooling capacity) of TVTC is compared with TVCR. Furthermore, the coefficient of structural bond is calculated in order to choose the most sensitive parameters for system's performance. Additionally, genetic algorithm-based multi-objective optimization has been performed to find a set of optimal solutions (pareto front) which shows a trade-off between two objectives.

#### **Chapter 5: Economic Analysis of Vortex Tube Coupled with Transcritical and Subcritical Vapour Compression Refrigeration Systems**

In this chapter, economic or cost analysis of transcritical and subcritical vapour compression refrigeration systems integrated with vortex tube has been done. The effect of evaporator temperature, gascooler exit temperature (condenser temperature in VTC) and cooling capacity has been studied on total plant cost, capital investment & maintenance cost, environment penalty cost and operational cost of TVTC and VTC. In addition to this, comparison of total plant cost rate has been done between TVTC & TVCR, and VTC & VCR.

## Chapter 6: Computational Fluid Dynamic Analysis of Vortex Tube

In this chapter, a computational fluid dynamic (CFD) study of a standalone counter flow straight vortex tube with two entry nozzles has been carried out by using ANSYS 2022R1 software. In this study, the effect of geometrical modification of vortex tube on energy separation phenomenon has been studied.

5

## Chapter 7: Overall Conclusion and Recommendations

In this chapter, overall conclusion of present investigations is presented. The appropriate suggestions and recommendation for future work are also mentioned in this chapter.

## CHAPTER 2: LITERATURE REVIEW

### 2.1 HISTORICAL BACKGROUND OF VORTEX TUBE

The vortex tube, also known as the Ranque–Hilsch vortex tube (RHVT), is a mechanical device that functions without any moving components. It divides a compressed gas stream into a cold stream and a hot stream, known as the temperature (or energy) separation effect. The vortex tube was initially discovered by Ranque[40], a metallurgist and physicist, who obtained a French patent for the device in 1932 and a United States patent in 1934[41]. Initially, the Vortex Tube failed to garner attention from the scientific and engineering communities for several years due to its significant thermodynamic inefficiency. In late 1945, interest in the vortex tube was rekindled by Hilsch[42], a German engineer, who enhanced its efficiency. He systematically analysed the impact of inlet pressure and the geometric parameters of the vortex tube on its performance, providing a plausible explanation for the energy separation process. The vortex tube is commonly referred to by various names. Ranque vortex tube, Hilsch vortex tube, or Ranque–Hilsch vortex tube, as well as Maxwell–Demon vortex tube (named after Maxwell and the Demon group who investigated the molecular dynamics of heated air within the tube). Despite the existence of multiple designations, this thesis will exclusively utilise the term "vortex tube."

Post-World War II, numerous scholars including Westley[43], Curley and McGree[44], Kalvinskas[45], Dobratz[46] and Nash[47] conducted comprehensive evaluations of vortex tube applications and improvements. Numerous practical applications of VT are available in literature which encompass quick start-up of steam power generation, liquefaction of natural gas [48], cooling of equipments in laboratories dealing with explosive chemicals[49, 50], regulating temperature of air systems for divers, manned underwater habitats and hyperbaric chambers [51-53], separating particles in the waste gas industry[54], cooling for low-temperature magic angle spinning nuclear magnetic resonance [55], nuclear reactors, and cooling of firemen's suits[56].

VT was identified as a cost-effective and efficient solution to numerous cooling issues in recent years. It was not until today that the separation mechanism within the vortex tube was fully comprehended [57]. VT can be employed in a variety of low-

temperature engineering applications, including the cooling of electronic control cabinets, cooling or heating of food items, and cooling of machine parts during operations, due to the ability to acquire either hot or cold flow streams using compressed gas [57].

The VT is highly beneficial for specific thermal management applications due to its simplicity, compactness, light weight, robustness, reliability, low maintenance cost, and safety, despite its limited capacity [58]. The VT can be categorised into two types: counter-flow VT and uni-flow VT [59]. In counter-flow VT, the cold stream flows in the opposite direction from the hot stream, whereas in uni-flow VT, both streams flow in the same direction. In general, the counter-flow VT is preferred over the uni-flow VT due to its effective energy separation [59].

## 2.2 WORKING PRINCIPLES OF VORTEX TUBE

Despite the straightforward design and functionality of a vortex tube, the flow dynamics remain inadequately understood, and the mechanism of energy separation has not been well elucidated, due to the very turbulent and intricate swirling flow within the tube. Numerous scholars have suggested valuable models to elucidate this phenomenon; nevertheless, none have been conclusively established to accurately describe the operational mechanism or quantitatively produce the optimal structures. A summary of the diverse theories from the open literature has been compiled.

### 2.2.1 Pressure Gradient

Researchers observed and examined the pressure gradient within the vortex tube at the initial stage. Ranque[40, 41] identified compression and expansion as the primary cause of temperature separation in the RHVT. It was elucidated that the vortex tube's configuration leads to abrupt expansion upon the injection of compressed air, resulting in a decrease in the temperature of the airflow within the core during the expansion process [60, 61]. The temperature decrease resulting from abrupt expansion can be estimated using the equations of adiabatic expansion. Furthermore, it was demonstrated that the peripheral flow exhibits a higher temperature than the core flow, attributable to the radial pressure distribution of the flow[62]. Certain studies have indicated that the formation of a forced vortex is the primary cause of the radial pressure gradient's existence. The pressure gradient of a forced vortex results in a



temperature distribution characterised by elevated temperatures in the periphery and reduced temperatures in the core, attributable to compression in the higher-pressure peripheral region and expansion in the lower pressure core region. The forced vortex and its impact on velocity distribution have been examined in previous studies[60, 63-66]. The velocity distribution in the vortex tube indicates the presence of a forced vortex; however, the rationale behind the radial pressure gradient of the forced vortex is still debatable. If the pressure within the tube exceeds the input pressure, peripheral compression will occur, leading to an increase in temperature. Investigations indicate that the pressure at any point within the tube is lower than the inlet pressure, implying that expansion occurs throughout the tube, including at the periphery[66, 67].

### 2.2.2 Viscosity and Turbulence

An investigation conducted by Fulton[68] showed that the tangential velocity of the peripheral layer was lower than that of the inner layer at the entrance of the tube, meaning that a free vortex was being formed. Because of the shear stress between different layers, the slow peripheral flow was accelerated by the inner flow, while the inner flow was decelerated. In this process, kinetic energy was transferred from the inner layer to the outer layer by inner friction. Temperature rise occurred because the energy transferred to the peripheral flow, and additional energy transported by turbulence between the two layers helped the formation of temperature gradient in the vortex tube. The concept of the inner friction and turbulence effect is supported by numerous experimental, theoretical and numerical studies conducted by other researchers[69-74]. Fulton [68] conducted an investigation that revealed the tangential velocity of the peripheral layer was lower than that of the inner layer at the tube's entrance, indicating the formation of a free vortex. The inner flow accelerated the slow peripheral flow, while the inner flow decelerated, as a result of the shear stress between different layers. Kinetic energy was transferred from the inner layer to the outer layer through inner friction during this process. The energy transferred to the peripheral flow and the additional energy transported by turbulence between the two layers contributed to the formation of a temperature gradient in the vortex tube, resulting in a temperature increase. Numerous experimental, theoretical, and numerical studies conducted by other researchers have substantiated the concept of the inner friction and turbulence

effect [69-74]. Furthermore, the viscous friction between the working fluid and the tube wall is the basis of some explanations found in literature [56, 60, 61, 75]. It has been reported that heat generation due to friction between the tube wall and working fluid converts kinetic energy of fluid into thermal energy, leads to increase in its temperature.

### 2.2.3 Secondary Circulation

The analysis of the counter-flow VT revealed that the amount of cold air redirected by the hot end plug exceeded the amount of cold air expelled from the cold nozzle [76]. Consequently, a portion of the cold air redirected by the hot plug must revert to the hot end, thereby establishing the secondary circulation. The influence of secondary circulation on temperature separation in a VT has been examined both experimentally and theoretically by numerous researchers [67, 76-80].

The secondary circulation within the tube was proposed to constitute a conventional refrigeration cycle that facilitated the transfer of thermal energy from the inner flow to the outer flow [76, 79, 80]. Upon its return to the cold end, the secondary circulation absorbed thermal energy along the centerline. This energy was subsequently transferred to the peripheral flow when it joined the primary flow at the hot end. Consequently, the temperature of the outer layer rose while the temperature of the core flow diminished.

Nonetheless, not all researchers have corroborated the presence of secondary flow in vortex tubes. A numerical analysis of the vortex tube indicated that secondary flow could occur when the cold nozzle's dimensions were sufficiently small [60]. As the diameter of the cold nozzle increases, the secondary circulation diminishes and ultimately ceases when the ratio of the cold end diameter to the tube diameter reaches 0.58. The secondary flow model was established using a single vortex tube with a small cold nozzle ( $d_c/d_t = 0.323$ ), thus restricting its applicability to this particular tube geometry.

The relationship between the secondary circulation and the size of the cold exit has been recently investigated by Nimbalkar and Muller[81]. They found that the formation of a secondary circulation dependent on the relative size of the cold nozzle.

According to the discussion above, clarification of the secondary circulation in different vortex tubes and an understanding of the influence of the secondary flow, when it is formed, are both required. Furthermore, the secondary circulation in a uni-flow vortex tube has not been investigated yet, so the existence and influence of the secondary flow in such a RHVT is still unclear. Nimbalkar and Muller [81] have examined the correlation between secondary circulation and the dimensions of the cold exit. The researchers discovered that the development of a secondary circulation is contingent upon the relative dimensions of the cold nozzle. In accordance with the preceding discussion, it is necessary to clarify the secondary circulation in various vortex tubes and to comprehend the impact of the secondary flow when it is generated. Moreover, the secondary circulation within a uni-flow vortex tube remains unexamined, leaving the existence and impact of the secondary flow in such a VT ambiguous.

#### 2.2.4 Acoustic Streaming

The noise generated during the VT experiments indicates that acoustics should be regarded as a significant factor in the analysis of the vortex tube. Acoustic signals generated by the VT have been quantified and examined in various studies[82-84].

During the 1980s, multiple experiments were conducted to examine acoustic streaming in a core-flow vortex tube lacking of a plug for the study of acoustic streaming[82]. This study involved the measurement and analysis of temperature along the centerline and near the tube entrance, as well as acoustic parameters including sound pressure level and noise frequency. The experimental results indicated that an increase in inlet pressure caused a sudden temperature rise from 35°C to 35.6°C. A simultaneous decrease of 25 dB in the sound pressure level was recorded. The abrupt change in temperature and sound pressure level illustrates the correlation between acoustic streaming and temperature distribution in the RHVT. Kurosaka[82] noted that a Rankine vortex formed at the inlet of the tube and the acoustic streaming always had the same direction as the steady vortex. He proposed that the tangential velocity of the swirl was accelerated by the acoustic streaming, and that the change in the velocity distribution indicated that the Rankin vortex was converted to a forced vortex by the acoustic streaming. The temperature distribution was then determined by the pressure

gradient of the forced vortex flow.

The above evidence is not sufficiently conclusive to support the acoustic streaming hypothesis. In Kurosaka's experiments, a hollow cylinder was used instead of vortex tube and only the cold temperature at the entrance of the tube was measured[82]. In these experiments, the acoustic streaming was investigated independently and other flow parameters such as velocity, temperature and pressure distribution were not measured. Also, as discussed in the previous section, the consideration of pressure gradient of forced vortex as the reason for the temperature separation is still debatable. Due to insufficient evidence, acoustic streaming cannot be claimed as the main reason for the temperature separation in a vortex tube. Furthermore, prediction of the temperature distribution from a three-dimensional numerical model of the Ranque–Hilsch vortex tube[60], which had no consideration of the acoustic effect, agreed well with the experimental results of Kurosaka[82]. The results show a strong correspondence between changes in the temperature separation and the sound pressure level. However, there is insufficient evidence to support the hypothesis that acoustic streaming altered the flow structure, hence the pressure gradient within the tube. Further investigation of the observed temperature and sound changes is required.

## 2.3 USE OF VORTEX TUBE IN CONVENTIONAL REFRIGERATION, AIR CONDITIONING AND HEAT PUMP SYSTEMS

### 2.3.1 Use of Vortex Tube in Transcritical Refrigeration Cycle

Extensive literature is available on the study of VT-integrated transcritical vapour compression refrigeration cycle (TVCR). A few researchers studied the Maurer model [11] when vortex tube is incorporated into trans-critical refrigeration cycle. Li et al. [85] studied the effect of the evaporator and gas cooler exit temperatures on the coefficient of performance (COP) of a VCR with a vortex tube. The maximum increase in COP was reported as 37% for CO<sub>2</sub> at an evaporation temperature of 5°C and gas cooler exit temperature of 40°C.

Sarkar [86] demonstrated the effect of various operating parameters on COP improvement and optimum compressor discharge pressure by using a vortex tube in transcritical CO<sub>2</sub> cycles based on the Maurer [11] and the Keller models [9]. He

reported that the effect of gas cooler exit temperature on optimal discharge pressure was more significant than that of evaporator temperature. Similarly, Sarkar[87] investigated the same cycles exergetically, and concluded that the maximum improvement in exergetic efficiency is recorded for isobutane (12.2%), followed by propane (11.5%) and ammonia (negligible).

Jain et al. [88] examined the effect of various operating parameters, like gas cooler exit temperature, evaporator temperature, cold mass fraction, and water inlet temperature, on the COP of transcritical cycle with vortex tube (TCVT) based on the Maurer model using  $N_2O$  as a refrigerant. The COP of TCVT was found to improve by 1.72–27.01% compared to the transcritical cycle with expansion valve (TCEV). Jain et al. [89] reported the effect of several operating parameters on exergetic efficiency and COP for TCVT. The exergetic efficiency and COP of TCVT were reported to be 10–12% higher than the TCEV for the considered operating conditions. In another study, Jain et al. [90] investigated the influence of various operating parameters on the COP and exergetic efficiency of a two-stage transcritical cycle with a vortex tube. Compared to a two-stage transcritical cycle with an expansion valve, the COP of the proposed cycle increased by 1.97–27.19% for  $N_2O$ .

Shet et al. [91] analysed the modified transcritical  $CO_2$  cycles with internal heat exchanger, vortex tube, and expansion turbine using EES software. The optimum COP and 2<sup>nd</sup> law efficiency at different evaporator and gas cooler exit temperatures are obtained. The expansion turbine improves COP by 25%, while vortex tube and internal heat exchanger have low COP improvements. Their results indicated that the COP of TCVT is 1.89% higher than the base case. However, all modifications decrease discharge pressure, with work recovery turbine achieving the best exergetic efficiency.

Xie et al. [92] employed the thermodynamics method to analyse the  $CO_2$  transcritical two-stage compression refrigeration cycle coupled with vortex tube. The proposed cycle is compared with  $CO_2$  trans-critical two-stage compression refrigeration cycle with expansion valve. The results indicate that the performance of the cycle with vortex tube is 2.4% to 16.3% superior to that of the cycle with expansion valve under the given conditions. COP of the cycle with vortex tube is maximised by

the optimal discharge pressure. When the evaporating temperature is lower or the gas cooler discharge temperature is higher, the COP of the system decreases, while the COP improvement increases. Moreover, cold mass fraction has no discernible impact on COP; however, the rate of COP improvement accelerates as the cold mass fraction increases.

Liu et al. [93] developed a transcritical CO<sub>2</sub> heat pump cycle utilizing vortex tube expansion and compared it to a transcritical CO<sub>2</sub> refrigeration cycle employing a throttle valve. Thermodynamic analysis indicates that the vortex tube expansion transcritical CO<sub>2</sub> heat pump cycle surpasses the transcritical CO<sub>2</sub> heat pump cycle utilizing a throttle valve regarding system performance. The coefficient of performance enhancement ranges from 5.8% to 13.9% under the designated conditions. The performance of the system is greatly affected by the temperature at the gas-cooler outlet. An enhanced COP improvement is noted when the cycle operates at a diminished evaporation temperature or an elevated gas-cooler outlet temperature.

Liu and Jin [94] thermodynamically studied a two-stage transcritical CO<sub>2</sub> refrigeration cycle with vortex tube expansion and compared it to the two-stage transcritical CO<sub>2</sub> refrigeration cycle with throttle valve. Thermodynamic analysis results suggest that the vortex tube cycle has an optimal heat rejection pressure, and the COP enhancement is between 2.4% to 16.3% under the specified conditions. The COP will diminish due to a reduction in evaporation temperature or an elevation in gas-cooler outlet temperature, whereas the COP will enhance. The cold mass fraction has a negligible impact on the COP; however, the COP enhancement will increase rapidly as the cold mass fraction increases.

Liu et al. [95] proposed utilizing a single vortex tube to substitute the expansion valve in a traditional CO<sub>2</sub> transcritical refrigeration system, aiming to minimize irreversible losses and enhance COP. A mathematical model was developed to evaluate the system's performance against conventional systems. The findings indicated that the proposed system could enhance energy conservation, with the vortex tube inlet temperature and discharge pressure exerting a substantial impact on the COP. The COP increased by 33.7% when the discharge pressure was 9 MPa and the vortex tube inlet

temperature was 45°C. The optimal discharge pressure correlation was determined, and its impact on COP enhancement was examined.

Dubey et al. [96] thermodynamically examined the performance of a cascade refrigeration-heat pump system utilizing a natural refrigerant for both heating and cooling applications. The system's topping cycle employs a vortex tube, yielding a 5.9% enhancement in the COP relative to the transcritical cascade cycle without an expansion valve. The model predicts performance parameters and operating conditions of the system and the same is optimised for overall COP by utilising multi-linear regression analysis. The research corroborates the cascade refrigeration-heat pump model utilizing carbon dioxide and propylene as refrigerants, potentially aiding in the advancement and optimal design of cascade refrigeration systems based on vortex tube.

Recently, Luo et al. [97] conducted a study on the transcritical CO<sub>2</sub> cycles with vortex tubes, which aimed to resolve the significant throttling loss and poor system performance of current transcritical CO<sub>2</sub> cycles. This work also introduces a two-stage compression transcritical CO<sub>2</sub> system with serial vortex tubes, which exhibits superior cooling performance and reduced exergy loss in comparison to current systems. The findings indicate that parallel vortex tubes are more effective in transcritical systems with evaporators that exceed two, while serial vortex tubes are more effective in systems with two evaporators and vortex tubes that have a cold mass fraction greater than 0.3. Moreover, the exergy analysis of the existing and improved transcritical CO<sub>2</sub> cycles demonstrates that the exergy loss resulting from the throttle valve is significantly reduced when the vortex tube is employed.

Singh [98] thermodynamically investigated vortex tube integrated transcritical CO<sub>2</sub> compression refrigeration cycle with single and double compressor. Moreover, he worked on feasibility study of vortex tube integrated transcritical CO<sub>2</sub> compression refrigeration system with ejector expansion device. The results shows that the vortex tube integrated transcritical CO<sub>2</sub> compression refrigeration cycle is observed to have higher thermodynamic performance in terms of COP and exergy efficiency than that of conventional CO<sub>2</sub> transcritical compression refrigeration cycle.



The above literature depicts the use of VT in refrigeration cycles based on the Maurer model. Nevertheless, employing this model does have a few drawbacks: the refrigerant stream enters VT and produces two phases cold stream, which further complicates the design of VT. Therefore, in terms of model feasibility, the Keller model is reported to be preferred over the Maurer model [99]. Therefore, a vortex tube coupled with trans-critical vapour compression refrigeration cycle (TVTC) based on the Keller model is a feasible alternative to the Maurer model.

### **2.3.2 Use of Vortex Tube in Subcritical Refrigeration Cycle**

Numerous studies have been conducted on the integration of VT in TVCR, but only a few [87] are focused on the application of VT in subcritical VCR. Sarkar [87] studied the effect of various operating and design parameters on thermodynamic performance utilising the Maurer and the Keller models for subcritical VCR employing isobutane, propane, and ammonia. Isobutane and propane both are hydrocarbons and have high flammability [100] whereas ammonia is toxic in nature [101]. Further, the drawback of the Maurer model is that the gaseous stream entering the VT generates a two-phase cold stream. The design of VT for the Maurer model is practically less feasible than for the Keller model due to difficulty of phase separation in VT [99]. Due to the absence of a two-phase cold stream, the ‘vortex tube integrated single-stage vapour compression refrigeration cycle’ (VTC) based on Keller model is the more realistic option.

### **2.3.3 Use of Vortex Tube in Power Cycles, Gas Liquification Cycles and other Thermodynamic Cycles**

Many experimental works involving novel cycles and application-based studies on VT also find place in the literature. Mansour et al. [102] formulated a novel real gas model to predict the cold and hot exit temperatures of a vortex tube, incorporating Bödewadt boundary layer flow and a correction factor for elevated cold mass fractions. The model is validated against an ideal gas model and experimental data for air, R134a, and carbon dioxide. The model markedly improves predictions for R134a and carbon dioxide. A parametric study evaluates carbon dioxide performance under transcritical conditions, demonstrating that cooling and heating capacities can increase up to 1 kW and exergy efficiency by at least 88.5%.



Mohiuddin and Elbel [103] experimentally studied the VT in refrigeration systems, assessing their performance for various working fluids like air and R134a. It identifies appropriate geometries and operating environments, and experimentally demonstrates work recovery effects. The findings suggest the development of novel vortex tube cycles that can enhance vapour compression systems, thereby enhancing performance.

Zhu and Elbel [104] investigated the potential of low-grade energy sources, including waste heat from internal combustion engine cycles, to enhance energy efficiency. It recommends the utilisation of vapour jet ejector cycles or absorption/adsorption cycles to produce cooling. The paper also investigates the feasibility of a vortex tube in enhancing the temperature-available levels of low-grade heat sources. The objective is to increase the temperature of the ejector cooling cycle by directing a stream of vapour heated by the waste heat source through the tube. The vortex tube heat booster has the potential to enhance the cycle's COP by 40% when operating with a low entrainment ratio, as indicated by the simulation results.

Acar et al. [105] designed and evaluated the Ranque-Hilsch vortex tube aided vapour compression cooling (RHVTC) and single vapour compression cooling systems. This study conducted the energy, exergy, and economic analyses for a vortex tube-aided vapour compression cooling (RHVTC) system employing R-143a for cooling and drying applications. The systems were designed for different evaporator temperatures and compressor discharge pressures for refrigerants. The Ranque-Hilsch vortex tube system had the highest net present value of 35836 €. Also, the COP and exergy efficiency were calculated for the summer and winter modes.

Puangcharoenchai et al. [106] experimentally studied the effect of subcooling of refrigerant on thermal performance of vapour compression refrigeration system by utilising vortex tube. Experiments were conducted on the evaporator section of a vapour compression refrigeration system by employing a variety of loads. The testing parameters included various loads (25%, 50%, 75%, and 100%) and cold mass fractions (25%, 50%, and 75%). The findings demonstrated that maximum efficiency was attained with a cold mass fraction of 25% and a load of 100%. Consequently, the

COP may be augmented by 5.16%, while the average power consumption could diminish by roughly 4.36%. This study is anticipated to provide improved guidelines for vapour compression refrigeration systems, which will improve the system's operation.

Mugdadi and Al-Nimr [15] introduced a novel cooling system that integrates an absorption cooler with a vortex tube. The cooling effects are generated by both devices. Compressed air is introduced into the vortex tube to produce a cooling effect, while the hot stream of air leaving from the vortex tube is utilized to operate the absorption cooler. A theoretical model has been developed to examine the performance of the hybrid cooling system concerning the specific cooling load and the COP. Moreover, the performance of the hybrid system is compared to that of the vortex tube independently. Results indicated that the system's cooling capacity increases as both the feed air temperature and pressure increase. In comparison to the standalone vortex tube, the system's maximum coefficient of performance under current design points is 29.3% higher.

Mansour et al. [107] analysed a transcritical carbon dioxide heat pump cycle integrating a vortex tube, aiming to increase heat pump efficiency. A conventional heat pump model is validated to determine feasibility. The vortex tube heat pump is analyzed to test its performance and the effect of different parameters under different conditions. The hot exit pressure and desuperheater glycol mass flow rate is found to be the most effective parameters for desuperheater heating capacity and overall COP. Hot exit pressure significantly controls desuperheater glycol exit temperature, but with limitations. The cold mass fraction variation shows insignificant changes in desuperheater glycol exit temperature. The heating COP of vortex tube coupled heat pump is improved by a maximum of 43.7% compared to a conventional heat pump.

Wang et al. [16] proposed a novel transcritical CO<sub>2</sub> Rankine cycle, which utilises a vortex tube to condense CO<sub>2</sub> under ambient conditions. The parametric effects on thermodynamic and economic performance are analysed using a mathematical model that is based on the cost of specific equipment investment. The model is subsequently verified using experimental data. In order to optimise

multiobjective systems for optimal cycle performance, the nondominated sorting genetic algorithm II is implemented. The results of the parametric analysis indicate that the exergy efficiency can be enhanced by increasing the turbine inlet temperature and vortex tube outlet pressure. A reduction in the turbine inlet temperature and pressure can lower the investment cost of the TCO<sub>2</sub> cycle equipment. In addition, the results of multiobjective optimisation suggest that a conflict exists between the economic and thermodynamic performance of the TCO<sub>2</sub> cycle, which is determined by the cost of specific equipment investment.

Majidi et al. [108] investigated various configurations of VTs in order to optimise their cooling and heating capabilities. The investigation examines the impact of thermo-physical parameters on the temperature gradient that is generated. Furthermore, a novel equation for estimating the hot outlet temperature has been developed and the same is validated by utilising the experimental data. Moreover, the maximum and minimum temperatures for hot and cold streams, respectively are determined by simulating various configurations. Finally, the optimal configuration for a triple vortex tube system and a double-pipe helical heat exchanger is recommended.

### 2.3.4 Self-Condensing Vortex Tube Cycle

Zhao et al. [109] introduced a self-condensation compressed carbon dioxide energy storage system utilizing a vortex tube to facilitate condensation without supplementary cooling sources. The findings demonstrate that the condensation process is more effective when the vortex tube inlet temperature approaches the critical temperature of carbon dioxide. The energy density, roundtrip electrical efficiency, and exergy efficiency of the system are 5.43 kWh/m<sup>3</sup>, 53.45%, and 61.83%, respectively. Increased pressure in low-pressure storage tanks enhances roundtrip efficiency, whereas high-pressure storage tanks improve both metrics. Increased isentropic efficiency of the compressor results in enhanced roundtrip efficiency and diminished energy density.

Cetin and Zhu [110] introduced a self-condensing supercritical CO<sub>2</sub> recompression system integrated with a vortex tube. This system accomplishes CO<sub>2</sub>

condensation without a low-temperature heat sink and recompression near the critical point, enhancing both energy and exergy efficiencies. The system's performance is assessed through the principles of thermodynamics. In a base case scenario with a 100-kW power output, energy efficiency is 35.50% and exergy efficiency is 58.21%. Under optimal operating conditions, the system can deliver a power output of 129.80 kW, with maximum energy and exergy efficiencies of 41.90% and 60.89%, respectively.

Wan et al. [10] worked on a novel self-condensing transcritical CO<sub>2</sub> power cycle coupled with vortex tube. This configuration has an advantage to achieve CO<sub>2</sub> condensation without an external low-temperature heat sink. The thermodynamic and economic models of the system are developed and parametric investigation has been conducted. Results shows that energy efficiency and exergy efficiency have been improved by 1.81% and 2.41%, respectively compared to the simple regenerative sCO<sub>2</sub> power cycle system, but increases the levelized cost of electricity by 3.37%. Moreover, the high temperature recuperator has the largest exergy destruction, which should be improved first.

### 2.3.5 Other Thermodynamic Cycles based on Vortex Tube

Xu et al. [111] studied the vortex tube coupled two-stage compression refrigeration cycle for hydrogen pre-cooling application. Analysis shows that vortex tube reduces power consumption by 26.4% to 41.5% when the pressure ratio increases from 1.5 to 20, COP is improved by 30.9% to 53.8% as compared to the conventional two-stage system without vortex tube. Moreover, the vortex tube component is numerically simulated using the standard k- $\epsilon$  turbulence model.

Chen et al. [112] investigated the inclusion of vortex tube in the precooling process of hydrogen refuelling stations for high-pressure hydrogen vehicles. Two innovative precooling processes are suggested, which result in substantial reductions in operating costs and capital expenditures. The results indicate that as the pressure ratio of hydrogen in the vortex tube increases, its energy separation performance improves, leading to a reduction in the cold exit temperature during the refuelling process.

Lagrandeur et al. [113] proposed a method to heat hydrogen using vortex tubes and heat exchangers. The system segregates compressed hydrogen gas into low and high enthalpy streams, utilizing excess pressure from the hydrogen tank as the driving force. A thermodynamic model for real gas and genetic algorithm is employed to optimize the hydrogen inlet temperature for a 100-kW fuel cell electric vehicle designed for four passengers. The system can increase hydrogen feeding temperature from  $-1.6^{\circ}\text{C}$  to  $18.3^{\circ}\text{C}$ , corresponding to a heating power of 622 W for hydrogen stored at  $-30^{\circ}\text{C}$ .

### 2.3.6 Application of Vortex Tube in IC engines

Celik et al. [114] suggested employing a VT to elevate the intake air temperature in a six-cylinder, four-stroke, direct injection diesel engine. At inlet to VT, compressed air was supplied by the truck's compressed-air brake system. The hot air at exit of VT was combined with the inlet air before entering the cylinders. The implementation of VT increases the intake air temperature in cylinders, thereby diminishing the durations of engine starting-cranking, cranking-idling, and idling-stabilizing. The findings indicate that vortex tubes may enhance cold starting performance in diesel engines.

In similar research, Celik et al. [115] obtained the exhaust emission characteristics for the engine with and without VT for carbon monoxide, hydrocarbons, nitrogen oxides, and particulate matter. Results showed that use of VT increased intake air temperature, reduced engine starting-cranking, cranking-idling, and idling-stabilizing durations, and reduced fuel consumption. Moreover, CO and PM emissions decreased, but HC and NO<sub>x</sub> emissions increased. The results indicated that the utilization of VT elevates the intake air temperature, diminishes engine starting-cranking, cranking-idling, and idling-stabilizing durations, and decreases the fuel consumption. Furthermore, emissions of CO and PM diminished, whereas emissions of HC and NO<sub>x</sub> escalated.

### 2.3.7 Vortex Tube in Liquefaction Process

Qyyum et al. [116] introduced an innovative, energy-efficient, secure, and simple refrigeration cycle to enhance the efficiency of nitrogen gas liquefaction

process. The cycle incorporates a vortex tube as an expansion mechanism alongside a turbo-expander to minimize the total energy needed for liquefied natural gas (LNG) production. The energy efficiency of the proposed hybrid configuration was found to be 68.5% greater than that of prior nitrogen expander-based processes.

In a similar research, Qyyum et al. [117] worked on a novel vortex tube-based natural gas liquefaction process to enhance efficiency by using computational fluid dynamics. The process structure and conditions were modified and optimized to maximize the benefits of the vortex tube using the knowledge-based optimization technique, with total energy consumption being the objective function. The vortex tube-based LNG process showed a 20% improvement in energy efficiency compared to the conventional  $N_2$ -expander liquefaction process. The high energy efficiency is largely dependent on refrigerant cold fraction, operating conditions, and refrigerant cycle configurations.

### 2.3.8 CFD Study of Vortex Tube

Based on cold mass fraction and inlet pressure, Markal et al. [118] conducted an experimental investigation of a counter-flow vortex tube at a constant angle of the conical valve ( $45^\circ$ ) and a constant value of  $L/D$  (30), followed by a thermodynamic analysis. It was discovered that irreversibility is proportional to length of the helical vortex generator and the pressure at vortex tube's inlet and inversely proportional to cold mass fraction.

In an another study, Dincer [119] conducted experiments on three and six cascade-type VTs. It was found that the six-cascade type VT had a greater temperature difference between its cold and hot ends than other types. In a similar study, Bej [120] explored the effect of cascading VT to enhance the heating effect of hot gas. It was found that tangential shear work is the primary driving mechanism of thermal separation in a vortex tube. Moreover, Bej [121] conducted an exergy analysis of hot cascade type VT. Recently, Dutta et al. [122] conducted an experiment and three-dimensional CFD study to assess energy separation between a counterflow and uniflow vortex tube with identical geometrical and operating parameters.

Some researchers have conducted CFD study of vortex tube related to the effect of nozzle shape and aspect ratio on the performance of vortex tube based on the computational studies. Manimaran [123] performed a 3D CFD simulation, comparing rectangular and trapezoidal inlets with differing aspect ratios. The trapezoidal inlet with the highest aspect ratio demonstrated superior thermal performance in the vortex tube, achieving a total temperature increase of 315 K at the hot exit and a decrease of 276 K at the cold exit with a 40% cold gas fraction. Air served as the working fluid, with an inlet pressure of 6 bar (absolute). He determined that turbulent viscous work transfer causes temperature separation in the counter-flow vortex tube.

In another study, Manimaran [124] performed a 3D CFD simulation to illustrate energy separation in the counter-flow vortex tube. Trapezoidal inlets, ranging from one to six in number, were compared and analyzed. The maximum temperature differential recorded was 25.4 K for a single inlet utilizing air as the working fluid. He also disclosed that an increased core flow layer diameter, reduced mean pitch distance, and extended residence time were the primary factors influencing energy separation.

Mete Avci [125] conducted experimental research on the influence of nozzle aspect ratio and quantity on the performance of a vortex tube. The author determined that nozzles with lower aspect ratios exhibit superior performance compared to those with larger aspect ratios in terms of refrigeration and heating efficiency. He discovered that a singular nozzle with a reduced aspect ratio of 0.25 exhibits a maximum air temperature differential of 71.1°C at an inlet pressure of 3 bars.

Xue and Arjomandi [126] experimentally demonstrated the impact of the rotating flow angle on the performance and efficiency of the Ranque–Hilsch vortex tube. The maximum cooling efficiency recorded was 0.156, achieved with a vortex angle of 6.7° at an input pressure of 3 bars. A reduced vortex angle exhibited a greater temperature differential and enhanced heating efficiency in the vortex tube. Nonetheless, minimal vortex angles yielded enhanced cooling efficiency solely at reduced input pressure levels.

Hamdan et. al. [127] experimentally demonstrated the influence of nozzle parameters on the energy separation within the vortex tube. The optimal energy

separation was attained with a tangential nozzle orientation at angles exceeding 30°. The study indicated that the optimal number of nozzles for maximum energy separation is four.

### 2.3.9 Economic Analysis of Vortex Tube

This section introduces literature collection based on the economic analysis of vortex tube coupled with thermodynamic cycles. Wang et al. [16] examined the transcritical CO<sub>2</sub> (tCO<sub>2</sub>) Rankine cycle, which has garnered increasing attention due to its reduced irreversible losses and superior thermophysical properties of CO<sub>2</sub>. A parametric investigation revealed that a reduction in turbine inlet pressure and temperature can lower the investment cost of tCO<sub>2</sub> cycle equipment.

Acar and arslan [128] conducted an exergo-economic assessment of an innovative drying system boosted by a vortex tube. The drying system was designed and thermodynamically evaluated. Furthermore, this innovative system was examined through life cycle analysis in conjunction with net present value (NPV) from an economic perspective. The maximum NPV of the system was determined to be 23,711.88 € for the given parameters of vortex tube.

Wan et. al [10] devised a novel self-condensing tCO<sub>2</sub> power cycle employing a vortex tube, enabling CO<sub>2</sub> condensation without requiring an external low-temperature heat sink. The thermoeconomic assessment and multi-objective optimization results demonstrate that, relative to the fundamental regenerative tCO<sub>2</sub> power cycle, the self-condensing tCO<sub>2</sub> power cycle improves thermal and exergy efficiencies by 1.81% and 2.41%, respectively, while resulting in a 3.37% rise in the levelized cost of electricity.

Lopez et al. [129] examined the operation of a natural gas decompression station incorporating a first-stage preheating process utilizing a vortex tube and a geothermal heat exchanger, succeeded by a second stage featuring a water bath heater. A study on energy, exergy, and exergoeconomics has been conducted using a mathematical model. The findings indicated a reduction in station fuel consumption by utilizing merely 2% of the natural gas in the system, alongside a 15.7% decrease in the cost of decompressed natural gas.



### 2.3.10 Optimisation of Vortex Tube Integrated Refrigeration Cycle

Various researchers have applied the concept of optimisation in their study associated with vortex tube. Wang et al. [16] performed the multi-objective optimisation of novel transcritical Rankine Cycle with a vortex tube. Shahsavari et al. [130] performed the optimisation study on combined vortex tube-photovoltaic system in city gate station.

## 2.4 RESEARCH GAPS AND OBJECTIVES

### 2.4.1 Research Gaps from Literature

1. The use of HFOs such as R1234yf and new refrigerants has not been utilised in vortex tube coupled subcritical cycle.
2. The previously done work on thermodynamic investigation of vortex tube cycle is limited to narrow range of operating parameters. Therefore, study for the broader ranges of parameters is scanty available.
3. With regard to exergy analysis, variation of component-wise efficiency defects and total irreversibility have not been computed for the wide range of operating parameters, in previous studies.
4. The comprehensive research on vortex tube coupled with subcritical and transcritical refrigeration cycle based on thermodynamic and optimisation study has not been conducted.
5. The economic analysis for vortex tube coupled with subcritical and transcritical refrigeration cycle is scanty available in the open literature.
6. The previously done work on transcritical refrigeration cycle coupled with vortex tube was optimised for '1 DOF' (degree of freedom), as reported by Sarkar for refrigerant CO<sub>2</sub> [86] but analysis with '2 DOF' is scanty available in literature.
7. Environmental penalty cost analysis for vortex tube coupled with subcritical and transcritical refrigeration cycles is scanty available.
8. Structural bond analysis to find the most sensitive parameters for system performance and multi-objective optimization (MOO) using GA to obtain the optimal system parameters have not been discussed yet.

9. The flow and temperature analyses using CFD of fluid entering the vortex tube for various entry angle are limited in open literature.

#### **2.4.2 Research Objectives of Thesis**

The present research deals with vortex tube coupled with subcritical vapour compression refrigeration cycle (VTC) and vortex tube coupled with transcritical vapour compression refrigeration cycle (TVTC) based on the Keller model, addresses the aforementioned gaps which also contributes to the originality and novelty of the current research. The objectives of the present work are as follows:

1. To perform energy and exergy analysis of vortex tube integrated refrigeration cycle.
2. To carry out optimization of vortex tube integrated refrigeration cycle.
3. To conduct economic analysis of vortex tube integrated refrigeration cycle.
4. To perform CFD analysis of vortex tube.

## CHAPTER 3: ENERGY, EXERGY AND MULTI-OBJECTIVE OPTIMIZATION OF VORTEX TUBE INTEGRATED SUBCRITICAL VAPOUR COMPRESSION REFRIGERATION CYCLE

### 3.1 INTRODUCTION

The present chapter deals with thermodynamic assessment of vortex tube integrated subcritical vapour compression refrigeration cycle (VTC), followed by multi-objective optimisation, which also add novelty to the present research work. Refrigerant R1234yf has been considered for analysis in VTC and has lower flammability and toxicity [100, 131]. It has many applications in refrigeration and air conditioning [24, 27]. The objectives of this chapter are as follows:

1. A comprehensive parametric investigation employing energy and exergy principles for VTC based on the Keller model is conducted for a wide range of operating and design parameters in order to compute cooling capacity, compressor power, COP, and exergetic efficiency. The results of VTC and VCR for the refrigerant R1234yf have been compared across a wide range of evaporator temperature ( $-25^{\circ}\text{C}$  to  $5^{\circ}\text{C}$ ), condenser temperature ( $35^{\circ}\text{C}$  to  $60^{\circ}\text{C}$ ), cold mass fraction (0.5 to 0.9), effectiveness of the heat exchanger (0.2 to 1), and isentropic efficiency of the VT-nozzle (0.2 to 0.9).
2. The component-wise efficiency defects and total irreversibility are also computed for the wide range of parameters as mentioned above in point 1.
3. From the parametric analysis, the most influential parameters are selected to formulate the objective functions for multi-objective optimization using the genetic algorithm (GA) in order to determine the optimal solutions and their utility for various applications.

### 3.2 SYSTEM DESCRIPTION

Fig. 3.1 and Fig. 3.2 depict schematic and P-h diagrams, respectively of VCR and VTC based on the modified Keller model. The cycle operates at three pressure levels, i.e., the lowest pressure in the evaporator ( $P_e$ ), an intermediate pressure in VT ( $P_{int}$ ), and the highest pressure in the condenser ( $P_c$ ). At the lowest pressure, the superheated

refrigerant vapour generated in the evaporator enters the compressor (state point 1), where it undergoes irreversible adiabatic compression and leaves at high pressure as a superheated refrigerant (process 1-2). The superheated refrigerant enters the condenser, where it gets condensed at constant pressure (process 2-3).

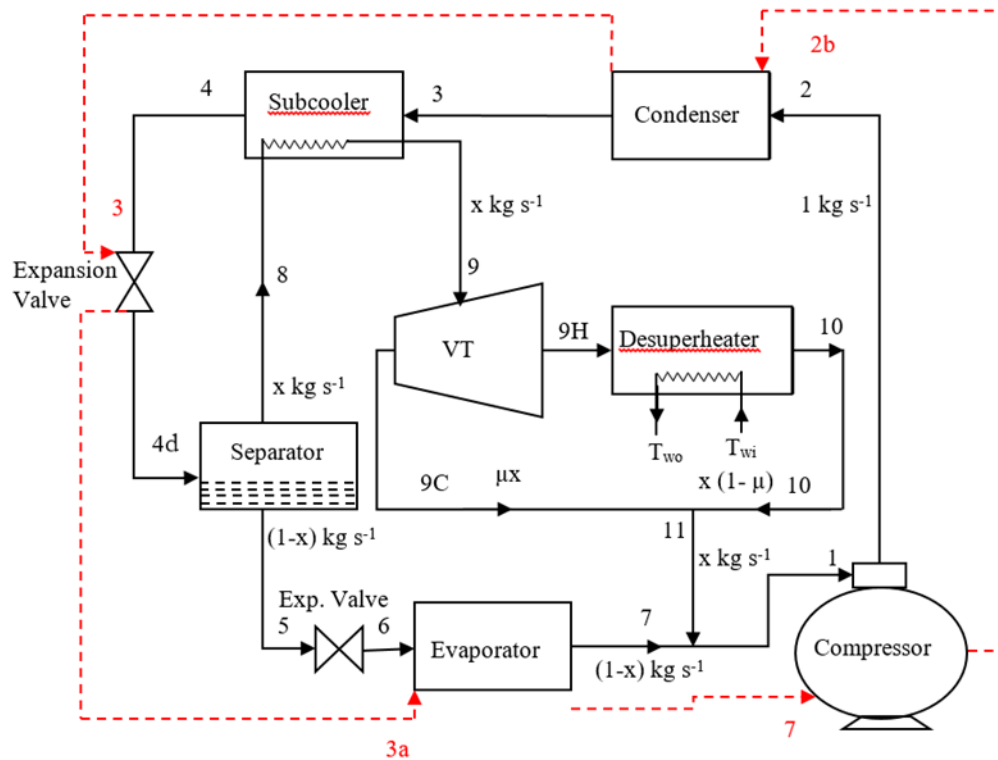


**Fig. 3.1** Block diagrams of VTC and VCR (7-2b-3-3a)

The saturated liquid refrigerant leaving the condenser is subcooled in the subcooler by saturated vapour refrigerant at low temperature leaving the separator (state point 8). For subcooling of liquid refrigerant (i.e., process 3-4) the temperature of saturated vapour refrigerant leaving the separator (state point 8) should be lower than the temperature of the refrigerant stream entering the sub-cooler (state point 3). It is achieved by throttling the subcooled refrigerant (process 4-4d) to an intermediate pressure (or intermediate temperature) and passing it through a separator where saturated liquid (state point 5) and saturated vapour (state point 8) are separated. The saturated liquid refrigerant (state 5) is throttled to evaporator pressure ( $P_e$ ) (state point 6), produces cooling effect and departs the evaporator (constant pressure process 6-7) as a saturated vapour (state point 7). The superheated vapour (state point 9) obtained

after the subcooler is expanded through the VT (process 9-9H and process 9-9C), separated into cold and hot streams. The hot stream (state point 9H) is passed through a desuperheater (at constant pressure, process 9H-10), which is utilised for heating applications. The refrigerant at state point 10 is mixed with a cold stream (state point 9C) coming out of VT. The resulting mixture (state point 11) combines with the dry saturated refrigerant (state point 7) leaves the evaporator, and goes into the compressor (state point 1).

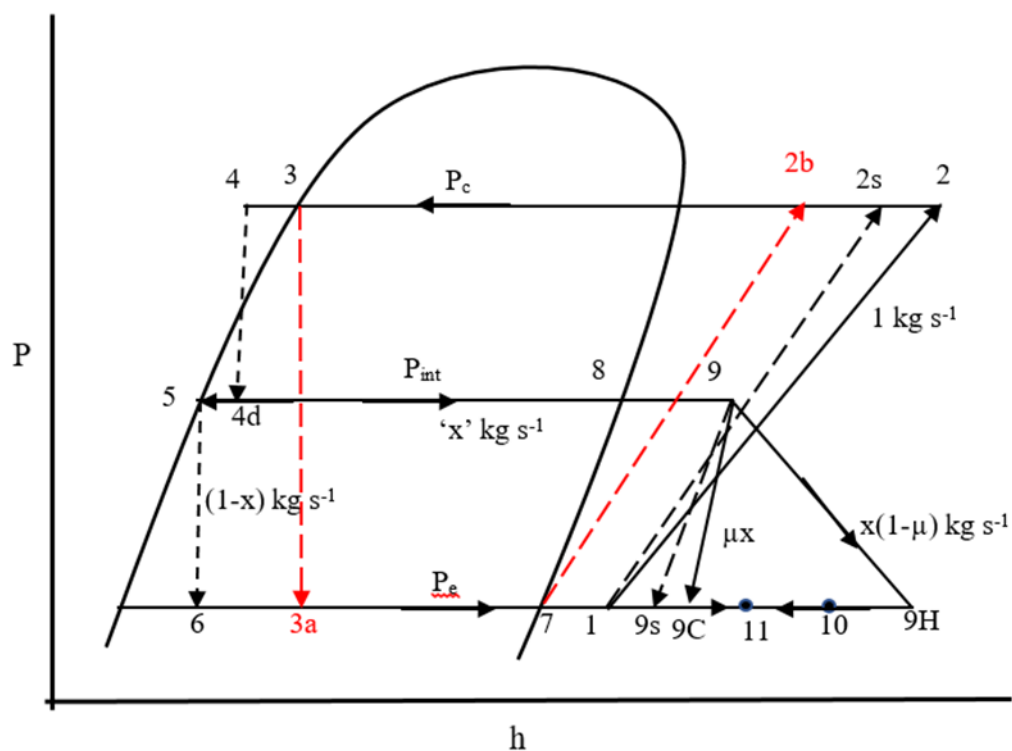


**Fig. 3.2** P-h diagram of VTC and VCR (7-2b-3-3a)

### 3.3 THERMODYNAMIC ANALYSIS AND MATHEMATICAL MODELLING OF VTC AND VCR

The mathematical modelling of VTC and VCR [86, 87] and their thermodynamic examination are presented in this section. The laws of conservation of mass, energy, and exergy balance are used to model and investigate VTC. The assumptions presented below are used for system modelling.

1. The pressure drops in connecting pipelines and heat exchangers are discarded.

2. Mixing and separation are isobaric.
3. The compression is irreversible and adiabatic.
4. The refrigerant leaving the evaporator is dry-saturated.
5. The hot and cold refrigerant streams leaving VT are assumed to be at same pressures.

### 3.3.1 Conservation of Mass

The mass flow rate of the refrigerant leaving the condenser is assumed to be  $1 \text{ kg s}^{-1}$ . Let the mass flow rate of saturated vapour refrigerant at 'state 8' be ' $x$ '  $\text{kg s}^{-1}$  and the mass flow rate of saturated liquid refrigerant expanding through the throttle valve (process 5-6) be ' $(1-x)$ '  $\text{kg s}^{-1}$ . The ratio of the mass of the cold stream to the total mass of the superheated refrigerant vapour entering the VT is called the 'cold mass fraction' and is denoted as ' $\mu$ '. The products ' $x(1-\mu)$ ' and ' $x\mu$ ' are the mass flow rates of cold and hot streams leaving the VT in  $\text{kg s}^{-1}$  (refer to Fig. 3.1). The Eqs. (3.1) to (3.4) are related to mass conservation for VTC.

The conservation of mass at the separator is given by Eq. (3.1).

$$\dot{m}_{4d} = \dot{m}_8 + \dot{m}_5 \quad (3.1)$$

The superheated vapour (state point 9) is expanded through the VT, where it is separated into cold (state point 9C) and hot (state point 9H) streams. The conservation of mass across the VT is given by Eq. (3.2).

$$\dot{m}_9 = \dot{m}_{9H} + \dot{m}_{9C} \quad (3.2)$$

The refrigerant at state 10 mixes with the cold stream (state point 9C) and leaves at state point 11. The conservation of mass at state 11 is given by Eq. (3.3).

$$\dot{m}_{11} = \dot{m}_{9C} + \dot{m}_{10} \quad (3.3)$$

The refrigerant at state 11 is combined with the saturated vapour refrigerant at the evaporator outlet (state 7) and goes into the compressor. The conservation of mass at state 1 is presented by Eq. (3.4).

$$\dot{m}_1 = \dot{m}_7 + \dot{m}_{11} \quad (3.4)$$

### 3.3.2 Energy Analysis

#### 3.3.2.1 Energy analysis of VTC

The equations (3.5) to (3.16) are used for the energy analysis:

The temperature of the refrigerant at the entry of VT is given by Eq. (3.5).

$$T_9 = T_8 + \varepsilon_{sc}(T_3 - T_8) \quad (3.5)$$

Energy balance across the subcooler is given by Eq. (3.6).

$$h_3 - h_4 = x(h_9 - h_8) \quad (3.6)$$

The energy balance across the separator is specified by Eq. (3.7).

$$h_{4d} = h_5(1 - x) + xh_8 \quad (3.7)$$

The isentropic efficiency of the VT-nozzle is defined as the ratio of the actual expansion of refrigerant vapour ( $h_9 - h_{9C}$ ) to the isentropic expansion of refrigerant vapour ( $h_9 - h_{9s}$ ) at the cold outlet. Therefore, the enthalpy of the cold stream coming of the cold end of VT is given by Eq. (3.8).

$$h_{9C} = h_9 - \eta_v(h_9 - h_{9s}) \quad (3.8)$$

Here, state 9s represent isentropic expansion in the VT-nozzle.

Energy balance across the vortex tube is given by Eq. (3.9).

$$h_9 = \mu h_{9C} + (1 - \mu)h_{9H} \quad (3.9)$$

In the desuperheater, the hot stream coming out of VT (at temperature  $T_{9H}$ ) is cooled by the external water (at temperature  $T_{wi}$ ) up to temperature  $T_{10}$ . The effectiveness of desuperheater ( $\varepsilon_{ds}$ ) is defined as the ratio of cooling of refrigerant (process 9H-10) to the maximum heat exchange between two streams. Hence, the temperature at the exit of the desuperheater is calculated using Eq. (3.10).

$$T_{10} = T_{9H} - \varepsilon_{ds}(T_{9H} - T_{wi}) \quad (3.10)$$

The enthalpy at state point 11 is calculated by applying energy balance to mixing of streams 9C and 10 (Eq. (3.11)).

$$h_{11} = \mu h_{9C} + (1 - \mu)h_{10} \quad (3.11)$$

The enthalpy at the inlet to the compressor at state point 1 is obtained by applying energy balance to mixing of streams at state points 7 and 11 (refer to Eq. (3.12)).

$$h_1 = (1 - x)h_7 + xh_{11} \quad (3.12)$$

The cooling capacity for the evaporator of VTC is presented using Eq. (3.13).

$$Q_{vtc} = (1 - x)(h_7 - h_6) \quad (3.13)$$

The isentropic efficiency of the compressor ( $\eta_{comp}$ ) is defined as the ratio of ideal compression work ( $h_{2s} - h_1$ ) to the actual compression work ( $h_2 - h_1$ ). So, enthalpy at state point 2 is given by Eq. (3.14).

$$h_2 = \frac{h_{2s} - h_1}{\eta_{comp}} + h_1 \quad (3.14)$$

Here, state point 2s is the state assuming isentropic compression in the compressor of VTC.

Compressor work (power) for VTC is calculated as given below:

$$W_{vtc} = \dot{m}_1(h_2 - h_1) \quad (3.15)$$

COP for VTC cycle is calculated using Eq. (3.16).

$$COP_{vtc} = \frac{Q_{vtc}}{W_{vtc}} \quad (3.16)$$

### 3.3.2.2 Energy Analysis of VCR

The cooling capacity for the evaporator of VCR is calculated using Eq. (3.17).

$$Q_{vcr} = \dot{m}_7(h_7 - h_{3a}) \quad (3.17)$$



The isentropic efficiency of the compressor of VCR is given by Eq. (3.18).

$$\eta_{comp,vcr} = \frac{h_{2bs} - h_7}{h_{2b} - h_7} \quad (3.18)$$

Here,  $h_{2bs}$ =specific enthalpy at the outlet of the compressor of VCR after isentropic compression. ‘State 2bs’ is not shown in Fig. 3.2

Compressor power for VCR is given by Eq. (3.19).

$$W_{vcr} = \dot{m}_7(h_{2b} - h_7) \quad (3.19)$$

COP for VCR cycle is represented by Eq. (3.20).

$$COP_{vcr} = \frac{Q_{vcr}}{W_{vcr}} \quad (3.20)$$

COP improvement of VTC over VCR is calculated using Eq. (3.21).

$$COP_{imp} = \frac{(COP_{vtc} - COP_{vcr})}{COP_{vcr}} \quad (3.21)$$

### 3.3.3 Exergy Analysis

#### 3.3.3.1 Exergy Analysis of VTC

The exergy balance equation has been employed for each component of VTC, establishing the following relations for computing component-level irreversibility:

Irreversibility in compressor

$$I_{comp,vtc} = T_o(s_2 - s_1) \quad (3.22)$$

Irreversibility in condenser

$$I_{c,vtc} = (h_2 - h_3) - T_o(s_2 - s_3) \quad (3.23)$$

Irreversibility in evaporator

$$I_{e,vtc} = (1 - x)T_o \left[ (s_7 - s_6) - \left( \frac{h_7 - h_6}{T_r} \right) \right] \quad (3.24)$$

Irreversibility in VT

$$I_{vt,vtc} = T_o x [\mu s_{9C} + (1 - \mu) s_{9H} - s_9] \quad (3.25)$$

Irreversibility in desuperheater,

$$I_{ds,vtc} = x(1 - \mu)[(h_{9H} - h_{10}) - T_o(s_{9H} - s_{10})] \quad (3.26)$$

Irreversibility in subcooler

$$I_{sc,vtc} = (h_3 - h_4) + x(h_8 - h_9) - T_o(s_3 - s_4) - T_o x(s_8 - s_9) \quad (3.27)$$

Irreversibility in the throttle valve

$$I_{th,vtc} = T_o[(1 - x)(s_6 - s_5) + (s_{4d} - s_4)] \quad (3.28)$$

The irreversibility in the separator due to separation is given as:

$$I_{s,vtc} = T_o[xs_8 + (1 - x)s_5 - s_{4d}] \quad (3.29)$$

Various streams at state points 9C, 10, and 7 mix with each other, resulting in a stream at the inlet of the compressor (state 1). Irreversibility due to the mixing of streams is given as

$$I_{mx,vtc} = T_o[s_1 - (1 - x)s_7 - \mu x s_{9C} - x(1 - \mu)s_{10}] \quad (3.30)$$

Total irreversibility for VTC is given as

$$\sum I_{vtc} = I_{comp,vtc} + I_{c,vtc} + I_{e,vtc} + I_{vt,vtc} + I_{ds,vtc} + I_{sc,vtc} + I_{th,vtc} + I_{mx,vtc} + I_{s,vtc} \quad (3.31)$$

For VTC, the exergy balance equation is given as:

$$W_{vtc} = Q_{vtc} \left( \frac{T_o}{T_r} - 1 \right) + \sum I_{vtc} \quad (3.32)$$

The term  $Q_{vtc} \left( \frac{T_o}{T_r} - 1 \right)$  is also known as exergy of product (EP) and compressor power is also termed as exergy of fuel (EF).

For VTC, exergetic efficiency is calculated by Eq. (3.33).

$$\eta_{ex,vtc} = \frac{W_{vtc} - \sum I_{vtc}}{W_{vtc}} = 1 - \frac{\sum I_{vtc}}{W_{vtc}} = \frac{Q_{vtc}}{W_{vtc}} \left( \frac{T_o}{T_r} - 1 \right) \quad (3.33)$$

### 3.3.3.2 Exergy Analysis of VCR

The second law of thermodynamics is employed for every component of VCR (7-2b-3-3a), establishing irreversibility relations for cycle components.

Irreversibility in compressor

$$I_{comp,vcr} = T_o(s_{2b} - s_7) \quad (3.34)$$

Irreversibility in condenser

$$I_{c,vcr} = (h_{2b} - h_3) - T_o(s_{2b} - s_3) \quad (3.35)$$

Irreversibility in evaporator

$$I_{e,vcr} = T_o \left[ (s_7 - s_{3a}) - \left( \frac{h_7 - h_{3a}}{T_r} \right) \right] \quad (3.36)$$

Irreversibility in the throttle valve

$$I_{th,vcr} = T_o(s_{3a} - s_3) \quad (3.37)$$

For the VCR, exergetic efficiency is calculated using Eq. (3.38)

$$\eta_{ex,vcr} = \frac{Q_{vcr}}{W_{vcr}} \left( \frac{T_o}{T_r} - 1 \right) \quad (3.38)$$

### 3.3.4 Efficiency Defect for VTC and VCR

Efficiency defect is the ratio of irreversibility or exergy destroyed in component 'j' and the compressor work [132], and is expressed by Eq. (3.39). If both parameters increase and irreversibility increases at a faster rate, the efficiency defect will increase, and vice versa. Similarly, if both parameters decrease and compressor work decreases at a faster rate, the efficiency defect will increase, and vice versa.

$$\delta_j = \frac{I_j}{W} \quad (3.39)$$

The relation between the efficiency defect and the exergetic efficiency of the system is given by Eq. (3.40).

$$\eta_{ex} = 1 - \sum \delta_j \quad (3.40)$$

A computational algorithm based on the present model described in ‘section 3’ is created in the Engineering Equation Solver (EES) software [133] for the parametric study of these cycles (VTC and VCR). Initially, the system performance is optimized to have the maximum COP of VTC using EES software, with the only variable being the intermediate pressure. The EES software offers a variety of optimization procedures. If there is only one degree of freedom, the EES software can calculate a variable's maximum or minimum value using ‘quadratic approximation’ or ‘golden section search’ methods [134]. The quadratic approximation method is generally faster, whereas the golden section search method is more consistent. Therefore, the golden section search method is utilised to determine the optimal intermediate pressure value.

### 3.4 RESULTS AND DISCUSSION

#### 3.4.1 Model Validation

In order to guarantee the accuracy of the developed code based on the mathematical model, the verification of COP for VTC is presented here. The developed computational code is utilised to the compute results corresponding to data given in Sarkar [135] for VTC with isobutane. Sarkar's research used the following input parameters: heat exchanger effectiveness = 85%, isentropic efficiency of VT-nozzle = 80%, isentropic efficiency of compressor = 75%, cold mass fraction = 0.7, and water inlet temperature = 300 K. The results reported by Sarkar [135] have been compared with those obtained using the present model. It is observed that the results obtained from the present work lie within -1.35% to -1.61% of the results reported by Sarkar [135], as shown in Table 3.1.

**Table 3.1** Comparison of results of present work with that of Sarkar

$T_e$ (°C)	$COP_{vtc,m}$ (Present work)	$COP_{vtc,m}$ [135]	Change in COP
-10	2.78	2.82	-1.41%
0	3.65	3.71	-1.61%
10	5.08	5.15	-1.35%

The data presented in Table 3.2 shows the input parameters for the computation of present results.

**Table 3.2** Base values and range of Input Parameters for VTC

S.No.	Input Parameters	Base Value	Range of Input Parameters [87, 89, 90, 132, 136]
1.	Cold mass fraction ( $\mu$ )	0.6	0.5 to 0.9
2.	Compressor isentropic efficiency ( $\eta_{comp}$ )	0.75	0.7 to 0.95
3.	Evaporator Temperature ( $T_e$ )	-25°C	-25° C to 5°C
4.	Condenser Temperature ( $T_c$ )	50°C	35°C to 60°C
5.	Ambient Temperature ( $T_o$ )	25°C	-
6.	Ambient Pressure ( $P_o$ )	101.325 kPa	-
7.	Refrigerated Space Temperature ( $T_r$ )	-15°C	-15°C to 15°C
8.	VT-nozzle isentropic efficiency ( $\eta_v$ )	0.8	0.2 to 1
9.	Effectiveness of subcooler ( $\varepsilon_{sc}$ )	0.85	0.5 to 1
10.	Effectiveness of desuperheater ( $\varepsilon_{ds}$ )	0.85	0.5 to 1
11.	Water inlet Temperature ( $T_{wi}$ )	25° C	-
12.	Mass flow rate ( $\dot{m}$ ) of refrigerant R1234yf	1 kg s <sup>-1</sup>	-

### 3.4.2 Results based on Energy Analysis

In this section, the effect of various operating parameters ( $T_e$ ,  $T_c$ ) and design parameters ( $\mu$ ,  $\varepsilon_{ds}$ ,  $\varepsilon_{sc}$ ,  $\eta_v$ ) have been studied on the cooling capacity, compressor power, and COP of both VTC and VCR.

Fig. 3.3 exhibits variation of  $COP_{vtc}$  and intermediate pressure ( $P_{int}$ ) with intermediate temperature ( $T_{int}$ ). As  $T_{int}$  increases,  $COP_{vtc}$  rises marginally up to a specific value of  $T_{int} = -20.05^\circ\text{C}$  and then decreases with a further increase in  $T_{int}$ .  $COP_{vtc}$  has a maximum value of 1.591 at  $T_{int} = -20.05^\circ\text{C}$  and the corresponding value of  $P_{int}$  is 150.7 kPa. The values of intermediate temperature and pressure corresponding to which  $COP_{vtc}$  is maximum are designated as optimum intermediate temperature ( $T_{int,opt}$ ) and pressure ( $P_{int,opt}$ ). With the variation of  $T_{int}$ , reduction in

$COP_{vtc}$  is observed to vary between 0.5% and 14.39% with respect to the maximum value of  $COP_{vtc}$ .

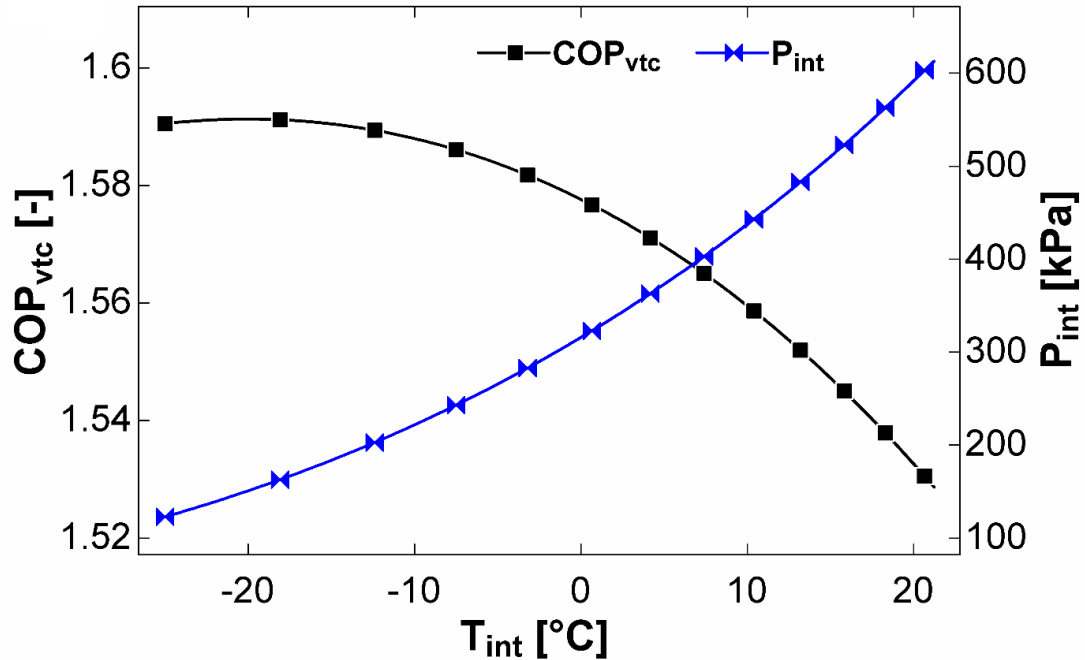


**Fig. 3.3** Effect of intermediate temperature on COP of VTC and intermediate pressure

In this study, computed values of COP presented in Fig. 3.3 and Fig. 3.4 are ‘maximum COP’ ( $COP_{vtc,m}$ ) that correspond to the optimum intermediate temperature ( $T_{int,opt}$ ) and pressure ( $P_{int,opt}$ ), and the same is computed using a single variable optimization method, i.e., the Golden Section Search Method [134].

Fig. 3.4 depicts the variation in cooling capacity, compressor power, and  $COP_{vtc,m}$  with  $T_e$  for VCR and VTC (corresponding to  $T_{int,opt}$  and  $P_{int,opt}$ ). The cooling capacity for VTC is 30.53% higher at  $T_e = -25^\circ\text{C}$  and 13.19% higher at  $T_e = 5^\circ\text{C}$  than that of VCR. This can be explained as, in case of VTC (refer to Fig. 3.1), the saturated liquid (state 5) and saturated vapour (state 8) are separated in the separator. The saturated vapour (at  $T_8$ ) is used to subcool the saturated liquid (at  $T_3$ ) in the subcooler. The saturated liquid (state 5) is further expanded in the expansion device and leaves it at a lower dryness fraction (state 6) than that obtained in VCR after expansion (state 3a) (refer to Fig. 3.2).

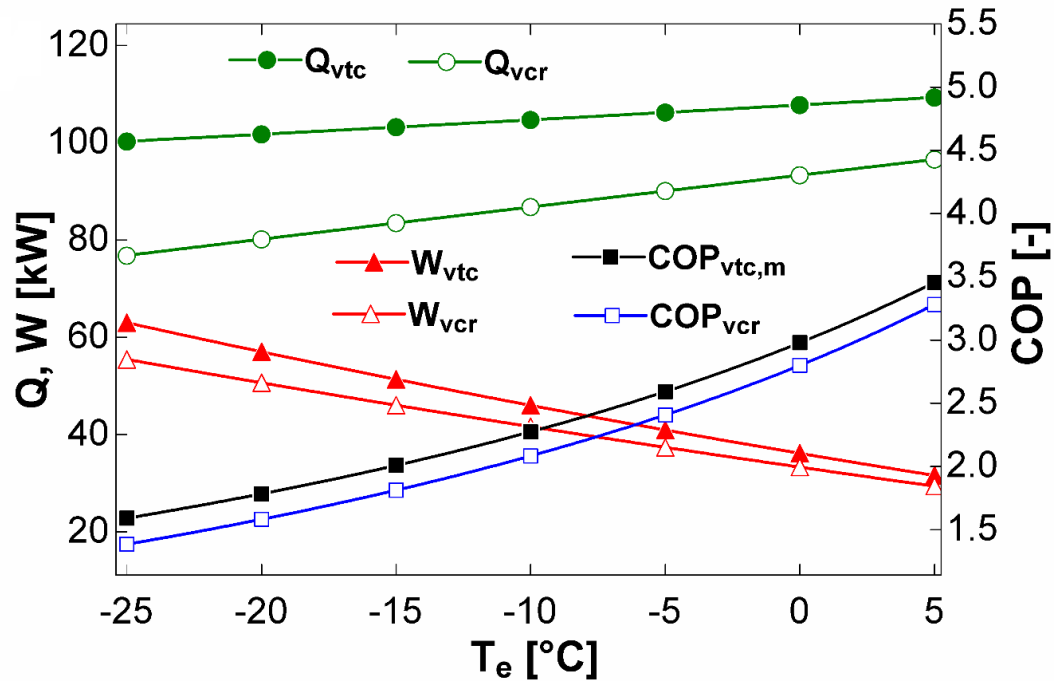


**Fig. 3.4** Effect of evaporator temperature on cooling capacity, compression power, and COP for VCR and VTC

The lower dryness fraction means that refrigerant has a greater mass of liquid than vapour, in the two-phase region (refer to Fig. 3.2). It is a well-known fact that the greater the amount of liquid refrigerant entering the evaporator, the greater the amount of heat absorbed by the evaporator until the liquid transforms into vapour. Therefore, these two factors, i.e., subcooling of refrigerant in the subcooler and a lower value of dryness fraction at the entry to the evaporator, are the primary reasons for the higher value of cooling capacity in VTC. Moreover, as  $T_e$  increases, cooling capacity increases for both cycles. This can be explained as follows: As  $T_e$  rises, the quality or value of dryness fraction of refrigerant at the evaporator's entry shifts toward the saturated liquid line, i.e., the dryness fraction reduces. As a result, the mass of liquid refrigerant increases, and thus the cooling capacity increases.

Fig. 3.4 shows that the compressor power for VTC is 13.59% higher at  $T_e = -25^\circ\text{C}$  and 7.51% higher at  $T_e = 5^\circ\text{C}$  than that of VCR. It is also observed that with an increase in  $T_e$ , compressor power is observed to reduce for both cycles. This can be explained by the fact that the compressor power is directly proportional to both pressure ratio and compressor inlet temperature. The compressor power required for

given pressure ratio in VTC is higher than that required in VCR since the refrigerant entering the compressor in VTC (state point 1) is in superheated state and the refrigerant entering the compressor in VCR (state point 7) is in saturated vapour state. Moreover, as the  $T_e$  increases, the pressure ratio across the compressor decreases, resulting in a reduction in compressor power for both VTC and VCR. The variation of  $COP_{vtc,m}$  with  $T_e$  is also depicted in Fig. 3.4. Since cooling capacity is increasing and compressor power is reducing with the increase in  $T_e$ , hence  $COP_{vtc,m}$  and  $COP_{vcr}$  increase. The  $COP_{vtc,m}$  is 14.87% and 5.3% higher than  $COP_{vcr}$  at  $-25^\circ\text{C}$  and  $5^\circ\text{C}$  evaporator temperatures, respectively.

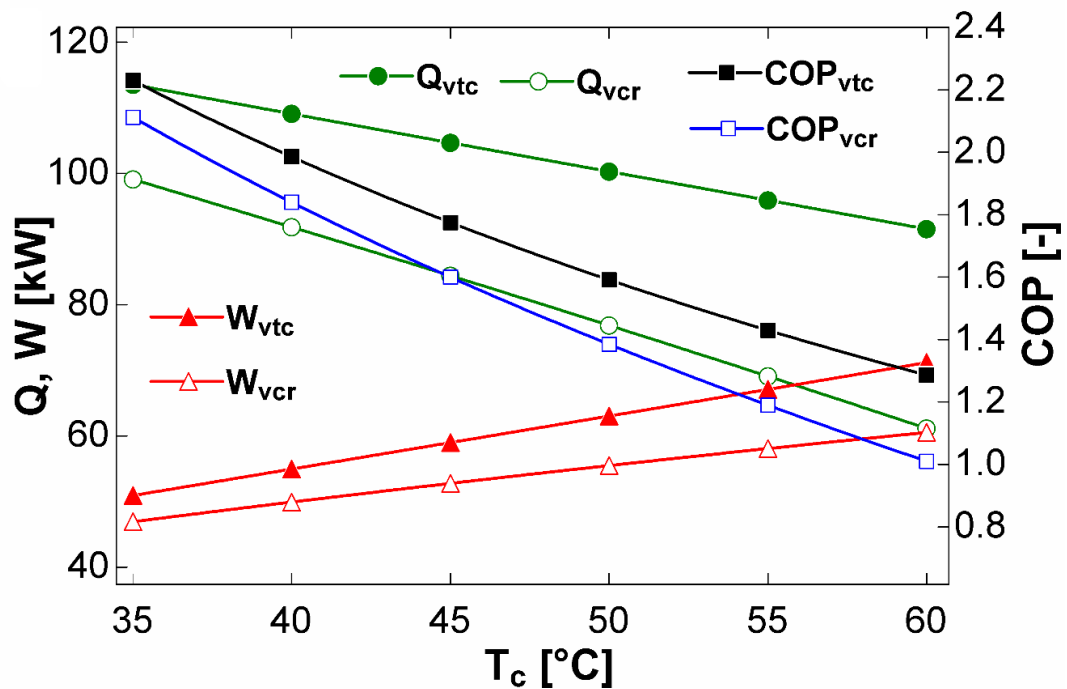


**Fig. 3.5** Effect of condenser temperature on cooling capacity, compression power, and COP for VCR and VTC

Fig. 3.5 shows the variation in cooling capacity, compressor power, and COP with condenser temperature ( $T_c$ ) for VCR and VTC (corresponding to  $T_{int,opt}$  and  $P_{int,opt}$ ). The cooling capacity for VTC is 14.53% higher at  $T_c=35^\circ\text{C}$  and 49.73% higher at  $T_c=60^\circ\text{C}$  than that of VCR. This demonstrates that an increase in condenser temperature has a significant impact on VTC's cooling capacity compared to VCR. The cooling capacity decreases with an increase in condenser temperature for both cycles. This trend can be explained as follows: With increase in  $T_c$ , it is observed that



the entry point to evaporator (state 6) shifts towards a higher value of dryness fraction. This reduces the mass of liquid refrigerant at entry to evaporator after expansion, thereby decreasing cooling capacity for VTC. Also, similar reasoning holds good for VCR. The reason why VTC has a greater cooling capacity than VCR with variation of  $T_c$  is similar to the explanation given for Fig. 3.4 in preceding paragraph. The compressor power required in VTC is higher than that of VCR, and with an increase in  $T_c$ , it is observed to increase for both cycles. The compressor power for VTC is 8.5% to 17.6% higher than that of VCR. The explanation for this trend is similar to that of Fig. 3.4, as mentioned in the earlier paragraph. The variation of  $COP_{vtc,m}$  with  $T_c$  is also depicted in Fig. 3.5. As  $T_c$  increases, both  $COP_{vtc,m}$  and  $COP_{vcr}$  decrease because cooling capacity decreases and compressor power increases. However, the reduction in  $COP_{vtc,m}$  per unit increase in  $T_c$  is lower with respect to VCR. The  $COP_{vtc,m}$  is 5.59% to 27.32% higher than  $COP_{vcr}$  at 35°C and 60°C condenser temperatures, respectively. Thus, the use of a vortex tube in the cycle enhances the performance in terms of cooling capacity and COP.

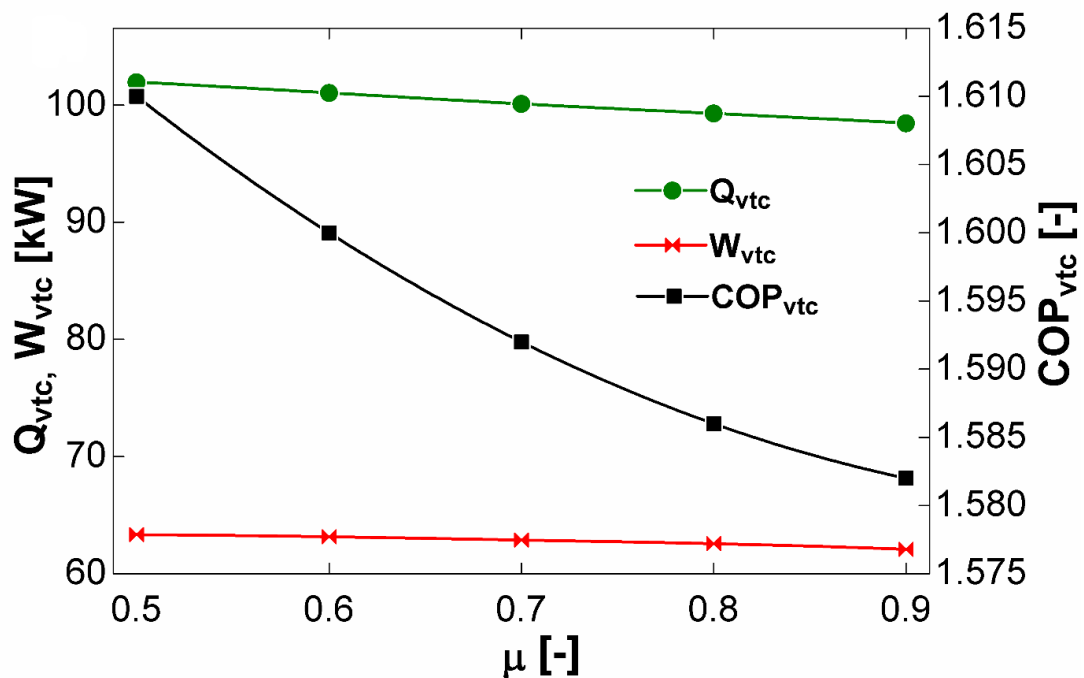


**Fig. 3.6** Effect of cold mass fraction on cooling capacity, compressor power and maximum COP of VTC

Fig. 3.6 shows the variation in the cooling capacity ( $Q_{vtc}$ ), compressor power ( $W_{vtc}$ ) and  $COP_{vtc,m}$  with  $\mu$ . The cold mass fraction ( $\mu$ ), which is the ratio of mass flow rate of cold streams to mass flow rate of inlet stream to VT, has a significant effect on hot and cold stream temperatures. As  $\mu$  increases, the temperature of cold stream ( $T_{9C}$ ) decreases and the temperature of hot stream ( $T_{9H}$ ) increases; consequently, the temperature difference between two streams ( $\Delta T_{vt}$ ) increases. This explanation is also supported by Markal's [118] research. Moreover, as the inlet pressure to VT increases,  $\Delta T_{vt}$  increases due to an enhanced energy separation phenomenon within the VT [99, 137]. Based on the analysis, it is observed that as  $\mu$  increases,  $P_{int,opt}$  increases and hence  $T_{int,opt}$  increases, being the saturation temperature corresponding to  $P_{int,opt}$ . The increase in  $T_{int,opt}$  (i.e.,  $T_5$  or  $T_8$ ) causes an increase in enthalpy of the saturated liquid refrigerant leaving the separator ( $h_5$  or  $h_6$ ). The mass flow rate of saturated vapour refrigerant ( $\dot{m}_8$ ) is observed to decrease, while the mass flow rate of saturated liquid leaving the separator ( $\dot{m}_5$ ) increases. The increase in  $h_6$  diminishes the specific refrigerant effect, which dominates the increase in mass flow rate entering the evaporator ( $\dot{m}_6$ ), resulting in a decline in cooling capacity. Further, the percentage variation in specific refrigerating effect and mass flow rate of refrigerant entering the evaporator is negligible; consequently, the decrease in  $Q_{vtc}$  is less than 3%.

As stated previously, with increase in  $\mu$ , the temperature of cold stream ( $T_{9C}$ ) decreases, resulting in a decrease in the refrigerant temperature at the compressor's inlet. Since the pressure ratio across the compressor is constant (for this particular case), it results in reduction in  $W_{vtc}$ . Thus, with an increase in value of  $\mu$ , both  $Q_{vtc}$  and  $W_{vtc}$  decrease. However, the relative reduction in  $W_{vtc}$  is smaller than reduction in  $Q_{vtc}$ . Consequently, COP decreases as  $\mu$  increases.

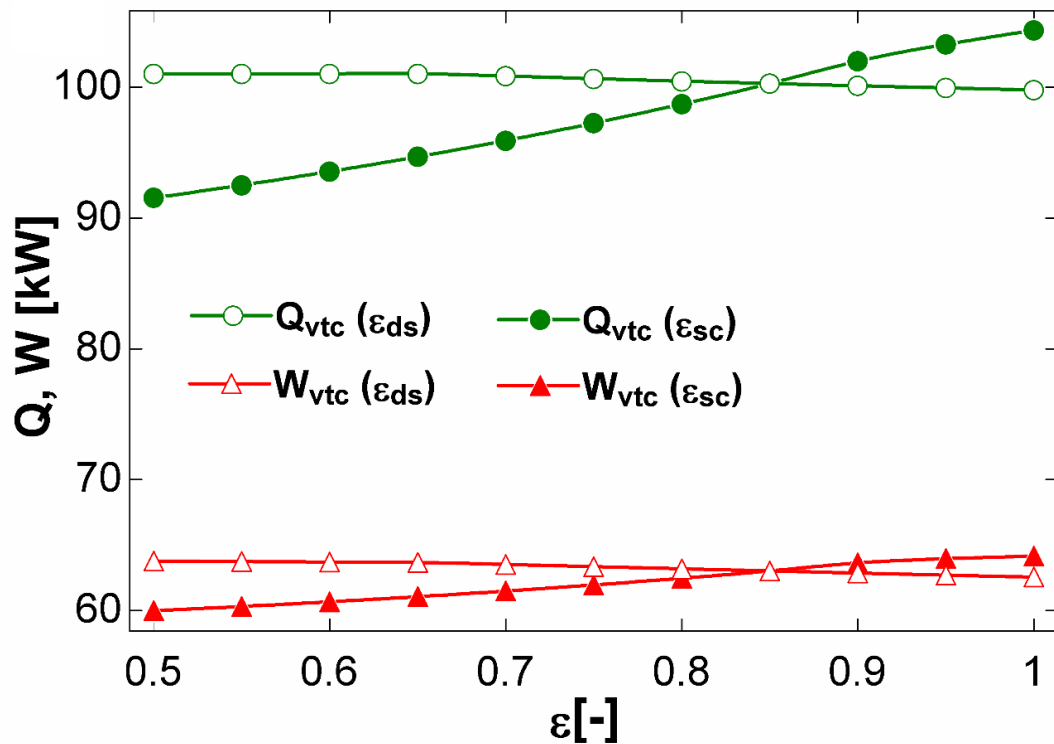


**Fig. 3.7** Effect of effectiveness of subcooler and desuperheater on cooling capacity and compressor power of VTC

Fig. 3.7 depicts the variation of  $Q_{vtc}$  and  $W_{vtc}$  with effectiveness of subcooler ( $\epsilon_{sc}$ ) and desuperheater ( $\epsilon_{ds}$ ) respectively. Both  $Q_{vtc}$  and  $W_{vtc}$  increase with increasing  $\epsilon_{sc}$  and decrease with increasing  $\epsilon_{ds}$ . This trend can be explained as follows: As  $\epsilon_{sc}$  increases, so does the degree of subcooling, leading to a decrease in both the enthalpy ( $h_6$ ) and mass flow rate of refrigerant entering the evaporator ( $\dot{m}_6$ ). The net effect of these two factors is to increase in both specific refrigerating effect and  $Q_{vtc}$ . Moreover, with an increase in  $\epsilon_{sc}$ , the temperature at entry to VT increases, resulting in an increase in the temperature of both hot and cold streams, which in turn leads to an increase in the temperature at entry to the compressor; consequently,  $W_{vtc}$  increases. As  $\epsilon_{ds}$  increases, the rate of heat exchange increases between the hot stream leaving the VT and cooling fluid entering the desuperheater. This increased rate of heat exchange is responsible for a higher reduction in the hot stream temperature of VT ( $T_{10}$ ) at the outlet of the desuperheater. This leads to decrease in the refrigerant temperature at entry to the compressor ( $T_1$ ), and as a result  $W_{vtc}$  decreases being the

direct function of  $T_1$ . Also, variation in  $\epsilon_{ds}$  indirectly affect the  $Q_{vtc}$ . As  $\epsilon_{ds}$  increases,  $P_{int,opt}$  and hence  $T_{int,opt}$  are observed to increase. It results in increase in both the enthalpy ( $h_6$ ) and mass flow rate of refrigerant entering the evaporator. However, it is observed that the net effect of these two factors is to diminish both the specific refrigerating effect and the  $Q_{vtc}$ .

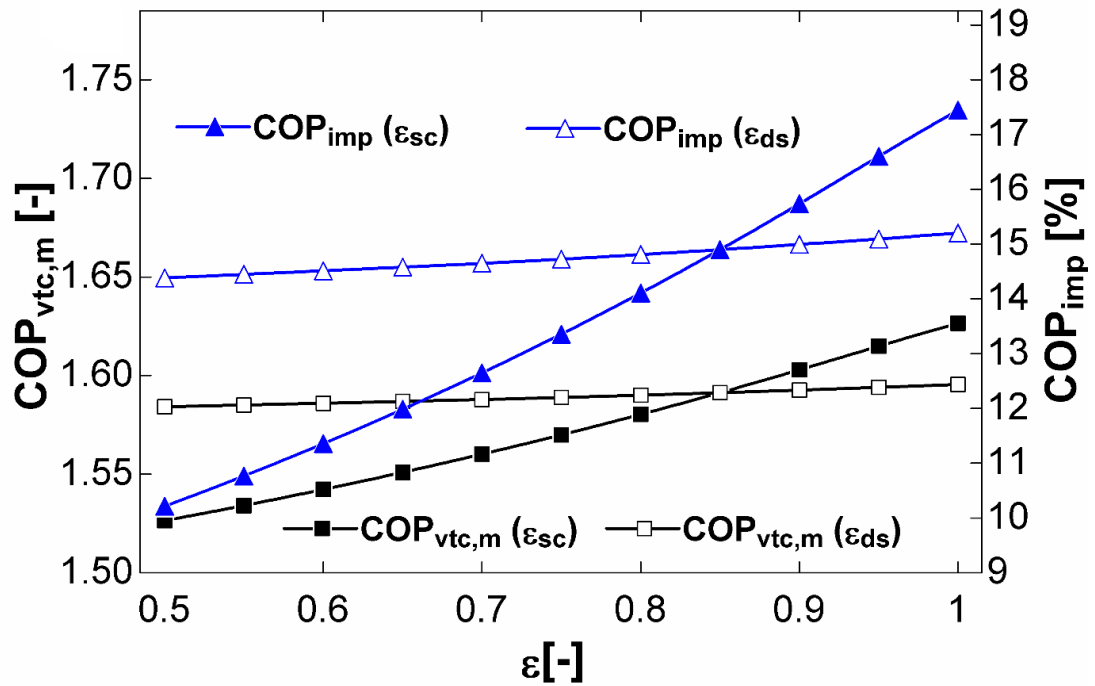


**Fig. 3.8** Effect of effectiveness of subcooler and desuperheater on COP of VTC and its improvement over VCR

Fig. 3.8 depicts the variation of  $COP_{vtc,m}$  and  $COP_{imp}$  with  $\epsilon_{sc}$  and  $\epsilon_{ds}$ . It can be observed that effect of increase in  $\epsilon_{sc}$  is more than that of  $\epsilon_{ds}$  as the relative increase in  $COP_{vtc,m}$  is more in the former case. It is shown in Fig. 3.8 that both cooling capacity and compressor power increase with an increase in  $\epsilon_{sc}$ . However, the rate of increase in cooling capacity dominates the rate of increase in compressor power. As a result,  $COP_{vtc,m}$  increases with increase in  $\epsilon_{sc}$ . On the contrary, with increase in  $\epsilon_{ds}$ , both  $Q_{vtc}$  and  $W_{vtc}$  decrease. However,  $COP_{vtc,m}$  increases as the relative decrease in  $W_{vtc}$  is observed to be higher than the decrease in  $Q_{vtc}$ .

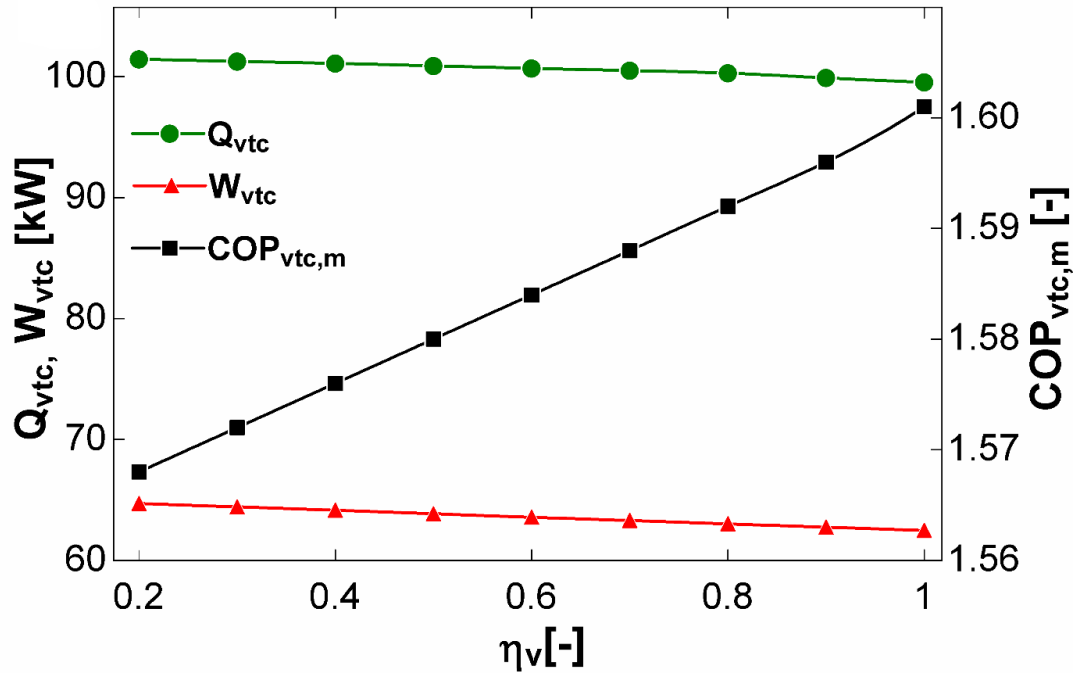


**Fig. 3.9** Effect of VT-nozzle efficiency on cooling capacity and compressor power of VTC

Fig. 3.9 demonstrates that as isentropic efficiency of the VT-nozzle ( $\eta_v$ ) increases, both cooling capacity and compressor power decrease while  $COP_{vtc,m}$  increases. This is so because as  $\eta_v$  increases, the cold stream temperature ( $T_{9c}$ ) decreases. This decreases  $T_1$  and consequently,  $W_{vtc}$  decreases (for a given pressure ratio). The variation of  $\eta_v$  indirectly affects the  $Q_{vtc}$  of the evaporator due to changes in  $P_{int,opt}$ . As  $\eta_v$  increases,  $P_{int,opt}$  increases, resulting in an increase in mass flow rate at entry to evaporator ( $\dot{m}_6$ ) and decrease in specific refrigerant effect. However, the  $Q_{vtc}$  has been observed to decrease. Furthermore, with increase in  $\eta_v$ ,  $COP_{vtc,m}$  increases because  $W_{vtc}$  decreases at a faster rate than  $Q_{vtc}$ .

Based on the results presented above, it is observed that the evaporator and condenser temperatures play a significant role in affecting the cooling capacity, compressor work and COP of VTC in comparison to other parameters.

### 3.4.3 Results based on Exergy Analysis

In this section, the effect of various operating parameters ( $T_e$ ,  $T_c$ ) and design parameters ( $\mu$ ,  $\eta_c$ ) on the exergetic efficiency, total irreversibility, and efficiency defect are examined. Table 3.3 illustrates the effect of  $T_e$  on efficiency defects in various

components of VCR. The compressor, condenser, and throttle valve are the primary contributors to the efficiency defect. Furthermore, the throttle valve and condenser have maximum efficiency defect of 30.56% at  $T_e = -25^\circ\text{C}$  and 33.39% at  $T_e = 5^\circ\text{C}$ , respectively.

**Table 3.3** Effect of evaporator temperature on efficiency defect in various components of VCR

$T_e(^{\circ}\text{C})$	$\delta_{comp}(\%)$	$\delta_c(\%)$	$\delta_e(\%)$	$\delta_{th}(\%)$
-25	22.84	18.78	6.35	30.56
-20	22.88	20.27	6.97	28.82
-15	22.92	22.03	7.69	27.08
-10	22.95	24.11	8.51	25.34
-5	22.97	26.61	9.48	23.62
0	22.98	29.65	10.63	21.90
5	23.00	33.39	12.03	20.20

The variation of efficiency defect in various components of VTC with  $T_e$  is depicted in Fig. 3.10. The condenser exhibits the highest efficiency defect among all the components (35.37%), followed by the compressor (22.3%) at a temperature of  $T_e = 5^\circ\text{C}$ . With the increase in  $T_e$  the efficiency defect of VT decreases from 6.5% to 1.2%. Moreover, the variation of the efficiency defect at various mixing points, the subcooler, and the desuperheater is insignificant. It is noticed that the total efficiency defect of all expansion devices in VTC is 20.31% to 12.81% lower than that of VCR (refer to Table 3.3). This shows the efficacy of VT.

As the evaporator temperature rises, the irreversibility of the compressor, condenser, evaporator, throttle valve, and VT decreases. As  $T_e$  increases, the pressure ratio across the compressor decreases, resulting in a decrease in compressor work and a decrease in the outlet temperature of compressor. It is evident that the lower the discharge temperature, the lower the entropy generation (for a particular value of compressor efficiency) and the lower the irreversibility or exergy destruction in the compressor. The expansion pressure ratio (EPR) determines the magnitude of frictional losses or irreversibility in the throttle valve, i.e., frictional losses increase with an increase in EPR and vice versa. With increase in  $T_e$ , the EPR decreases, leading

to a reduction in frictional losses or irreversibility in the throttle valves. With an increase in  $T_e$ , the cooling capacity increases while the compressor power decreases. However, the overall heat rejected by the condenser decreases. The reduction in the condenser's overall heat rejection decreases its irreversibility.

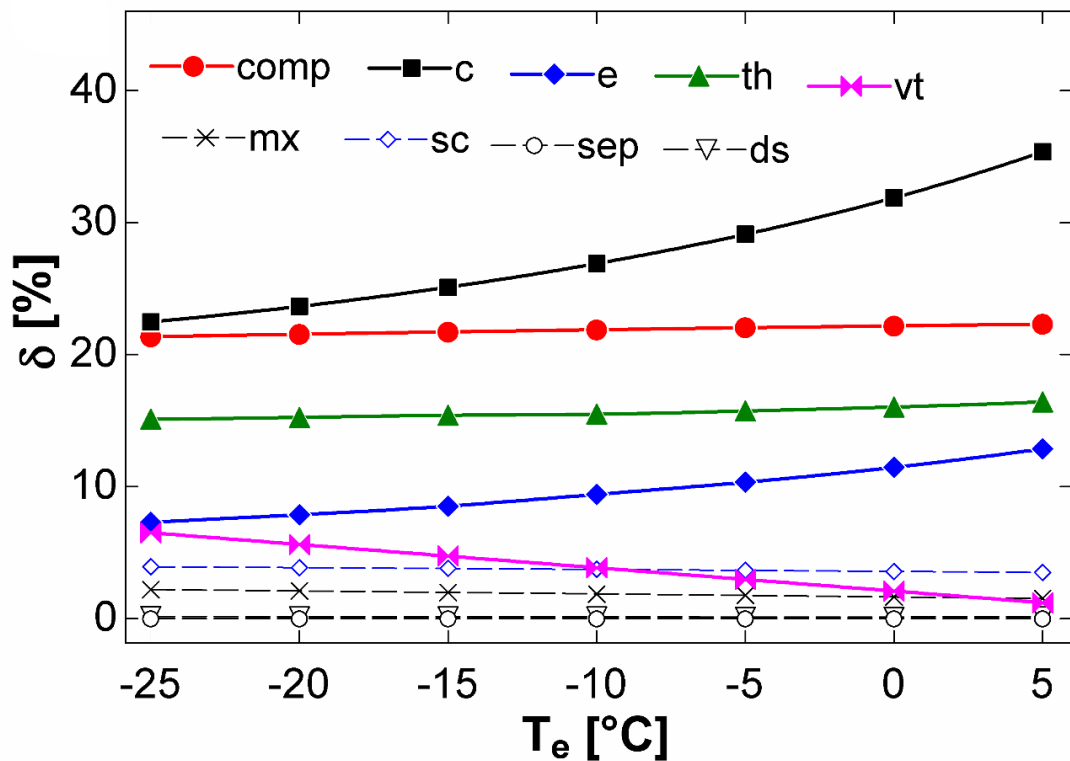


**Fig. 3.10** Effect of evaporator temperature on efficiency defect of VTC

It is already explained in that with increase in  $T_e$  cooling capacity increases. Also, with increase in  $T_e$ , the difference between the  $T_e$  and  $T_o$  decreases, which reduces both the exergy of product (EP, i.e., exergy associated with cooling capacity) and exergy of fuel (EF, i.e., compressor work), resulting in a decrease in the irreversibility of the evaporator. Another way of understanding the variation in EP with change in  $T_e$  is presented in the following lines. The ambient (at  $T_o$ ) and evaporator (at  $T_e$ ) can be considered as constituting a heat engine, producing work that decreases as the difference between these two temperatures decreases when the evaporator temperature increases and vice versa. Similarly, the exergy of product will reduce when the  $T_e$  increases since the  $T_o$  is considered as constant.

As  $T_e$  increases, both evaporator saturation pressure ( $P_e$ ) and optimum intermediate pressure ( $P_{int,opt}$ ) rise. The net effect is to decrease in the expansion pressure ratio (EPR) across the VT, which causes an increase in the cold end temperature of VT and a decrease in VT's irreversibility (for a given value of  $\eta_v$ ). This explanation is also supported by Markel[118].

The reasoning for the irreversibility in various components of VTC is already explained in the preceding paragraphs. Further, the first paragraph under section 3.3.4 gives the definition of efficiency defect and explains the reasons due to which efficiency defect increases or decreases in a particular component. Accordingly, one can understand, why the efficiency defect increases in the condenser, compressor, throttle valves, evaporator and decreases in the VT, as shown in Fig. 3.10.

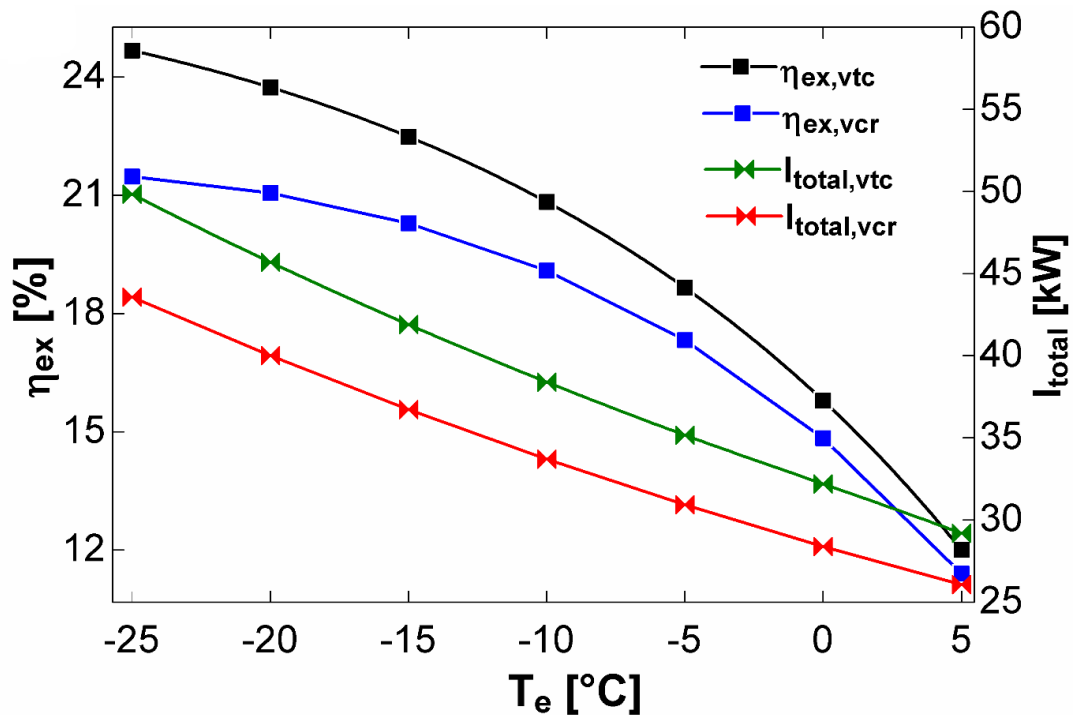


**Fig. 3.11** Effect of evaporator temperature on exergetic efficiency and total irreversibility of VTC and VCR

Fig. 3.11 demonstrates the effect of  $T_e$  on exergetic efficiency ( $\eta_{ex}$ ) and total irreversibility ( $I_{total}$ ) of VTC and VCR. Both the parameters decrease with increase in  $T_e$ . The total irreversibility as well as exergetic efficiency of VTC is higher than that of VCR. The higher irreversibility in condenser, compressor and evaporator in VTC



compared to VCR (as shown in Table 3.4), leads to a higher total irreversibility in VTC than that of VCR. However, the irreversibility in expansion valve of VCR is 6.83% to 24.61% higher in comparison to total of irreversibility in expansion valve and VT of VTC. The reduction in the irreversibilities of expansion processes in VTC is the reason for its higher exergetic efficiency.

**Table 3.4** Comparison of irreversibility in various components of VTC and VCR

Component	$I_{vtc}$ (kW)		$I_{vcr}$ (kW)	
	$T_e$ (-25 to 5°C)	$T_c$ (35 to 60°C)	$T_e$ (-25 to 5°C)	$T_c$ (35 to 60°C)
Condenser	14.16 – 11.19	6.33 – 19.00	10.42 – 9.82	4.92 – 12.96
Compressor	13.46 – 7.05	11.62 – 14.56	12.67 – 6.76	11.23 – 13.41
Throttle valve(s)	9.52 – 5.19	5.84 – 12.27	16.96 – 5.94	10.86 – 21.88
Evaporator	4.59 – 4.06	5.20 – 4.19	3.52 – 3.48	4.54 – 2.80
Subcooler	2.47 – 1.10	1.15 – 3.61	-	-
Vortex Tube	4.09 – 0.37	2.23 – 1.40	-	-
Mixing	1.38 – 0.48	0.89 – 1.73	-	-
Desuperheater	0.09 – 0.03	0.02 – 0.19	-	-
Separator	0.07 – 0.01	0.01 – 0.09	-	-
<b>Total</b>	<b>49.83 – 29.48</b>	<b>33.28 – 57.04</b>	<b>43.57 – 26.00</b>	<b>31.55 – 51.05</b>

Furthermore, it is observed that  $\eta_{ex,vtc}$  is 14.90% higher at  $T_e = -25^\circ\text{C}$  and 5.26% higher at  $T_e = 5^\circ\text{C}$  than  $\eta_{ex,vcr}$ . The variation in EP is already explained in fourth paragraph of section 4.3.1. Also, as  $T_e$  increases, exergy of fuel, i.e., compressor power decreases (as depicted in Fig 3.2(b)). The exergetic efficiency is the ratio of exergy of product (EP) to the exergy of fuel (EF). Both EP and EF are observed to decrease; however, the relative decrease in EP is greater than that of EF, resulting in a decrease in exergetic efficiency. Mathematically, this can also be explained with Eqs. (3.33) and (3.38). The exergetic efficiency of VTC depends on two terms, i.e., COP and  $\left(\frac{T_o}{T_r} - 1\right)$ . As refrigerated space temperature ( $T_r$ ) increases, the term  $\left(\frac{T_o}{T_r} - 1\right)$  decreases. The rate of decrease in the term  $\left(\frac{T_o}{T_r} - 1\right)$  is more than the rate of increase in COP. As a result, as  $T_e$  increases,  $\eta_{ex,vtc}$  and  $\eta_{ex,vcr}$  decrease.

The effect of  $T_c$  on the efficiency defect in various components of the VCR is shown in Table 3.5. The throttle valve, compressor, and condenser are significant contributors to the efficiency defect in VCR. The throttle valve is observed to have a maximum efficiency defect of 36.14% in VCR at  $T_c=60^\circ\text{C}$ , followed by compressor (i.e., 23.56%) at  $T_c=35^\circ\text{C}$ , respectively.

**Table 3.5** Effect of condenser temperature on efficiency defect in various components of VCR

$T_c(^{\circ}\text{C})$	$\delta_{comp}(\%)$	$\delta_c(\%)$	$\delta_e(\%)$	$\delta_{th}(\%)$
35	23.93	10.5	9.68	23.15
40	23.56	13.97	8.44	25.51
45	23.20	16.69	7.33	27.98
50	22.84	18.87	6.35	30.56
55	22.50	20.33	5.45	33.28
60	22.16	21.41	4.63	36.14

Fig. 3.12 illustrates the variation of efficiency defect in all components of VTC with  $T_c$ . The foremost contributors to efficiency defect in VTC are the condenser and compressor. The condenser shows a maximum efficiency defect of 26.7% at  $T_c = 60^\circ\text{C}$ , followed by 22.32% in the compressor at  $T_c=35^\circ\text{C}$ . The efficiency defect in VT decreases from 3.84% to 1.97%. It is noticed that the total efficiency defect of all the expansion devices (VT and two throttle valves) in VTC is 47.24% to 53.76% lower than that of the single expansion device in VCR. Moreover, the variations in efficiency defect in mixing at various locations, the subcooler, and the desuperheater is negligible. The reasons for these variations are provided below.

As  $T_c$  increases, the irreversibility of the condenser, compressor, and throttle valve increases, while the irreversibility of the evaporator and VT decreases. As  $T_c$  increases, the pressure ratio rises; consequently, the work input to the compressor rises, as does the temperature at the compressor's outlet, leading to an increase in its irreversibility. The rise in irreversibility of throttle valves is attributed to an increase in frictional losses caused by an increase in expansion pressure ratio (EPR). Also, the rise in net heat rejection from the condenser increases its irreversibility. In addition, as  $T_c$  increases, the optimum intermediate pressure decreases, resulting in a reduction in

the pressure ratio across VT; consequently, irreversibility in VT decreases with increase in  $T_c$ .

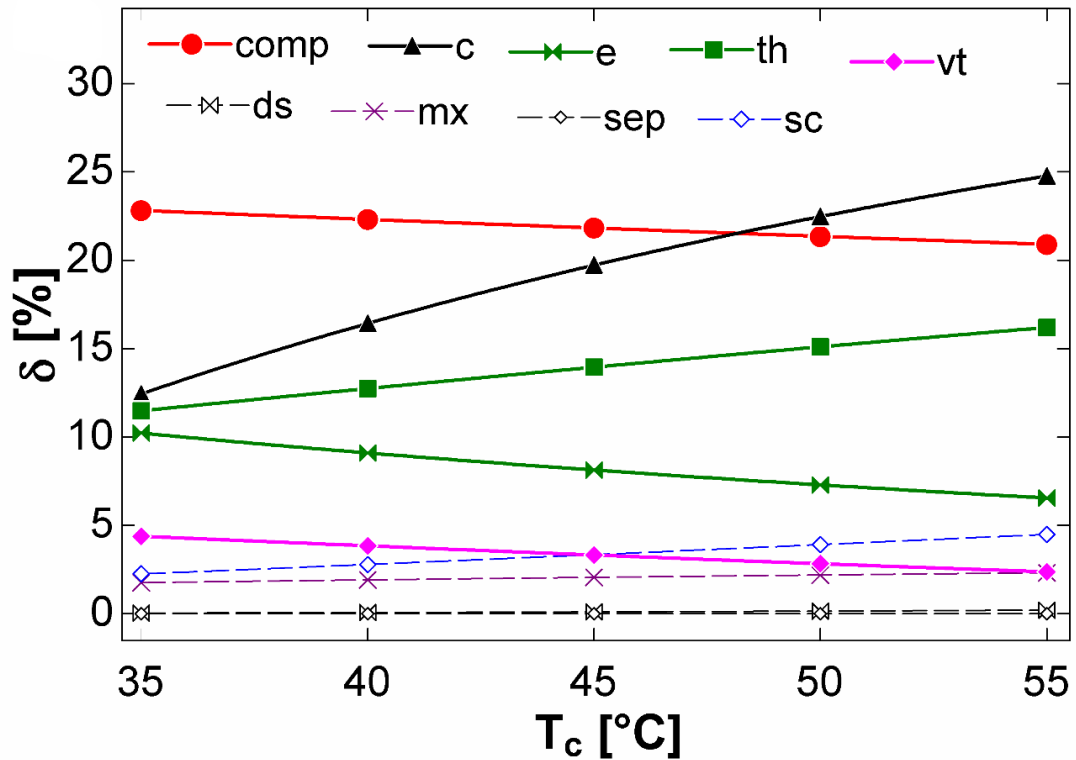


**Fig. 3.12** Effect of condenser temperature on efficiency defect of VTC and VCR

Additionally, a similar trend is observed for the irreversibility of VT in the preceding section. As a result, the efficiency defect increases in the condenser and throttle valves due to the fact that irreversibilities in these components increase at a faster rate than the compressor work. On the contrary, efficiency defect decreases in the compressor, evaporator, and VT.

The effect of  $T_c$  on exergetic efficiency ( $\eta_{ex}$ ) and total irreversibility ( $I_{total}$ ) of VTC and VCR is demonstrated in Fig. 3.13. The total irreversibility increases while exergetic efficiency decreases with an increase in condenser temperature. It is observed that  $\eta_{ex,vtc}$  is 5.62% higher at  $T_c=35^\circ\text{C}$  and 27.33% higher at  $T_c=60^\circ\text{C}$  than  $\eta_{ex,vcr}$ . Both parameters have a higher value for VTC than for VCR. This is explained as the fact that the higher value of irreversibility in the condenser, compressor and evaporator of VTC compared to VCR (as shown in Table 3.4), leads to higher total irreversibility in VTC than that of VCR. The explanation for the declining trend of

exergetic efficiency is as follows: With increase in  $T_c$ , compressor power or exergy of fuel increases, while exergy of product decreases; consequently,  $\eta_{ex}$  decreases. Mathematically, the above explanation can also be understood from Eqs. (3.33) and (3.38). The exergetic efficiencies of both cycles depend on two terms, i.e., COP and  $\left(\frac{T_o}{T_r} - 1\right)$ . As  $T_c$  increases, COP decreases, but the second term  $\left(\frac{T_o}{T_r} - 1\right)$  remains constant; consequently,  $\eta_{ex}$  decreases.

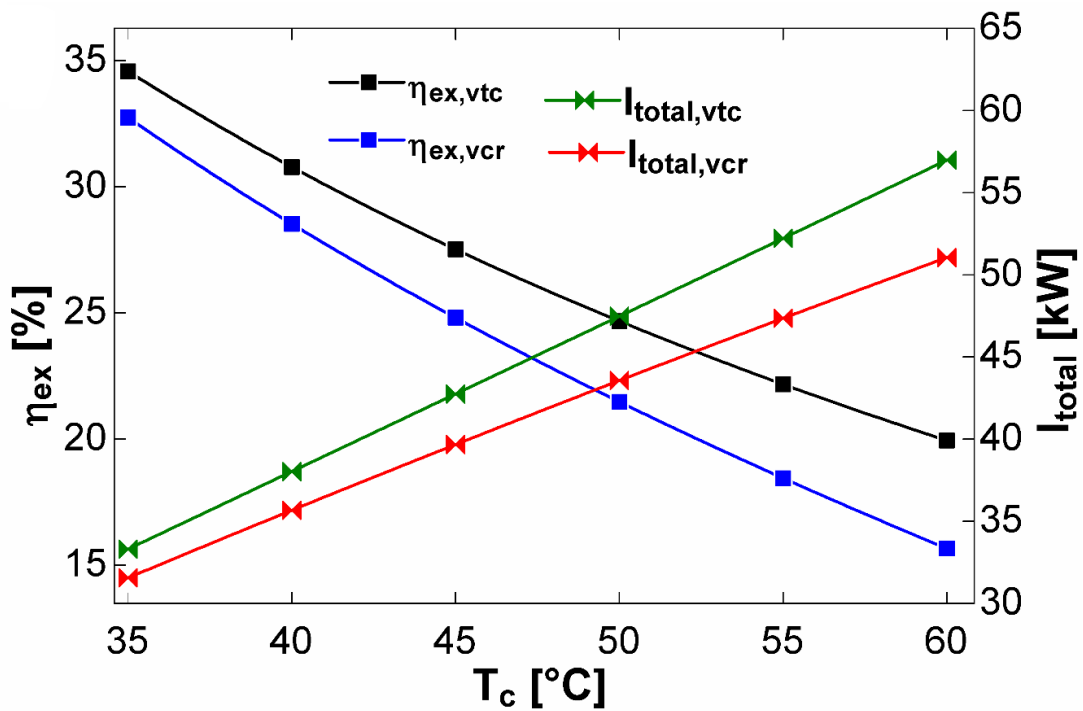


**Fig. 3.13** Effect of condenser temperature on exergetic efficiency and total irreversibility of VTC and VCR

The effect of isentropic efficiency of compressor ( $\eta_{comp}$ ) on exergetic efficiency of VTC ( $\eta_{ex,vtc}$ ) and VCR ( $\eta_{ex,vcr}$ ) is demonstrated in Fig. 3.14. It is discovered that  $\eta_{ex,vtc}$  is 14.63% to 17.37% higher than  $\eta_{ex,vcr}$ . The exergetic efficiency of both cycle rises as  $\eta_{comp}$  increases. The  $\eta_{comp}$  plays a vital role in compressor power consumption. The higher the  $\eta_{comp}$ , the lower the required compressor power or exergy of fuel. Since the value of EP is constant at a given evaporator temperature, an increase in  $\eta_{comp}$  will lead to an increase in  $\eta_{ex}$  of both cycles. Since there is no VT in VCR,  $\eta_{ex,vcr}$  is independent of  $\mu$ . The effect of cold mass fraction ( $\mu$ ) on exergetic efficiency is displayed by Table 3.6. As  $\mu$  increases,  $\eta_{ex,vtc}$  exhibits a slightly

decreasing trend from 24.72% at  $\mu=0.5$  to 24.58% at  $\mu=0.9$ . This trend can be interpreted similarly to the effect of  $\mu$  on  $COP_{vtc}$  (refer to Fig. 3.6). As  $\mu$  increases, both cooling capacity and compressor power decrease, as shown in Fig. 3.6. This leads to decrease in exergy of product (exergy associated with cooling capacity) and exergy of fuel (compressor power). However, the increase in  $\mu$  results in a net decrease in exergetic efficiency because the relative decrease in EP is greater than the decrease in EF.

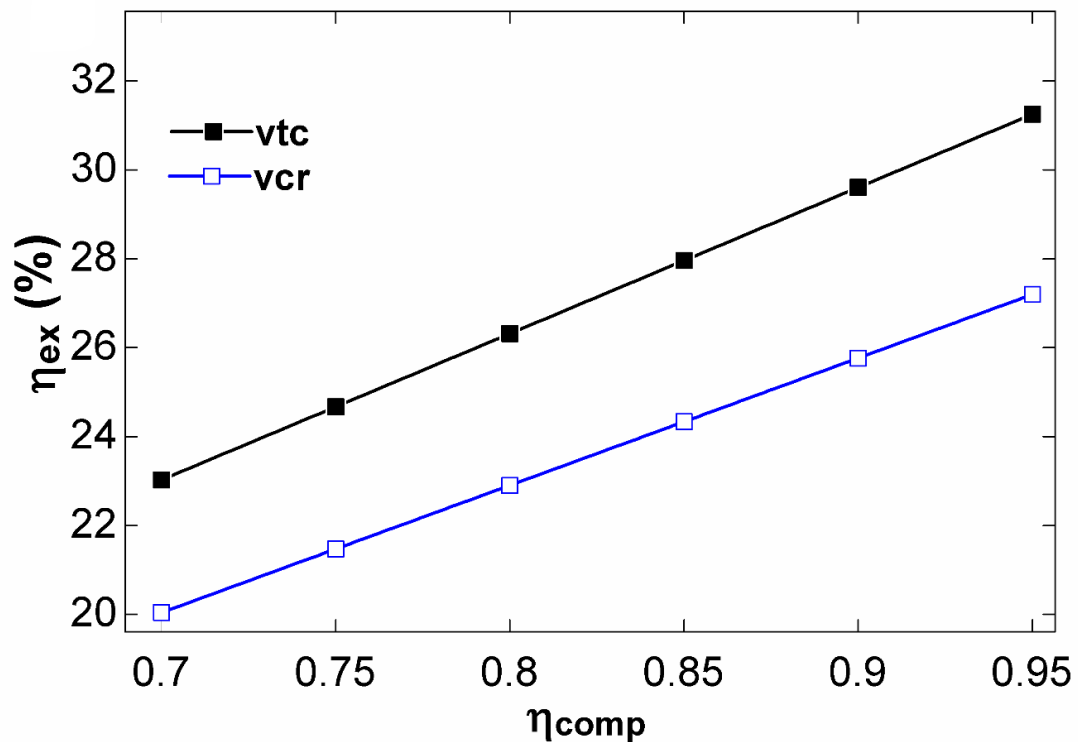


**Fig. 3.14** Effect of isentropic efficiency of compressor on exergetic efficiency of VTC and VCR

**Table 3.6** Effect of cold mass fraction on exergetic efficiency of VTC

$\mu$	$\eta_{ex, vtc} (%)$
0.5	24.72
0.6	24.67
0.7	24.63
0.8	24.60
0.9	24.58

It is evident from the antecedent discussion that operating parameters, such as evaporator temperature and condenser temperature, and design parameters, such as the compressor's isentropic efficiency, have a greater impact on exergy-related outcomes.

### 3.4.4 Multi-Objective Optimization

The operating and design parameters of the system working on VTC must be optimized to function in an effective manner. From the above parametric investigation, the evaporator temperature, condenser temperature, along with the isentropic efficiency of the compressor are observed to influence both the energy and exergy performances of VTC. The selected performance factors are compressor work and exergetic efficiency. The reason for the selection of these performance parameters is that compressor work is an indicator of operational cost, while exergetic efficiency provides a thermodynamic perspective on the system. Increased exergy efficiency is preferable, while an increase in compressor work is undesirable. Therefore, input variables should be optimized to minimise the increase in compressor work.

In order to obtain the summarised actual equations for compressor work and exergetic efficiency, the regression analysis is conducted using Design Expert software. The input variables for regression analysis, along with their ranges, are evaporator temperature ( $-25^{\circ}\text{C}$  to  $5^{\circ}\text{C}$ ), condenser temperature ( $35^{\circ}\text{C}$  to  $60^{\circ}\text{C}$ ), and isentropic efficiency of compressor (0.75 to 0.85). Three distinct regression models from the Design Expert software have been tested, i.e., linear, 2FI, and quadratic. Moreover, each regression model uses three terms: predicted  $R^2$  ( $R_p^2$ ), adjusted  $R^2$  ( $R_a^2$ ), and adequate precision (AP). The higher the difference between  $R_p^2$  and  $R_a^2$ , the higher is AP value, indicates the higher accuracy of particular regression model. If a model's AP value is less than 4, it is not recommended for further examination [138]. As shown in Table 3.7, the quadratic model is superior for regression analysis as it reflects the highest accuracy among all models.

**Table 3.7** Statistical data for different Regression Models

Performance Factor	Linear			2FI			Quadratic		
	$R_a^2$	$R_p^2$	AP	$R_a^2$	$R_p^2$	AP	$R_a^2$	$R_p^2$	AP
$\eta_{ex,vtc}$	0.9265	0.8770	29.17	0.9141	0.7329	20.40	0.9944	0.9608	66.89
$W_{vtc}$	0.9928	0.9887	93.02	0.9956	0.9896	89.4097	1.0000	0.9999	1324.99

Based on the selected quadratic regression model, a set of equations (Eqs. (3.41) and (3.42)) for both performance parameters are derived.

$$\begin{aligned} \eta_{ex,vtc} = & 37.3962 - 0.49370 * T_e - 0.858937 * T_c + 10.62167 * \eta_{comp} + \\ & 0.005059 * T_e * T_c - 0.5833 * T_e * \eta_{comp} - 0.7760 * T_c * \eta_{comp} - 0.013064 * \\ & T_e^2 + 0.009971 * T_c^2 + 30.80 * \eta_{comp}^2 \end{aligned} \quad (3.41)$$

$$\begin{aligned} W_{vtc} = & 49.43 - 1.6252 * T_e + 1.3252 * T_c - 119.5766 * \eta_{comp} - 0.004427 * \\ & T_e * T_c + 1.21333 * T_e * \eta_{comp} - 0.864 * T_c * \eta_{comp} + 0.005411 * T_e^2 + \\ & 0.000144 * T_c^2 + 75 * \eta_{comp}^2 \end{aligned} \quad (3.42)$$

Subsequently, these equations are implemented for the optimization. The objective function consists of  $W_{vtc}$  (to be minimised) and  $\eta_{ex,vtc}$  (to be maximized). The above mentioned problem is then solved using multi-objective optimization using a genetic algorithm (MOGA) [139]. MOGA is a metaheuristic technique that provides a large population of solutions that seeks to provide all possible trade-offs between two or more objective functions. As a result, Pareto optimality has been obtained. While carrying out the genetic algorithm [140], the following values were chosen as its parameters: population size of 200, crossover probability of 0.8, and Pareto front population percentage of 0.35 are the GA parameters. In addition, the selection function used is 'tournament' with a size of 2 and 'intermediate' crossover functions selected.

The Pareto front shown in Fig. 3.15 illustrates a set of optimal solutions that show the trade-off between compressor work and exergetic efficiency since the maximum values of exergetic efficiency exist correspond to maximum compressor work and vice

versa. Hence, two extreme points ('A' and 'C') and one intermediate point ('B') have been chosen arbitrarily to demonstrate the several parameters and their patterns. At 'A', both compressor work and exergetic efficiency are at a minimum. On the other hand, at 'C', both the parameters are maximum. The location of 'B' lies somewhere between 'A' and 'C'. Along the pareto front,  $T_c$  and  $\eta_{comp}$  are observed to be near their minimum and maximum values, respectively. The major variation (i.e., decrement) is witnessed in  $T_e$ , as one moves from 'A' to 'C'. At 'A', the  $T_e$  is  $4.98^\circ\text{C}$ , decreasing continuously to  $-24.98^\circ\text{C}$  at 'C'.

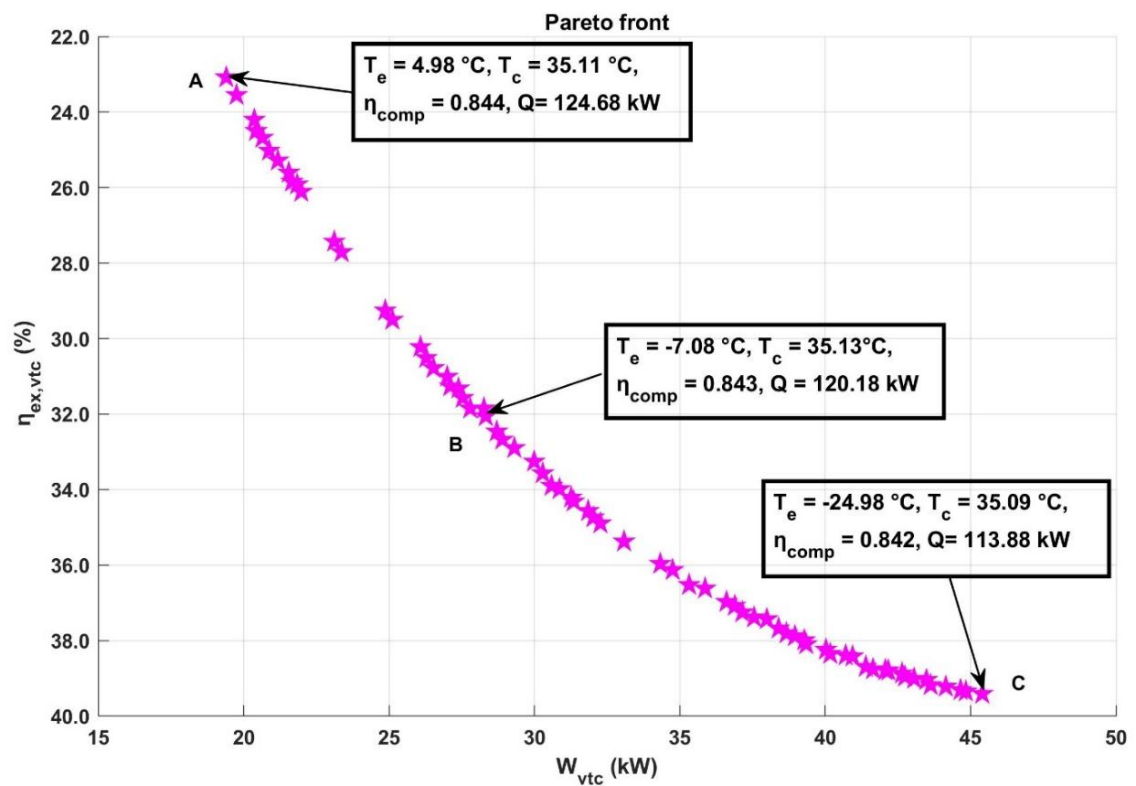


**Fig. 3.15** Pareto front calculated using GA for compressor work and exergetic efficiency of VTC

The system consisting of VTC designed at 'A' could be suitable for the application of mobile air-conditioners since the temperature of evaporator coil lies in the proximity of  $5^\circ\text{C}$ . At this point, the required compressor work is minimal; however, the exergetic efficiency is also minimal. Considering the operational cost, operating the system at this point would be economically beneficial, and moreover, cooling capacity is higher than at other points. In a similar way, designing the system



comprising VTC would work suitably for deep freezing applications while operating at 'C'. Though the operational cost is high at this point, but the irreversibility associated with the system is minimal as the exergetic efficiency is the highest. Even though the cooling capacity at 'C' is lower than at 'A', the difference between the evaporator coil temperature and the ambient temperature is substantially greater at 'C,' resulting in a higher exergy of product at 'C' than at 'A'. Therefore, the cost associated with exergy destruction is lower at 'C' than that at 'A'. Also, the product exergy cost is the highest at 'C'. Moreover, the system consisting of the VTC designed neighbouring 'B' could be employed for various suitable applications based on evaporator temperature. Hence,  $T_e$  is the major decisive factor for finding the suitability of VTC in various applications.

## CHAPTER 4: ENERGY, EXERGY, ENVIRONMENTAL (3E) ANALYSES AND MULTI-OBJECTIVE OPTIMIZATION OF VORTEX TUBE COUPLED WITH TRANS-CRITICAL VAPOUR COMPRESSION REFRIGERATION CYCLE

### 4.1 INTRODUCTION

The present chapter deals with vortex tube coupled with trans-critical vapour compression refrigeration cycle (TVTC) based on the Keller model, which contributes to the originality and novelty of the current research. The objectives of this chapter are as follows:

- To compute the results of TVTC by considering intermediate pressure and gascooler pressure as independent variables (2 DOF) and comparing results with those of '1 DOF' as reported by Sarkar for refrigerant CO<sub>2</sub> [86].
- To perform a comprehensive parametric investigation for computing compressor power, cooling capacity, COP, exergetic efficiency, component-level, and total irreversibility of TVTC.
- To compare the results of TVTC and TVCR based on energy and exergy principles.
- To perform the environmental analysis for determining the penalty cost per unit cooling capacity for both cycles.
- To compute the coefficient of structural bond in order to find the most sensitive parameters to system's performance.
- To conduct multi-objective optimization for TVTC using the genetic algorithm (GA) for finding the optimal solutions and assessing their applicability across a variety of contexts.

### 4.2 VORTEX TUBE COUPLED WITH TRANS-CRITICAL VAPOUR COMPRESSION REFRIGERATION CYCLE (TVTC)

Fig. 4.1 and Fig. 4.2 depict the schematic and p-h diagram, respectively of both TVTC and TVCR. TVTC is based on the Keller model and works at three distinct pressure levels: the highest pressure in the gascooler ( $P_{gc}$ ), the intermediate pressure ( $P_{int}$ ) in VT, and the lowest pressure in evaporator ( $P_e$ ). The various thermodynamic processes are explained in next few lines. The superheated refrigerant enters the

compressor (state 1) and gets compressed by irreversible adiabatic process (process 1-2), thereby increasing pressure and temperature of refrigerant above the critical point. The high temperature fluid (state 2) is cooled in the gascooler at constant pressure, i.e.,  $P_{gc}$  (process 2-3) by rejecting its heat into the atmosphere. The refrigerant is further cooled in subcooler (process 3-4), by exchanging heat with saturated vapour stream exiting the separator (state 8). A subcooler is employed to further cool the refrigerant stream passing through the gascooler. In order to ensure efficient heat exchange in the subcooler, the temperature of the refrigerant stream at 'state 8' must be lower than the temperature of the stream at the exit of the gas cooler (state 2). This subcooled refrigerant stream is throttled (process 4-4d), which in turn reduces its pressure to  $P_{int}$ .

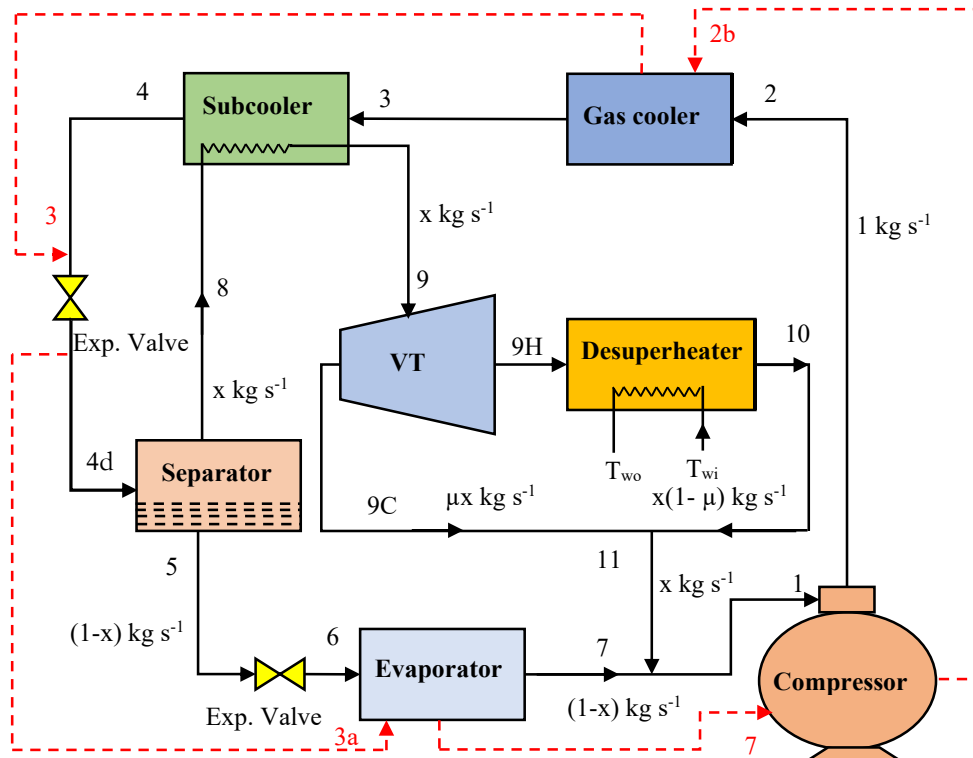


**Fig. 4.1** Schematic diagram of TVTC and TVCR (7-2b-3-3a)

Further, refrigerant is separated into saturated liquid stream ( $(1-x) \text{ kg s}^{-1}$ ) at state 5, and saturated vapour stream ( $x \text{ kg s}^{-1}$ ) at state 8, in the separator. The saturated liquid stream of refrigerant (state 5) is further expanded in expansion valve (process 5-6) and enters the evaporator (state 6) in two-phase region, where it absorbs heat at constant

pressure ( $P_e$ ) from the space to be cooled and becomes saturated vapour (state 7). Simultaneously, the saturated vapour refrigerant exiting the separator at intermediate pressure (state 8), enters the vortex tube after exchanging heat in the subcooler. The VT divides vapour refrigerant into two streams: the hot stream (state 9H) and the cold stream (state 9C). The state of both these streams are in superheated region as shown in Fig. 4.2. The mass flow rate of cold stream and hot streams are  $x\mu$  and  $\mu(1 - x)$  kg s<sup>-1</sup>, respectively. The hot stream is cooled in the desuperheater at constant pressure, i.e.,  $P_{int}$  (process 9H-10) and then combines with the cold stream (state 11). The heat obtained from the desuperheater can be utilised in numerous heating applications. The resulting mixture (state 11) is united with the dry saturated refrigerant coming out of evaporator (state 7) and enters the compressor in superheated region (state 1).

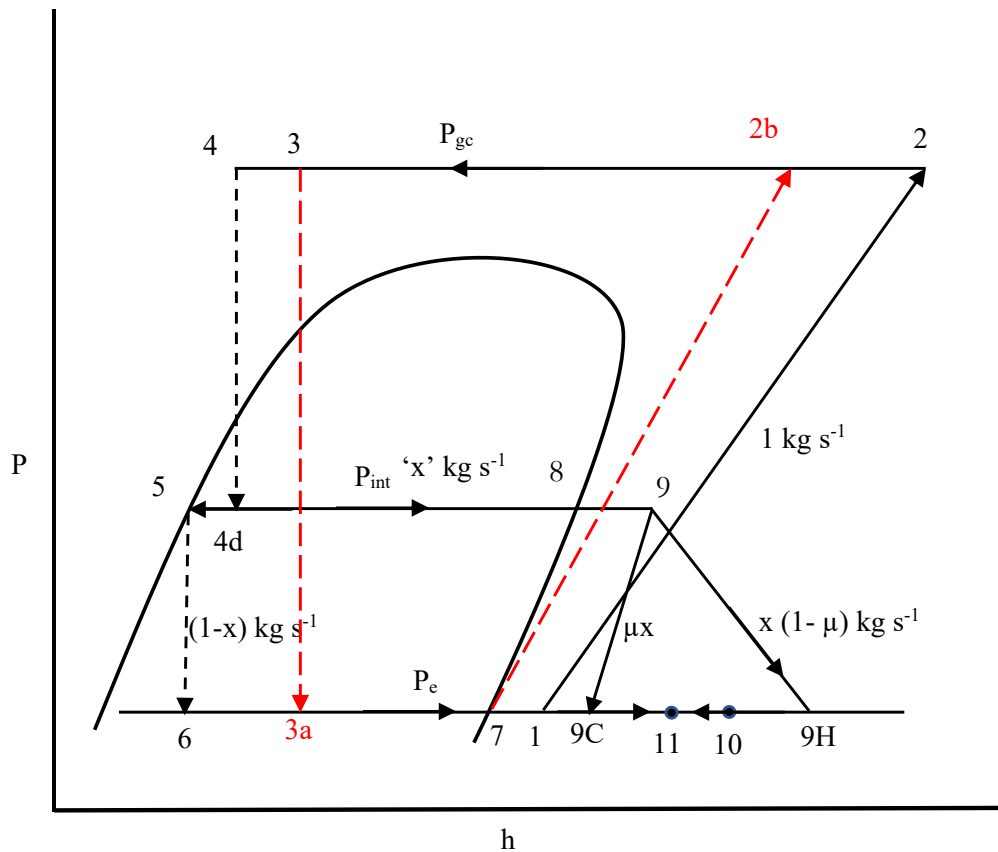


**Fig. 4.2** P-h diagram of TVTC and TVCR (7-2b-3a)

### 4.3 MATHEMATICAL MODELLING OF TVTC

The study of TVTC involves the application of the fundamental principles of mass conservation, energy conservation, and exergy balance [86, 87]. The model employed in this context is developed using the principles of the 1<sup>st</sup> and 2<sup>nd</sup> laws of thermodynamics, which are detailed below. The thermodynamic model outlined in the following paragraph is based on the following assumptions:

1. Pressure losses in heat exchangers and connecting pipelines are disregarded.
2. Mixing and separation processes occur at constant pressure (isobaric).
3. Compression process is assumed to be irreversible adiabatic.
4. The refrigerant's state at the exit of the evaporator is assumed as dry saturated.
5. The heat exchange processes in the evaporator and the gascooler are assumed as isobaric.
6. The ambient temperature and pressure considered for analysis are assumed as 25°C and 101.325 kPa, respectively.

#### 4.3.1 Mass Conservation

$$\sum \dot{m}_i = \sum \dot{m}_e \quad (4.1)$$

#### 4.3.2 Energy Conservation

$$\sum \dot{Q} - \sum \dot{W} = \sum \dot{m}_e h_e - \sum \dot{m}_i h_i \quad (4.2)$$

In this context,  $\dot{Q}$  represent the rate of heat transfer between the control volume and its surrounding, and  $\dot{W}$  signifies the work transfer rate. The coefficient of performance (COP) for the system is defined by the Eq. (4.3).

$$COP = \frac{\dot{Q}}{\dot{W}} \quad (4.3)$$

#### 4.3.3 Exergy Balance

The 2<sup>nd</sup> law of thermodynamics plays a pivotal role in the evaluation of a system's performance, primarily through the concept of exergy. Exergy consistently diminishes due to inherent irreversibilities within the system. The exergy balance of a control volume (CV) for a steady-state process can be mathematically expressed as follows [132]:

**Table 4.1** Various equations for Mass balance and Energy Balance in TVTC

Components/ Process	Mass Balance	Eq. No.	Energy Balance [90, 145]	Eq. No.
Gascooler	$\dot{m}_2 = \dot{m}_3 = 1$		$Q_{gc} = \dot{m}_2(h_2 - h_3)$	(4.9)
Subcooler	$\dot{m}_3 = \dot{m}_4 = 1$		$\dot{m}_3(h_3 - h_4) = \dot{m}_8(h_9 - h_8)$	(4.10)
	$\dot{m}_8 = \dot{m}_9 = x$		$T_9 = T_8 + \varepsilon_{sc}(T_3 - T_8)$	(4.11)
Separator	$\dot{m}_{4d} = \dot{m}_8 + \dot{m}_5$	(4.5)	$\dot{m}_{4d}h_{4d} = \dot{m}_5h_5 + \dot{m}_8h_8$	(4.12)
Vortex Tube	$\dot{m}_9 = \dot{m}_{9H} + \dot{m}_{9C}$	(4.6)	$h_{9C} = h_9 - \eta_v(h_9 - h_{9s})$	(4.13)
	$\dot{m}_{9H} = x(1 - \mu)$		$\dot{m}_9h_9 = \dot{m}_{9H}h_{9H} + \dot{m}_{9C}h_{9C}$	(4.14)
	$\dot{m}_{9C} = x\mu$			
Desuperheater	$\dot{m}_{9H} = \dot{m}_{10} = x(1 - \mu)$		$T_{10} = T_{9H} - \varepsilon_{ds}(T_{9H} - T_{wi})$	(4.15)
			$Q_{ds} = \dot{m}_{10}(h_{9H} - h_{10})$	(4.16)
Throttle valves	$\dot{m}_4 = \dot{m}_{4d} = 1$		$h_4 = h_{4d}$	(4.17)
	$\dot{m}_5 = \dot{m}_6 = 1 - x$		$h_5 = h_6$	(4.18)
Evaporator	$\dot{m}_6 = \dot{m}_7 = 1 - x$		$Q_{tvtc} = \dot{m}_6(h_7 - h_6)$	(4.19)
Mixing	$\dot{m}_{11} = \dot{m}_{9C} + \dot{m}_{10}$	(4.7)	$\dot{m}_{11}h_{11} = \dot{m}_{9C}h_{9C} + \dot{m}_{10}h_{10}$	(4.20)
	$\dot{m}_1 = \dot{m}_7 + \dot{m}_{11}$	(4.8)	$\dot{m}_1h_1 = \dot{m}_7h_7 + \dot{m}_{11}h_{11}$	(4.21)
Compressor	$\dot{m}_1 = 1$		$W_{tvtc} = \dot{m}_1(h_2 - h_1)$	(4.22)
			$(h_2 - h_1) = (h_{2s} - h_1)/\eta_{comp}$	(4.23)
System	$COP_{tvtc} = \frac{Q_{tvtc}}{W_{tvtc}}$			(4.24)

**Table 4.2** Various equations for Exergy Balance in TVTC

Components/ Process	Exergy Balance (Irreversibility and Exergetic efficiency) [91, 145]	Eq. No.
Gas-cooler	$I_{gc} = \dot{m}_2[(h_2 - h_3) - T_o(s_2 - s_3)]$	(4.25)
Subcooler	$I_{sc} = \dot{m}_3[(h_3 - h_4) - T_o(s_3 - s_4)] + \dot{m}_8[(h_8 - h_9) - T_o(s_8 - s_9)]$	(4.26)
Separator	$I_{sep} = T_o[\dot{m}_8s_8 + \dot{m}_5s_5 - \dot{m}_{4d}s_{4d}]$	(4.27)
Vortex Tube	$I_{vt} = T_o[\dot{m}_{9c}s_{9c} + \dot{m}_{9H}s_{9H} - \dot{m}_9s_9]$	(4.28)
Evaporator	$I_e = \dot{m}_6T_o \left[ (s_7 - s_6) - \left( \frac{h_7 - h_6}{T_r} \right) \right]$	(4.29)
Throttle valves	$I_{th} = T_o[\dot{m}_5(s_6 - s_5) + \dot{m}_4(s_{4d} - s_4)]$	(4.30)
Compressor	$I_{comp} = \dot{m}_1T_o(s_2 - s_1)$	(4.31)
Desuperheater	$I_{ds} = \dot{m}_{9H}[(h_{9H} - h_{10}) - T_o(s_{9H} - s_{10})]$	(4.32)
Mixing	$I_{mx} = T_o[\dot{m}_1s_1 - \dot{m}_7s_7 - \dot{m}_{9c}s_{9c} - \dot{m}_{10}s_{10}]$	(4.33)
System	$\sum I = I_{gc} + I_{sc} + I_{sep} + I_{vt} + I_e + I_{th} + I_{comp} + I_{ds} + I_{mx}$	(4.34)
	$W_{tvtc} = Q_{tvtc} \left( \frac{T_o}{T_r} - 1 \right) + \sum I$	(4.35)
	$\eta_{ex,tvtc} = \frac{W_{tvtc} - \sum I}{W_{tvtc}} = \frac{Q_{tvtc}}{W_{tvtc}} \left( \frac{T_o}{T_r} - 1 \right) = \frac{EP}{EF}$	(4.36)

\* Exergy of product (EP) =  $Q_{tvtc} \left( \frac{T_o}{T_r} - 1 \right)$ ; Exergy of Fuel (EF) =  $W_{tvtc}$

$$\sum (\dot{m}e)_{in} + \sum \left( \dot{Q} \left( 1 - \frac{T_o}{T} \right) \right)_{in} = \sum (\dot{m}e)_{out} + \sum \left( \dot{Q} \left( 1 - \frac{T_o}{T} \right) \right)_{out} \pm \sum \dot{W} + E\dot{D}_i \quad (4.4)$$

In this equation, terms  $\sum (\dot{m}e)_{in}$  and  $\sum (\dot{m}e)_{out}$  represent the sum of exergies of refrigerant streams entering and leaving the control volume (CV). The product

$\dot{Q} \left(1 - \frac{T_o}{T}\right)$  [141] signifies the exergy associated with the heat transfer rate ( $\dot{Q}$ ), and is defined as the work obtained by a Carnot engine working between constant source temperature  $T$ , and ambient temperature  $T_o$  as sink. This term can also be defined as the product of heat transfer rate and Carnot efficiency  $\left(1 - \frac{T_o}{T}\right)$ . Moreover, term  $\pm \sum \dot{W}$  is the mechanical work transfer to or from the CV. Lastly, the term  $E\dot{D}_i$  represents the exergy destruction rate (irreversibility) occurring in a process. Table 4.1 demonstrates the various equations for mass and energy balance, and Table 4.2 illustrates the equations for irreversibilities occurring in various components of TVTC along with the exergetic efficiency of the system.

#### 4.3.4 Environmental Analysis

Environmental analysis is an essential component in the modelling of thermal systems due to the increase in environmental-related issues such as global warming, which have a significant impact on the environment. Pertaining to this, the amount of CO<sub>2</sub> emission and its associated cost of environmental damage are considered important factors in the current study [142]. Consequently, for a unit cooling capacity of TVTC, the annual penalty cost of CO<sub>2</sub> emissions into the environment resulting from the generation of electricity using fossil fuels is calculated by Eq. (4.37)

$$C_{env} = m_{CO_2} * C_{CO_2} \quad (4.37)$$

where  $C_{CO_2}$  is the damage cost of the environment per unit kg of CO<sub>2</sub> emission or cost of CO<sub>2</sub> avoided, and is given by 0.09 USD/kg of CO<sub>2</sub> emission [142]. Additionally, the mass of CO<sub>2</sub> emission per unit cooling capacity ( $m_{CO_2}$ ) is given by Eq. (4.37) [142]. Since both TVTC and TVCR are compared for a constant mass flow rate of refrigerant, that is why emission in Eq. (4.38) is taken per unit of cooling capacity.

$$m_{CO_2} = (\lambda_{CO_2} * W * t_{op})/Q \quad (4.38)$$

Where  $t_{op}$  is the annual operational hours of TVTC (5000 h) and  $\lambda_{CO_2}$  is the emission conversion factor of electricity from the power grid (0.968 kg/kWh).



### 4.3.5 Structural Bond Analysis

Structural bond method is applied to the exergetic performance of various components by identifying the most sensitive parameters of the system. In the current study, the irreversibilities of various components have been investigated on the basis of coefficient of structural bond (CSB). According to this principle, a change in any component's irreversibility results in a change in the total irreversibility of the system when a particular parameter of the component is varied. Mathematically, the CSB of any  $n^{\text{th}}$  component is given by the following relation [143]:

$$CSB_n = \left[ \frac{\delta I_t}{\delta z_i} \right] / \left[ \frac{\delta I_n}{\delta z_i} \right] \quad (4.39)$$

TVTC,  $\forall n \in \text{EoE} \cap (\text{Evaporator Gascooler, Compressor, VT, Subcooler, Desuperheater})$

Here,  $z_i$  is the input parameter of the  $i^{\text{th}}$  component. In the structural bond method, this parameter is also termed as the 'system efficiency parameter'. There can be more than one parameter for a component affecting its irreversibility. Like in TVTC, evaporator temperature is the only system efficiency parameter for the evaporator, thus having one CSB value, whereas cold mass fraction and isentropic efficiency of VT are two system efficiency parameters affecting the irreversibility of VT; i.e., having two CSB values. Similarly, CSB values for other components can be considered.

On the basis of CSB values, three cases are under consideration, which are  $CSB > 1$ ,  $CSB = 0$ , and  $CSB < 1$ ; their meanings are as follows [144]:

When CSB is greater than one, it simply shows that, the change in system efficiency parameter ( $z_i$ ) causes the variation in irreversibility of the  $n^{\text{th}}$  component, which results in a significant change in total irreversibility. It means that the variation in total irreversibility of the system is higher than that of the  $n^{\text{th}}$  component. Therefore, the  $n^{\text{th}}$  element should receive more design attention to improve the performance of the system.

When CSB is zero, there is negligible change in the total irreversibility of the system with respect to change in irreversibility of  $n^{\text{th}}$  component. It means that an increase (or decrease) in irreversibility of  $n^{\text{th}}$  component would be compensated by a

decrease (or increase) in the irreversibilities of other components. This shows that there is no scope for improvement in system's overall performance.

When CSB is less than one and positive, total irreversibility decreases at a slower rate than the  $n^{\text{th}}$  component's irreversibility when system efficiency parameter is varied. It means that decrease in the irreversibility of the  $n^{\text{th}}$  component results in rise in the irreversibility of other components at comparatively lower rate. As a result, the structure of the system gives the least preferred choice over  $\text{CSB} > 1$ .

When CSB is negative, there is an inverse relationship between total irreversibility and irreversibility of  $n^{\text{th}}$  component when system efficiency parameter is varied. It means that the increase in the irreversibility of  $n^{\text{th}}$  component results in a decrease in the irreversibility of other components at comparatively higher rates.

#### 4.4 MODEL VALIDATION

Validation of results is a crucial step that essentially verifies the correctness of the model's code by comparing it to prior research. In order to accomplish this, the program was formulated in Engineering Equation Solver (EES) software [133] for current model and compared with Sarkar's model [86], employing the input conditions, refrigerant, and methodology of Sarkar [86].

**Table 4.3** Comparison of the present work with Sarkar

$T_e$ ( $^{\circ}\text{C}$ )	$\text{COP}_{\text{tvtc}}$ (Sarkar [86])	$\text{COP}_{\text{tvtc}}$ (Present Model)	% Error in COP	$P_{gc}$ (kPa) (Sarkar, [86])	$P_{gc}$ (kPa) (Present Model)	% Error in $P_{gc}$
-20	0.98	0.97	1.03%	13709	13841	0.96%
-10	1.21	1.19	1.68%	13243	13370	0.96%
0	1.52	1.49	2.02%	12782	12900	0.92%

The input conditions utilised by Sarkar [86] are as follows: intermediate pressure in VT = 5.7 MPa, effectiveness of heat exchangers = 85%, isentropic efficiency of compressor = 75%, and water inlet temperature = 27 $^{\circ}\text{C}$ . Moreover, for VT, the cold mass fraction and isentropic efficiency of nozzle were 0.5 and 80%, respectively.

Further, a comparison was made between the results stated by Sarkar [86] and those produced by the present model. Table 4.3 illustrates the discrepancy between the outcomes acquired in the current study and those obtained by Sarkar [86], which lies within 0.96 % to 1.65 % for COP and 0.92% to 0.96% for  $P_{gc}$ .

#### 4.5 RESULTS AND DISCUSSION

In this section, results based on energy analysis, exergy analysis, environmental analysis, structural bond method, and multi-objective optimization are shown and discussed in detail. The following input parameters are used to compute all energy and exergy-based results, as shown in Table 4.4.

**Table 4.4** Base values and range of Input Parameters for TVTC

S. No.	Input Parameters	Base Value	Range of Input Parameters [91, 93, 94, 135, 139]
1.	Evaporator Temperature ( $T_e$ )	-20°C	-50°C to 0°C
2.	Gascooler exit temperature ( $T_{gc}$ )	50°C	35°C to 55°C
3.	Refrigerated space temperature ( $T_r$ ) ( $T_r = T_e + 10^\circ\text{C}$ )	-10°C	-
4.	Cold mass fraction ( $\mu$ )	0.6	0.4 to 0.9
5.	VT-nozzle isentropic efficiency ( $\eta_v$ )	0.8	0.5 to 1
6.	Effectiveness of subcooler ( $\varepsilon_{sc}$ )	0.85	0.5 to 1
7.	Effectiveness of desuperheater ( $\varepsilon_{ds}$ )	0.85	0.5 to 1
8.	Water inlet temperature to desuperheater ( $T_{wi}$ )	25°C	25°C to 55°C
9.	Compressor isentropic efficiency ( $\eta_{comp}$ )	0.75	0.7 to 0.95
10.	Ambient Temperature ( $T_o$ )	25°C	-
11.	Ambient Pressure ( $P_o$ )	101.325 kPa	-
12.	Mass flow rate ( $\dot{m}$ ) of refrigerant CO <sub>2</sub>	1 kg s <sup>-1</sup>	-

The mass flow rate of refrigerant, evaporator temperature, gascooler exit temperature, and other parameters of TVCR have been considered the same as those of TVTC, as shown in Table 4.4.

#### 4.5.1 Results of Energy Analysis

It is to be noted that Sarkar [86] has taken intermediate pressure as a constant value of 5.7 MPa and gascooler pressure as the only independent variable, i.e., results were computed with one degree of freedom (1 DOF). In contrast, the present study considers the intermediate pressure and the gascooler pressure as independent variables, i.e., two degrees of freedom (2 DOF) for the computation of results. The methodology used is ‘Direct Algorithm’ [145] of EES to compute the present mathematical model. To demonstrate the efficacy of the direct algorithm of EES, a comparison has been made between Sarkar’s results and those of the present work by using input values of Sarkar [86]. As shown in Table 4.5, COP and  $P_{gc}$  of the present work are 2.6% to 3.3% higher and 2.4% to 3.1% lower, respectively, than those of Sarkar [86]. This shows that the present work is adding a novelty with improved results by using the ‘Direct Algorithm’.

**Table 4.5** Comparison of present work’s outcomes (2 DOF) to those of Sarkar (1 DOF)

$T_e$ (°C)	$COP_{tvtc}$ (Sarkar [86])	$COP_{tvtc}$ (Present Model)	$\Delta COP_{tvtc}$	$P_{gc}$ (kPa) (Sarkar [86])	$P_{gc}$ (kPa) (Present Model)	$\Delta P_{gc}$
-20	0.98	1.01	+3.1%	13709	13290	-3.1%
-10	1.21	1.25	+3.3%	13243	12883	-2.7%
0	1.52	1.56	+2.6%	12782	12475	-2.4%

The variation of COP of TVTC and TVCR with gascooler pressure ( $P_{gc}$ ) for different values of evaporator temperature is depicted in Fig. 4.3. The procedure for obtaining plot in Fig. 4.3 is as follows. Initially, intermediate pressure of TVTC is adjusted in order to obtain the maximum COP at constant values of  $T_e = -20^\circ\text{C}$ ,  $T_{gc} = 50^\circ\text{C}$  and  $P_{gc} = 12$  MPa. A local maximum COP is present, which corresponds to a local optimum intermediate pressure. Further, subsequent gascooler pressure value is established

while intermediate pressure is adjusted at constant value of  $T_e = -20^\circ\text{C}$ ,  $T_{gc} = 50^\circ\text{C}$ . A new local maximum COP is present, which corresponds to a new local optimum intermediate pressure. The iteration is repeated for subsequent gascooler pressure values until a global maximum COP is obtained. The pressure value that corresponds to global maximum COP is referred to as optimum gascooler pressure. At  $T_e = -20^\circ\text{C}$ , the maximum COP for TVTC is 1.02, and the corresponding optimum gascooler pressure is 13.2 MPa.

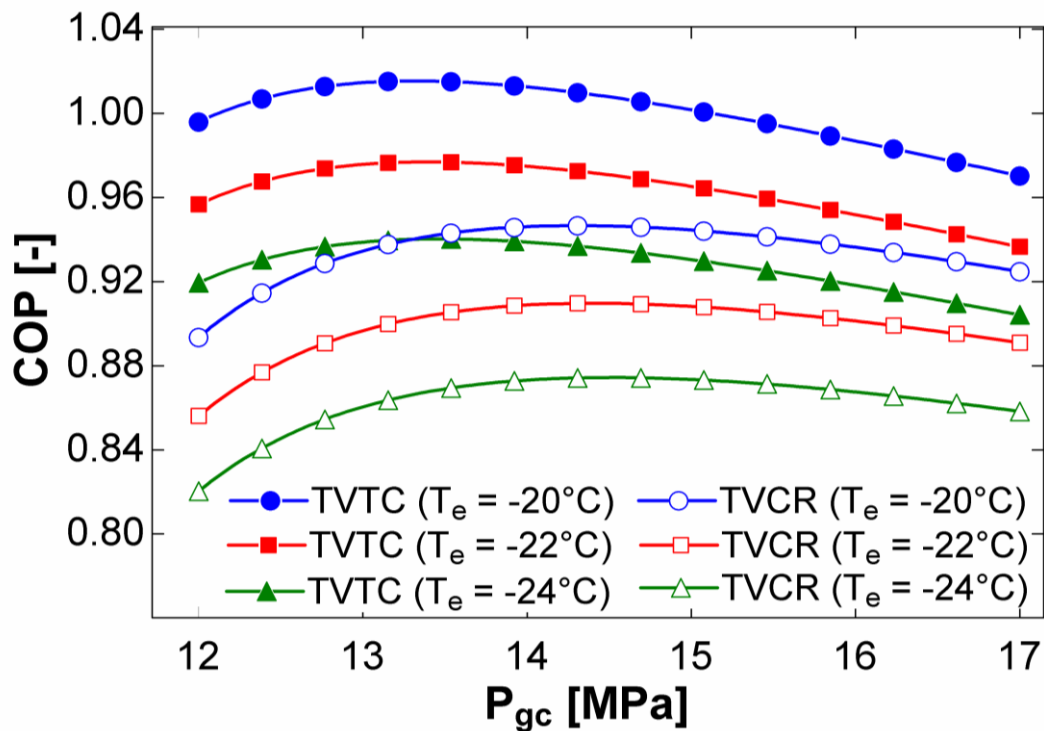


**Fig. 4.3** Effect of gascooler pressure on COP of TVTC and TVCR

For TVCR, since there is no intermediate pressure, the COP is computed for the given range of gascooler pressure only. There exists a maximum COP and a corresponding optimum gascooler pressure for TVCR. At  $T_e = -20^\circ\text{C}$ , the maximum COP is 0.92 and the corresponding optimum gascooler pressure is 14.3 MPa. Therefore, it can be concluded that TVTC exhibits a higher value of COP and a lower value of optimum gascooler pressure than those of TVCR. This provides a rationale for utilising VT in a transcritical refrigeration cycle.

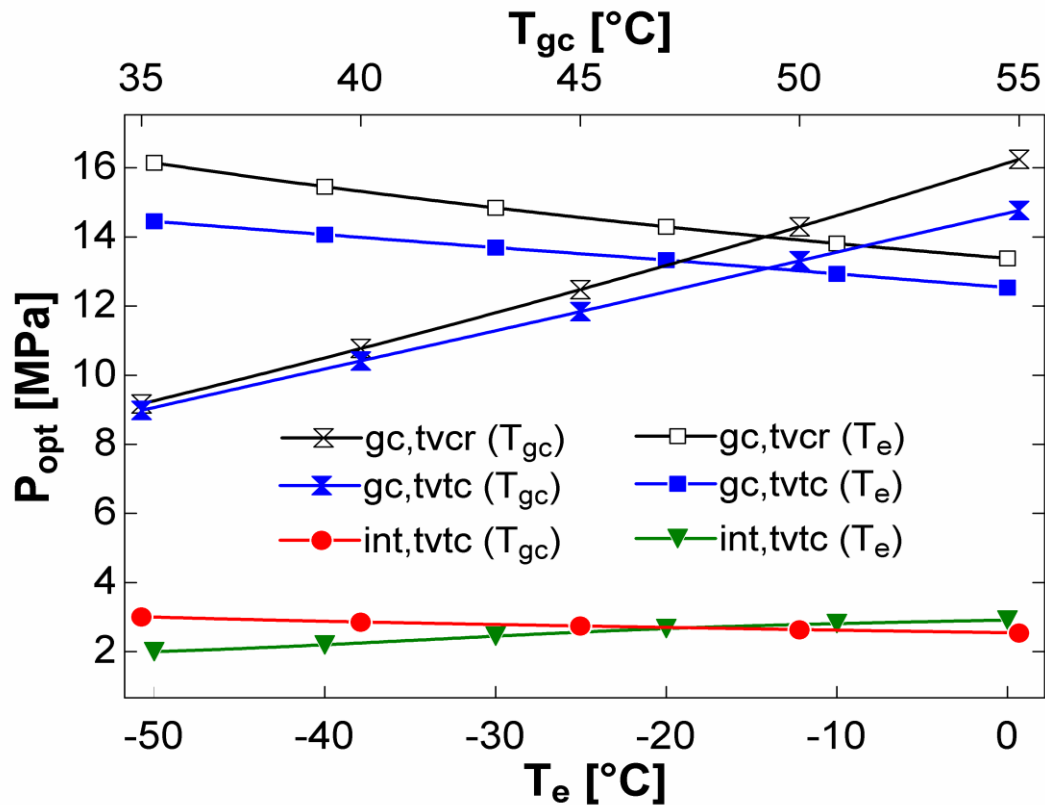


**Fig. 4.4** Effect of evaporator and gascooler exit temperatures on optimum gascooler and intermediate pressures

The variation of optimum gascooler pressure ( $P_{gc,opt}$ ) and optimum intermediate pressure ( $P_{int,opt}$ ) for both cycles with respect to evaporator temperature ( $T_e$ ) and gascooler exit temperature ( $T_{gc}$ ) is depicted in Fig. 4.4.

The procedure for determining the optimum pressure values for computation of maximum COP of TVTC is as follows. At first, the intermediate pressure is adjusted while keeping the evaporator temperature constant at  $-20^{\circ}\text{C}$  and gascooler exit temperature at  $50^{\circ}\text{C}$ . There exists a local maximum COP corresponding to a local optimum intermediate pressure. Further, gascooler pressure is adjusted while maintaining a constant local optimum intermediate pressure and keeping all other parameters unchanged. There exists a local maximum COP corresponding to a local optimum gascooler pressure. Once again, the intermediate pressure is adjusted at local optimum gascooler pressure, to discover a new local maximum COP and its corresponding local optimum intermediate pressure. The process is repeated until the discrepancy between two consecutive events diminishes to a negligible extent. A single

global optimum point is achieved, which corresponds to a global maximum COP. The identical iteration is performed for subsequent values of evaporator temperature while maintaining all other parameters as constant. Similarly, the global maximum COP values and corresponding global optimum pressure values are obtained by adjusting gascooler temperature while keeping evaporator temperature fixed at  $-20^{\circ}\text{C}$ . Further, all of these global optimum pressure points are plotted against evaporator and gascooler temperatures, as shown in Fig. 4.4.

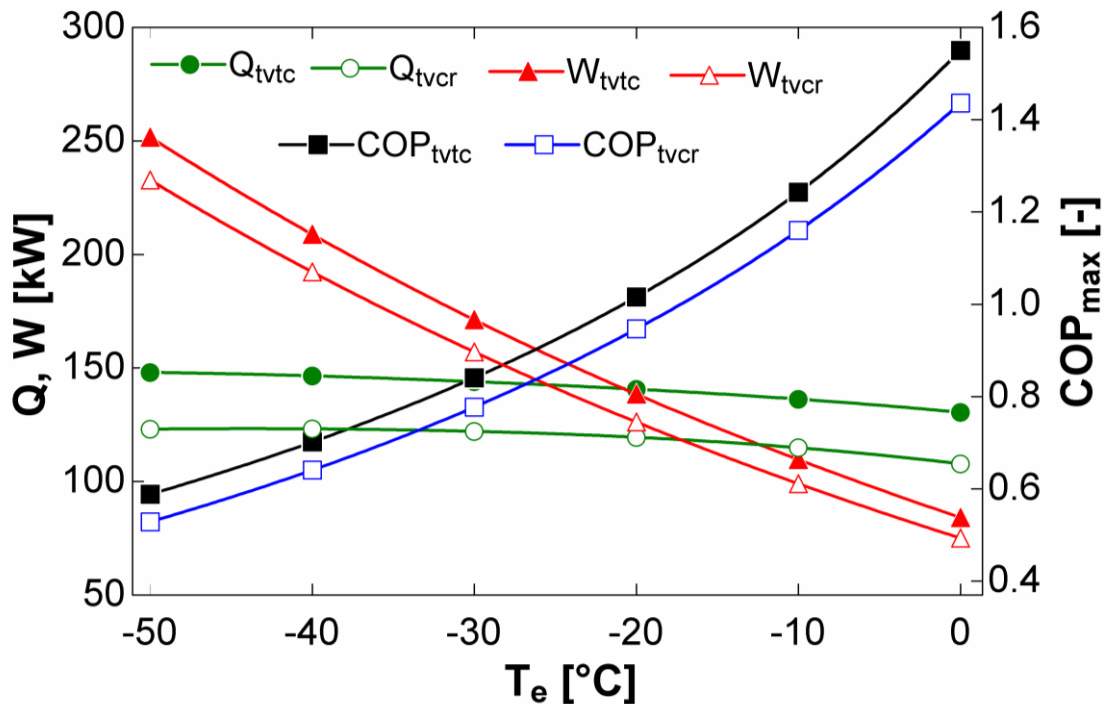
Alternatively, in order to reduce computational time, one can employ EES algorithms to obtain the same range of optimal pressure values. The 'direct algorithm' of EES is used to compute the maximum COP of TVTC (i.e., 2DOF) because it has two independent variables,  $P_{gc,tvtc}$  and  $P_{int,tvtc}$ . The 'golden search method' of EES is utilised to compute the maximum COP (i.e., 1DOF) of TVCR since there is only one independent variable,  $P_{gc,tvcr}$ .

An increase in  $T_e$  (at  $T_{gc} = 50^{\circ}\text{C}$ ) leads to an increase in the optimum intermediate pressure of TVTC ( $P_{int,opt,tvtc}$ ), a decrease in the optimum gascooler pressure of TVTC ( $P_{gc,opt,tvtc}$ ), and a decrease in the optimum gascooler pressure of TVCR ( $P_{gc,opt,tvcr}$ ). With an increase in  $T_{gc}$  (at  $T_e = -20^{\circ}\text{C}$ ),  $P_{int,opt,tvtc}$  decreases, while both  $P_{gc,opt,tvtc}$  and  $P_{gc,opt,tvcr}$  increase. It is observed that  $P_{gc,opt,tvcr}$  is 6.7% to 11.7% greater than  $P_{gc,opt,tvtc}$  for the studied range of  $T_e$ . Moreover, for the studied range of  $T_{gc}$ ,  $P_{gc,opt,tvcr}$  exhibits 2.1% to 10.1% increase compared to  $P_{gc,opt,tvtc}$ . Given that the gascooler pressure of TVTC is lower than that of TVCR, it can be inferred that the capital cost of TVTC's gascooler would be lower than that of TVCR.

When evaporator temperature increases while maintaining a constant gascooler exit temperature, the optimum gascooler pressure decreases while optimum intermediate pressure increases. This increased value of optimum intermediate pressure leads to a decrease in the dryness fraction at 'state 4d'. As a result, there is an augmentation in the mass flow rate at entry to evaporator (i.e., state 6). In contrast, an increase in evaporator temperature leads to a corresponding increase in evaporator pressure. As a result, the dryness fraction at 'state 4d' increases, causing a decrease in mass flow rate at entry to the evaporator. The overall impact of raising the evaporator

temperature is that mass flow rate at entrance of evaporator initially rises and subsequently declines.

When gascooler exit temperature is increased while keeping the evaporator temperature constant leads to increase in the optimum gascooler pressure while decrease in the optimum intermediate pressure. This results in an increase in the dryness fraction at 'state 4d', causing a decrease in the mass flow rate at 'state 6' i.e. at the entry to the evaporator. Moreover, the decrease in the optimum intermediate pressure results in a decrease in enthalpy at entry to evaporator, i.e., refrigeration effect increases. Nevertheless, the cooling capacity diminishes as the gascooler exit temperature rises (as illustrated in Fig. 4.6).



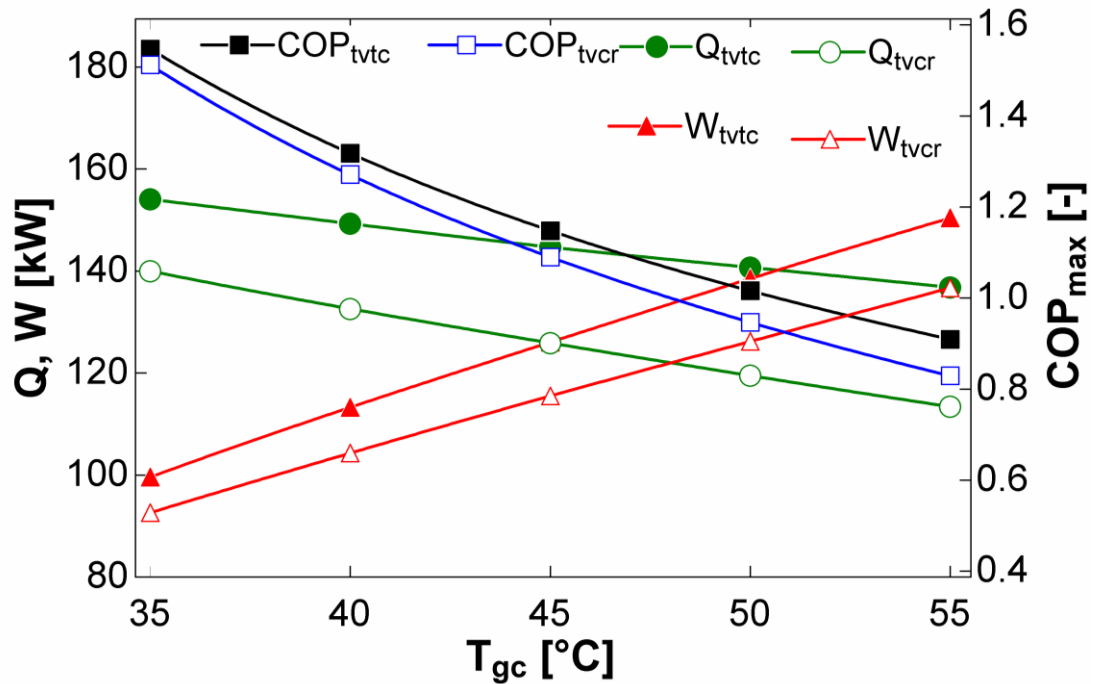
**Fig. 4.5** Effect of evaporator temperature on compressor power, cooling capacity, and COP

Fig. 4.5 depicts the effect of evaporator temperature ( $T_e$ ) on compressor power, cooling capacity, and COP for TVTC and TVCR. The cooling capacity for TVTC ( $Q_{tvtc}$ ) is 20.3% to 21.1% higher than that of TVCR ( $Q_{tvcr}$ ) for the examined range of  $T_e$ . The higher value of  $Q_{tvtc}$  than  $Q_{tvcr}$  can be attributed to two factors: initially, cooling of refrigerant to a lower temperature in the subcooler, and secondly, reduced



value of dryness fraction (at state 6) at entry to evaporator of TVTC as compared to TVCR. This reduced dryness fraction indicates that within the two-phase region, there is a larger proportion of liquid than vapour in the refrigerant. It is a widely recognised fact that the greater the amount of liquid refrigerant that enters the evaporator, the higher the quantity of heat absorbed by the refrigerant until the liquid transforms into vapour. Furthermore, the cooling capacity diminishes with a rise in  $T_e$ . This is explicable as, as  $T_e$  rises, both the evaporator pressure and the optimum intermediate pressure experience an increase (as shown in Fig. 4.4). Consequently, the mass flow rate within the evaporator initially goes up and then decreases. Also, the refrigeration effect within the evaporator diminishes as  $T_e$  increases since the enthalpy at the entry to evaporator increases. However, the cooling capacity, which is the product of the mass flow rate and refrigeration effect in the evaporator, is observed to exhibit a slight decline with rise in  $T_e$ .

Additionally, Fig. 4.5 demonstrates that as  $T_e$  increases, the compressor power of both cycles decreases. The compressor power of TVTC ( $W_{tvtc}$ ) is 8.1-12.1% greater than that of TVCR ( $W_{tvcr}$ ) across the studied range of  $T_e$ . This can be explained by the fact that the compressor power is proportional to the inlet temperature of compressor and the pressure ratio. The value of  $W_{tvtc}$  is greater than  $W_{tvcr}$  for a given pressure ratio since refrigerant that enters the compressor in TVTC (state point 1) is in superheated state, while in TVCR (state point 7), it is in a saturated vapour state. Also, with an increase in  $T_e$ , the pressure ratio in the compressor diminishes, leading to a decrease in compressor work for both TVTC and TVCR. The maximum COP of TVTC ( $COP_{max,tvtc}$ ) is observed to be 7.9-11.2% greater than that of TVCR ( $COP_{max,tvcr}$ ), over the entire range of  $T_e$ . Additionally, for both cycles, the COP increases as  $T_e$  rises. This phenomenon can be elucidated by the fact that as  $T_e$  increases, there is a corresponding decrease in both compressor power and cooling capacity. Nevertheless, compressor power diminishes at higher rate than that of cooling capacity, resulting in an increase in COP.



**Fig. 4.6** Effect of gascooler exit temperature on compressor power, cooling capacity, and COP

Fig. 4.6 depicts the variation of compressor power, cooling capacity, and COP with gascooler exit temperature ( $T_{gc}$ ) for both cycles. The cooling capacity for TVTC ( $Q_{tvtc}$ ) is 10.1% to 20.6% higher than that of TVCR ( $Q_{tvcr}$ ). This demonstrates that a rise in  $T_{gc}$  has a notable influence on the cooling capacity of TVTC in comparison to TVCR. Moreover, the cooling capacities for both cycles decrease with an increase in  $T_{gc}$ . The explanation for this behaviour is as follows: with an increase in  $T_{gc}$ , optimum intermediate pressure decreases (as shown in Fig. 4.4), which leads to decrease in the mass flow rate at entry to evaporator more than the increase in the specific refrigeration effect in the evaporator. Hence, the cooling capacities for both cycles decline as  $T_{gc}$  increases.

Fig. 4.6 also demonstrates that with increase in  $T_{gc}$ , the compressor power of both cycles increase. The compressor power of TVTC ( $W_{tvtc}$ ) is 7.5% to 10.1% greater than that of TVCR ( $W_{tvcr}$ ) over the range of  $T_{gc}$ . The reasoning for this trend is similar to that discussed for Fig. 4.5. Moreover, the variation of COP is illustrated in Fig. 4.6. The COPs for both cycles decrease, as  $T_{gc}$  increases. Over the studied range

of  $T_{9C}$ ,  $COP_{max,tvtc}$  is 2.3% to 9.7% higher than  $COP_{max,tvcr}$ . The higher COP and cooling capacity of TVTC compared to those of TVCR justifies the use of VT in trans-critical refrigeration cycles.

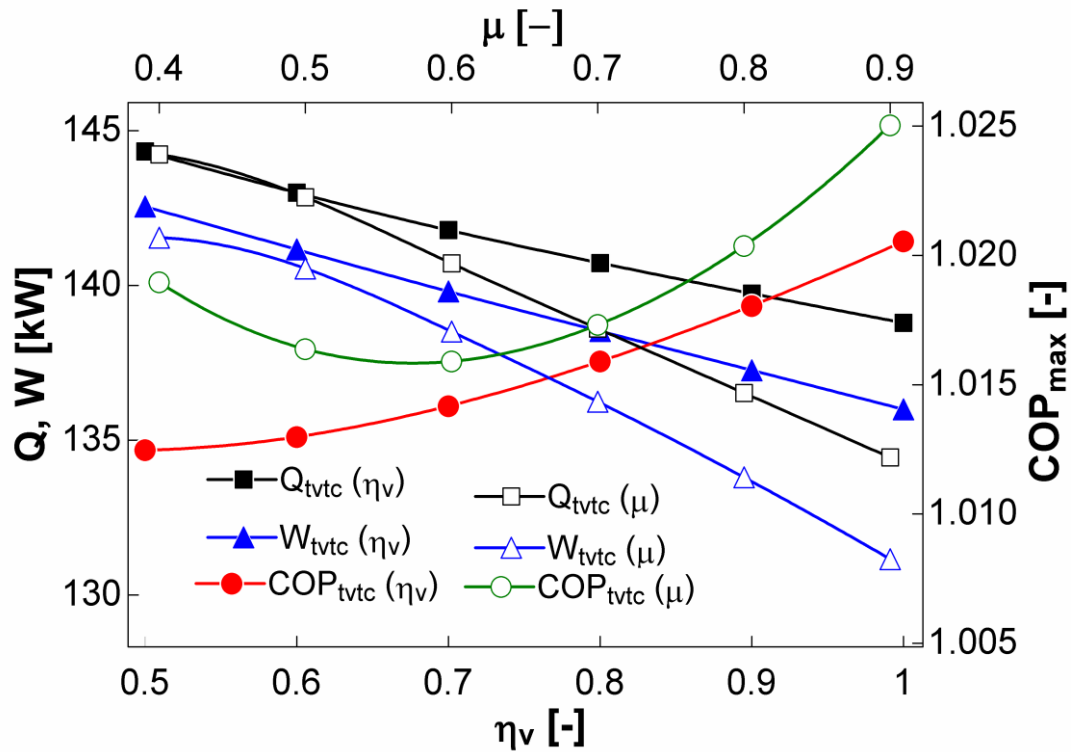


**Fig. 4.7** Effect of cold mass fraction and isentropic efficiency of VT-nozzle on cooling capacity, compressor power and COP of TVTC

Fig. 4.7 shows the variation of  $Q_{tvtc}$ ,  $W_{tvtc}$  and  $COP_{max,tvtc}$  with cold mass fraction ( $\mu$ ) and isentropic efficiency of VT-nozzle ( $\eta_v$ ). It is observed that as  $\mu$  increases, both  $Q_{tvtc}$  and  $W_{tvtc}$  decrease. The term  $\mu$ , which is the ratio of mass flow rate of the cold stream to that of the stream entering VT, has a notable influence on the temperatures of both the hot and cold streams. The temperature of the cold stream ( $T_{9C}$ ) is influenced by two parameters; cold mass fraction ( $\mu$ ) and corresponding optimum inlet pressure to VT i.e.,  $P_{int,opt}$ . Further it is observed that as  $\mu$  increases, so does the value of  $P_{int,opt}$ . The increase in values of  $\mu$  and  $P_{int,opt}$  exhibits opposing effect on  $T_{9C}$ . Specifically, an increase in  $\mu$  results in a corresponding increase in  $T_{9C}$ , while  $P_{int,opt}$  induces a reduction in  $T_{9C}$ . However, the combined effect of  $\mu$  and  $P_{int,opt}$  results in a reduction in  $T_{9C}$  since the increase in  $P_{int,opt}$  has greater influence

on  $T_{9C}$  compared to  $\mu$ . It is also observed that as  $\mu$  increases, temperature of hot stream ( $T_{9H}$ ) and the temperature difference between hot and cold streams ( $\Delta T_{vt}$ ) increases [118, 146]. Moreover, as  $P_{int}$  increases,  $T_{9H}$  increases and  $\Delta T_{vt}$  increases at a given value of cold mass fraction [118, 147, 148].

This net decrease in  $T_{9C}$  results in a lower temperature of refrigerant at entry to the compressor ( $T_1$ ), thereby decrease in  $W_{tvtc}$  is observed for a constant pressure ratio. Thus, both  $Q_{tvtc}$  and  $W_{tvtc}$  decrease as  $\mu$  increases. However,  $COP_{max,tvtc}$  follows a specific trend. Initially, it decreases as  $\mu$  increases, reaching its minimum value (at  $\mu = 0.58$ ), and then it starts to increase with further increase in  $\mu$ . This behaviour occurs because, up to  $\mu = 0.58$ ,  $Q_{tvtc}$  decreases at a faster rate than  $W_{tvtc}$ , resulting in a decrease in  $COP_{max,tvtc}$ . After this point, the situation reverses, and  $COP_{max,tvtc}$  begins to increase as  $\mu$  rises.

As illustrated in Fig. 4.7, an augmentation in  $\eta_v$ , results in simultaneous decline of both  $Q_{tvtc}$  and  $W_{tvtc}$ , while concurrently enhancing  $COP_{max,tvtc}$ . This phenomenon can be elucidated by considering the fact that as  $\eta_v$  increases,  $P_{int,opt}$  is observed to increase in order to compute maximum COP. This leads to increase in pressure ratio across VT which results in decrease in the temperature of the cold stream ( $T_{9C}$ ). Consequently, temperature of refrigerant at the entry to the compressor ( $T_1$ ) decreases, thereby causing a decrease in  $W_{tvtc}$  for a given pressure ratio. The fluctuation in  $\eta_v$  indirectly influences  $Q_{tvtc}$  due to increase in  $P_{int,opt}$ . This increase in  $P_{int,opt}$  brings a rise in mass flow rate in the evaporator and simultaneously decreases the specific refrigeration effect. This leads to a decrease in  $Q_{tvtc}$ . Furthermore, with an increase in  $\eta_v$ , the  $COP_{max,tvtc}$  demonstrates an increase due to the fact that  $W_{tvtc}$  decreases at more rapid pace than  $Q_{tvtc}$ .

The impact of  $\mu$  on heat rejected by the desuperheater ( $Q_{ds}$ ) for various values of  $\varepsilon_{ds}$  is presented in Table 4.6. The heat rejection from the desuperheater to the cooling water is estimated to be approximately 3-6% of the cooling capacity of TVTC. Additionally,  $Q_{ds}$  exhibits a maximum value at higher and lower values of cold mass fraction, as shown in Table 4.6. When  $\mu$  is in the range of 0.4 to 0.5,  $Q_{ds}$  is at its

minimum. This demonstrates that desuperheater usage is justified at higher values of  $\mu$ . Furthermore, in the absence of a desuperheater in the cycle, the hot stream and cold stream of VT would be mixed directly at the evaporator's exit. This configuration of the cycle would have minimal impact on the effectiveness of the proposed system, given that the cooling capacity of TVTC is approximately 20 - 21% greater than that of TVCR, as shown in Fig. 4.5.

**Table 4.6** Effect of on the heat rejected by the desuperheater at different values of effectiveness of desuperheater

$\mu$	$Q_{ds}$ (kW) (at $\varepsilon_{ds} = 0.85$ )	$Q_{ds}$ (kW) (at $\varepsilon_{ds} = 0.90$ )	$Q_{ds}$ (kW) (at $\varepsilon_{ds} = 0.95$ )
0.1	5.40	5.70	6.02
0.2	4.83	5.11	5.41
0.3	4.27	4.52	4.76
0.4	3.76	3.99	4.12
0.5	3.56	3.90	4.16
0.6	4.22	4.53	5.05
0.7	4.99	5.51	5.86
0.8	6.35	6.61	7.23
0.9	7.52	8.20	8.62

Additionally, the requirement for a desuperheater and the ranges of cold and hot temperatures at the exit of VT may differ depending on the type of VT selected. Three conditions govern the requirement of a desuperheater: first, the type of VT employed; second, the state of the refrigerant at inlet of VT; and third, the temperature differential between the hot stream exiting the VT and the temperature of cooling water utilised in the desuperheater. Nevertheless, the effect of geometrical parameters of VT on cycle performance is not the focus of the present work. Therefore, the preceding discussion

(related to Table 4.6) is based solely on the thermodynamic analysis of the current research.

**Table 4.7** Effect of water inlet temperature on cooling capacity, compressor power and COP of TVTC

$T_{wi}$ ( $^{\circ}C$ )	$Q_{tvtc}$ (kW)	$W_{tvtc}$ (kW)	$COP_{max,tvtc}$
25	140.6	136.4	1.03
30	140.7	137.5	1.02
35	140.7	138.7	1.01
40	140.7	140.3	1.00
45	140.8	141.0	0.99
50	140.7	141.5	0.99
55	140.8	142.9	0.98

Table 4.7 depicts the variation of  $Q_{tvtc}$ ,  $W_{tvtc}$  and  $COP_{max,tvtc}$  with water inlet temperature to desuperheater ( $T_{wi}$ ). As  $T_{wi}$  increases,  $Q_{tvtc}$  remains unchanged,  $W_{tvtc}$  increases and  $COP_{max,tvtc}$  decreases. This is due to the fact that  $T_{wi}$  has no relationship with  $Q_{tvtc}$ . Also, for a given effectiveness of desuperheater ( $\epsilon_{ds}$ ), temperature of refrigerant stream at the outlet of desuperheater ( $T_{10}$ ) increases, as  $T_{wi}$  increases. This elevated temperature increases the refrigerant temperature at compressor's inlet ( $T_{10}$ ). Therefore, for a given pressure ratio,  $W_{tvtc}$  is observed to increase. Since  $Q_{tvtc}$  remains constant and  $W_{tvtc}$  increases, therefore,  $COP_{max,tvtc}$  decreases.

The slight variation in COP observed in Table 4.7 can be attributed to the fact that the amount of heat rejected by the hot stream (exiting VT) in the desuperheater ( $Q_{ds}$ ) is small in comparison to  $Q_{tvtc}$  (as shown in Table 4.6). Consequently, when  $T_{wi}$  increases, there is a slight decrease in  $Q_{ds}$ . This results in an insignificant increase in  $W_{tvtc}$  and a corresponding decrease in the COP.

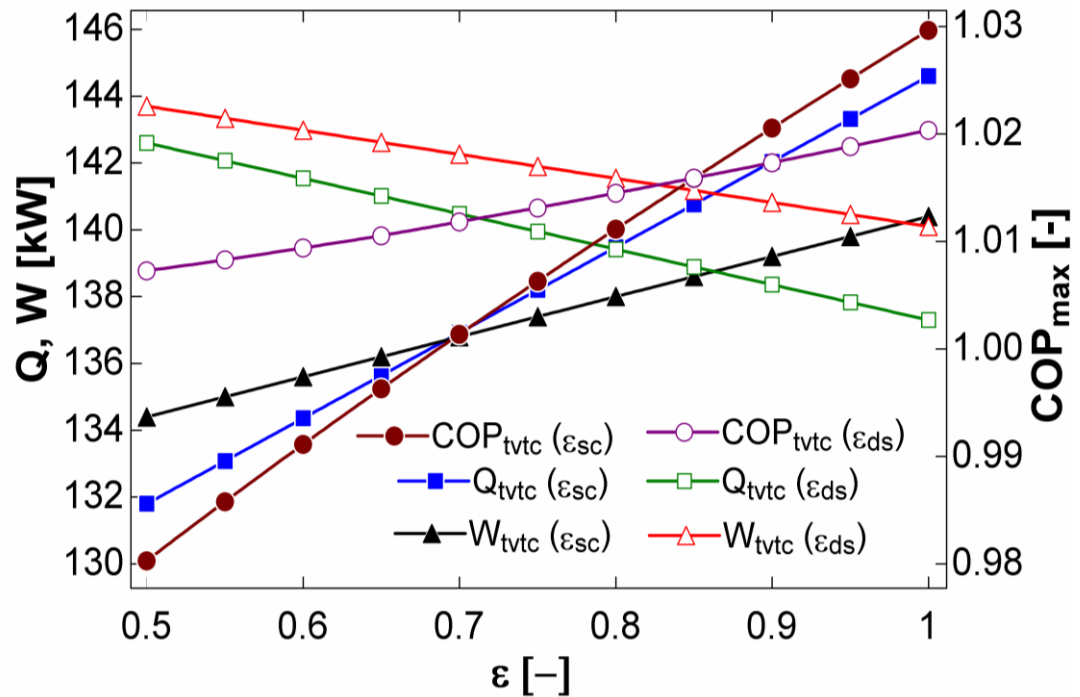


**Fig. 4.8** Effect of effectiveness of subcooler and desuperheater on cooling capacity, compressor power and COP of TVTC

Fig. 4.8 depicts the variation of  $Q_{tvtc}$  and  $W_{tvtc}$  with effectiveness of subcooler ( $\epsilon_{sc}$ ) and desuperheater ( $\epsilon_{ds}$ ). As  $\epsilon_{sc}$  increases, both  $Q_{tvtc}$  and  $W_{tvtc}$  increase, while as  $\epsilon_{ds}$  increases, both  $Q_{tvtc}$  and  $W_{tvtc}$  decrease.

As  $\epsilon_{sc}$  rises, the process of heat exchange in the subcooler improves due to the subcooling of the stream leading to the evaporator via the separator. This results in an increase in the net refrigerating effect and  $Q_{tvtc}$  due to decrease in refrigerant's enthalpy at the evaporator's entry being the primary cause of this trend. An increase in  $\epsilon_{sc}$  has a secondary effect on the VT by increasing the inlet stream's temperature ( $T_9$ ) as a result of heat exchange in the subcooler. Moreover, the optimum intermediate pressure decreases, this results in decrease in the pressure ratio across the VT. This leads to an increase in temperature of cold stream ( $T_{9c}$ ), which plays an important role in raising the temperature of refrigerant at the inlet of compressor ( $T_1$ ); consequently,  $W_{tvtc}$  increases. Nevertheless, the rate of increase in  $Q_{tvtc}$  is higher than that of  $W_{tvtc}$ . Consequently, as  $\epsilon_{sc}$  increases, so does  $COP_{max,tvtc}$ .

As  $\varepsilon_{ds}$  rises, the heat transfer rate from the hot fluid leaving VT to the cold fluid approaching the desuperheater increases. This increased heat transfer rate is accountable for a more substantial decrease in the temperature of refrigerant leaving the desuperheater ( $T_{10}$ ). As a result, the temperature of refrigerant at the entrance of the compressor ( $T_1$ ) decreases. As a direct consequence of this temperature decrease,  $W_{tvtc}$  diminishes. Furthermore, rise in  $\varepsilon_{ds}$  have an indirect influence on  $Q_{tvtc}$ . As  $\varepsilon_{ds}$  increases, it is observed that  $P_{int,opt}$  also rises in order to compute the maximum COP. Consequently, there is a simultaneous increase in the mass flow rate and enthalpy of refrigerant stream inflowing the evaporator. However, the combined outcome is a decrease in the specific refrigerating effect and  $Q_{tvtc}$ . It has already been stated that as  $\varepsilon_{ds}$  increases, both  $Q_{tvtc}$  and  $W_{tvtc}$  decrease. However,  $COP_{max,tvtc}$  exhibits an augmentation in response to this change. This is primarily attributed to the fact that the reduction in  $W_{tvtc}$  is relatively greater than the reduction in  $Q_{tvtc}$ . Moreover, it is noted that the impact of increase in  $\varepsilon_{sc}$  on  $COP_{max,tvtc}$  is greater than that of  $\varepsilon_{ds}$ .

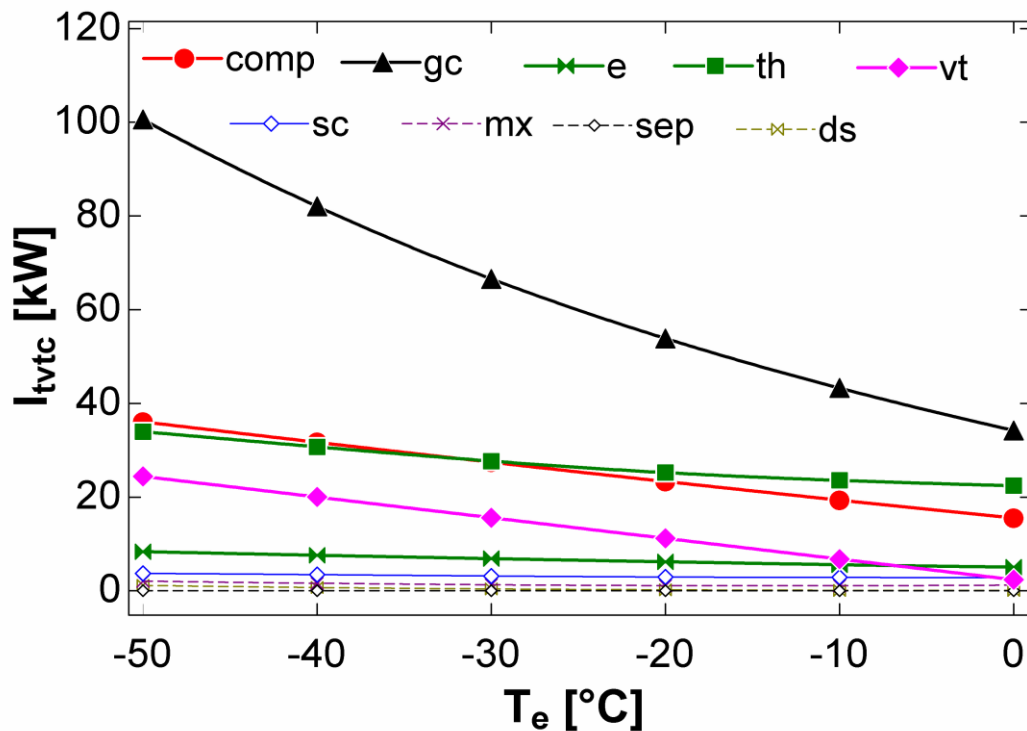
#### 4.5.2 Results of Exergy Analysis

Table 4.8 illustrates the effect of  $T_e$  on irreversibilities in numerous components of TVCR. The gas cooler and throttle valve have the greatest degree of irreversibility in TVCR. In addition, the maximum irreversibility in the gascooler and the throttle valve at  $T_e = -50^\circ\text{C}$  are 86.9 kW and 69.5 kW, respectively.

**Table 4.8** Effect of evaporator temperature on irreversibilities in various components of TVCR

$T_e(^{\circ}\text{C})$	$I_{comp}(\text{kW})$	$I_{gc}(\text{kW})$	$I_e(\text{kW})$	$I_{th}(\text{kW})$
-50	35.2	86.9	6.9	69.5
-40	30.8	70.1	6.4	57.3
-30	26.5	56.2	5.8	46.8
-20	22.3	44.8	5.3	37.9
-10	18.4	35.2	4.7	30.2
0	14.5	27.1	4.1	23.7





**Fig. 4.9** Effect of evaporator temperature on irreversibilities of various components of TVTC

The variation in irreversibility of each component of TVTC with  $T_e$  is depicted by Fig. 4.9. The gascooler demonstrates the highest irreversibility of 100.6 kW among all the components, followed by the compressor at 36.1 kW, at  $T_e = -50^\circ\text{C}$ . As  $T_e$  increases, the irreversibility of VT decreases from 24.4 kW to 2.3 kW, which is much lower than that of the throttle valve of TVCR. This justifies the use of VT from an exergetic viewpoint. Furthermore, there is minimal variation in irreversibility observed at different mixing points, desuperheater, and subcooler.

The irreversibility of the gas cooler, compressor, throttle valve, evaporator, and VT diminishes as  $T_e$  increases. The reasoning behind these variations can be explained in the next few lines. With an increase in  $T_e$ , pressure ratio decreases across the compressor, which leads to reduced compressor work, consequently lowering the temperature of refrigerant at compressor's outlet ( $T_2$ ). It is apparent that, for a given value of isentropic efficiency of compressor, a decline in discharge temperature corresponds to a decrease in entropy generation and exergy destruction within the compressor. With an increase in  $T_e$ , there is a decrease in both cooling capacity and

compressor power (as shown in Fig. 4.5), leading to a reduction in the overall heat rejection by the gas cooler, which causes decrease in its irreversibility. Further, as  $T_e$  increases, the temperature difference between  $T_e$  and  $T_o$  diminishes. As a result, exergy of the product (EP) as well as exergy of the fuel (EF) simultaneously decrease. The term ‘EP’ is denoted as the exergy related to cooling capacity while ‘EF’ is associated with compressor power. Consequently, irreversibility of the evaporator goes down. With increase in  $T_e$ , there is a concurrent increase in both evaporator pressure ( $P_e$ ) and the optimal intermediate pressure ( $P_{int,opt}$ ). The cumulative effect of increase in both of these pressures results in a reduction of pressure ratio across the VT, which leads to decrease in irreversibility of VT. This interpretation is corroborated by the findings of Markel [118].

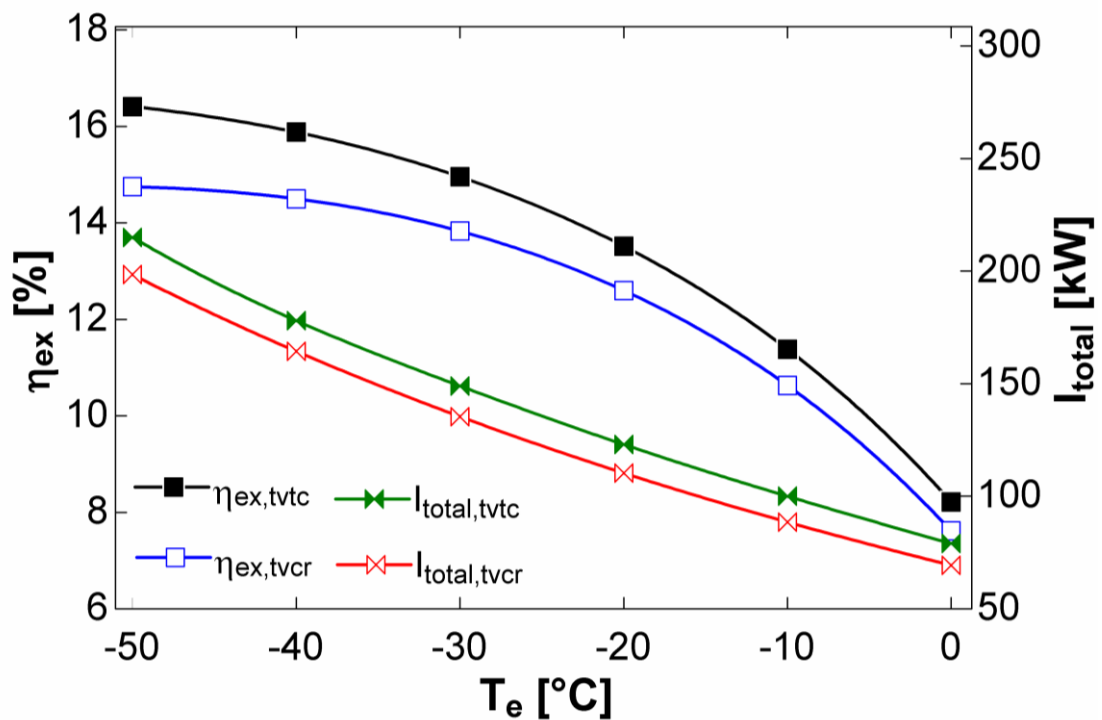


**Fig. 4.10** Effect of evaporator temperature on exergetic efficiency and total irreversibility of TVTC and TVCR

Fig. 4.10 depicts the trends of exergetic efficiency ( $\eta_{ex}$ ) and total irreversibility ( $I_{total}$ ) concerning the evaporator temperature for both TVTC and TVCR. It is observed that  $\eta_{ex}$  and  $I_{total}$  diminish as  $T_e$  rises. TVTC exhibits a greater degree of total irreversibility and exergetic efficiency in comparison to TVCR. This

pertains to the fact that a greater amount of irreversibility in the gascooler results in a greater amount of total irreversibility in TVTC than that of TVCR, as evidenced in Fig. 4.9 and Table 4.8. Nevertheless, the irreversibility of throttle valve of TVCR is found to be at most 18.9% higher compared to cumulative irreversibilities of expansion valves and VT of TVTC. This reduced irreversibility of expansion processes in TVTC over TVCR is the underlying cause of higher exergetic efficiency and justifies the use of VT in trans-critical refrigeration cycles.

Additionally, it is observed that the exergetic efficiency of TVTC ( $\eta_{ex,tvtc}$ ) is 11.3% higher at  $T_e = -50^\circ\text{C}$  and 7.9% higher at  $T_e = 0^\circ\text{C}$  compared to that of TVCR ( $\eta_{ex,tvcr}$ ). As  $T_e$  increases, cooling capacity and compressor power decrease, as depicted in Fig. 4.5. EP and EF both decrease concurrently, resulting in a reduction in exergetic efficiency, which is defined as the ratio of EP to EF. This phenomenon can be elucidated mathematically using Eq. (4.36). The exergetic efficiency of TVTC relies on two factors, namely COP and  $\left(\frac{T_o}{T_r} - 1\right)$ . With an increase in the refrigerated space temperature ( $T_r$ ), the second factor diminishes. The rate of decrease in the second factor exceeds the rate of increase in COP. Consequently, as  $T_e$  increases, both  $\eta_{ex,tvtc}$  and  $\eta_{ex,tvcr}$  exhibit a decrease.

The influence of  $T_{gc}$  on the irreversibility of different components of TVCR is presented in Table 4.9. Notably, both the throttle valve and the gascooler of TVCR contribute significant irreversibility. Specifically, the gascooler exhibits a maximum irreversibility of 51.1 kW, followed by 42.1 kW in throttle valve at  $T_{gc}=55^\circ\text{C}$ .

Fig. 4.11 depicts the trend of irreversibility in various components of TVTC with  $T_{gc}$ . The primary contributors to irreversibility of TVTC are the gas cooler, throttle valve, and compressor. Specifically, the gas cooler exhibits a maximum irreversibility of 61.6 kW, followed by the throttle valve (28.7 kW) and the compressor (24.5 kW) at  $T_{gc}=55^\circ\text{C}$ . The irreversibility of VT decreases from 7.7 kW to 6.1 kW. Notably, the cumulative irreversibility of VT and throttle valves of TVTC is 10.2% to 17.3% lower than that of sole throttle valve of TVCR. Additionally, negligible variations in

irreversibility are observed in the desuperheater, subcooler, and at various mixing points. Furthermore, the underlying reasons for the aforesaid variations are elucidated below.

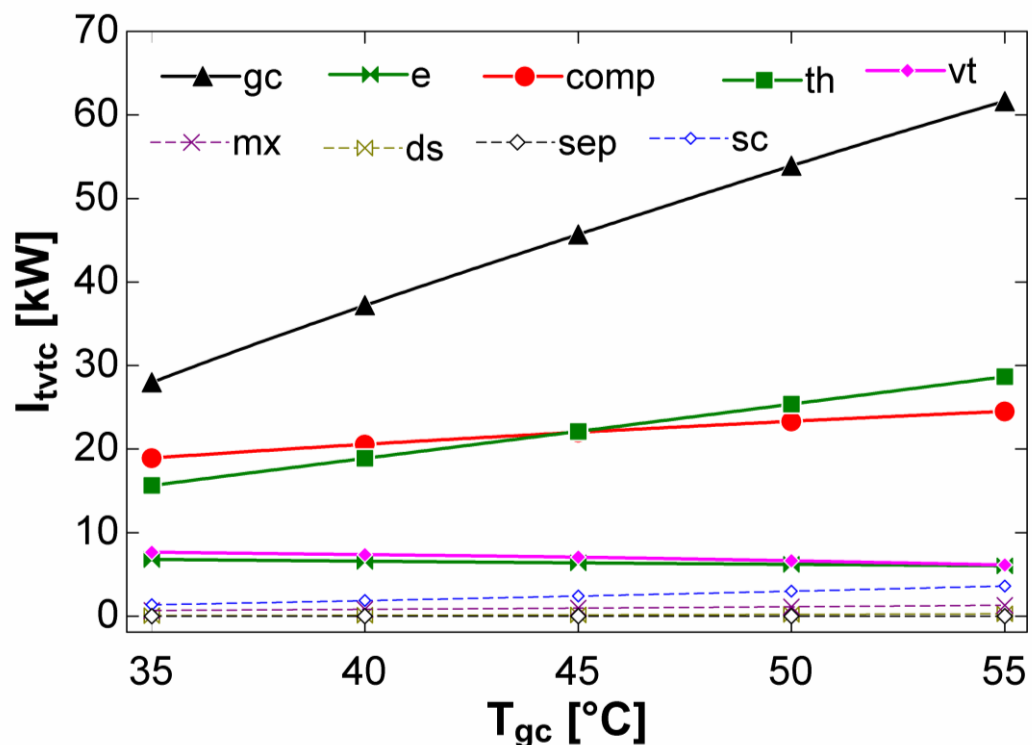


**Fig. 4.11** Effect of gascooler exit temperature on irreversibility of various components of TVTC

**Table 4.9** Effect of gascooler exit temperature on irreversibilities in various components of TVCR

$T_{gc}(^{\circ}C)$	$I_{comp}(kW)$	$I_{gc}(kW)$	$I_e(kW)$	$I_{th}(kW)$
35	18.2	23.6	6.2	25.9
40	19.8	31.2	5.6	29.8
45	21.1	38.3	5.5	33.8
50	22.3	44.8	5.3	37.9
55	23.5	51.1	4.1	42.1

As  $T_{gc}$  increases, the irreversibilities of the compressor, gas cooler, and throttle valve experience an increase; in contrast, the irreversibilities of evaporator and VT

witness a reduction. The increase in  $T_{gc}$  corresponds to an increase in pressure ratio across the compressor. This leads to an increase in compressor power and its discharge temperature, which causes an increase in its irreversibility. Furthermore, with an increase in the pressure ratio, frictional losses are witnessed to increase in the throttle valve, which leads to an augmentation in its irreversibility. Likewise, due to an increase in overall heat rejection, the irreversibility of gascooler increases.

Moreover, as  $T_{gc}$  increases,  $P_{int,opt}$  experiences a decline, which leads to a decrease in the pressure ratio across the VT. This results in a decrease in the irreversibility of VT. A similar trend for irreversibility of VT was observed in Fig. 4.9.

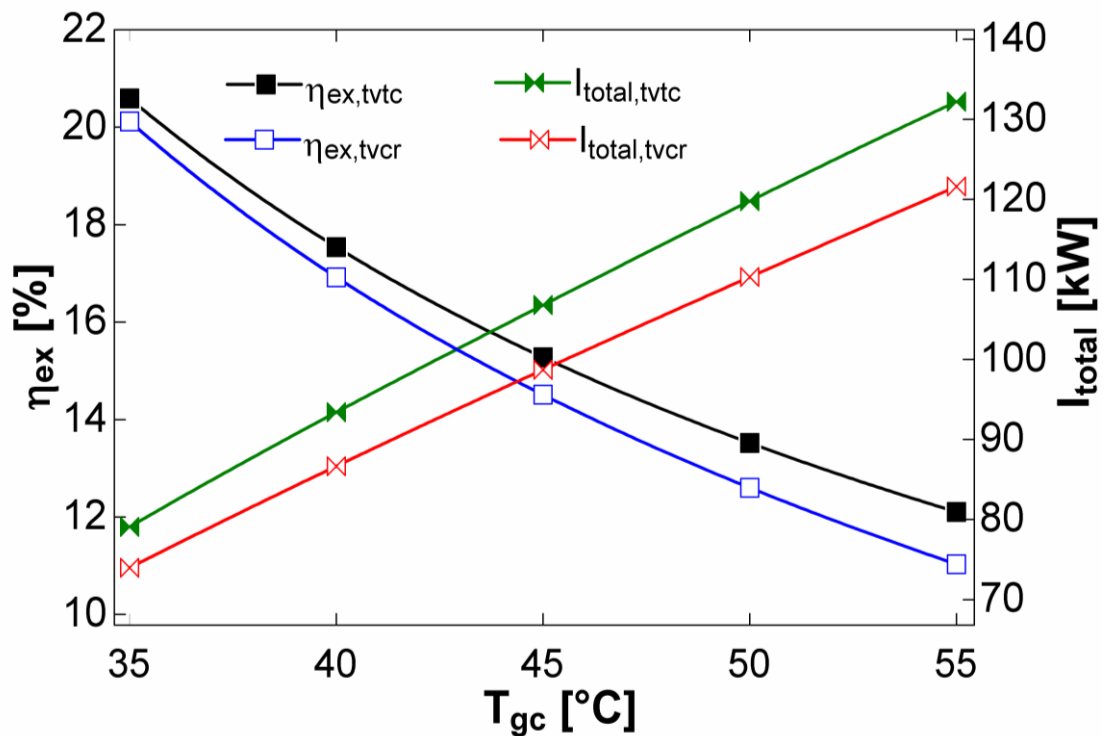


**Fig. 4.12** Effect of gascooler exit temperature on exergetic efficiency and total irreversibility of TVTC and TVCR

Fig. 4.12 illustrates the fluctuation of exergetic efficiency and total irreversibility with  $T_{gc}$  for both cycles. With increase in  $T_{gc}$ , total irreversibility increases while exergetic efficiency decreases. Specifically,  $\eta_{ex,tvtc}$  is noted to be 2.3% higher at  $T_{gc}=35^{\circ}\text{C}$  and 9.7% higher at  $T_{gc}=55^{\circ}\text{C}$  compared to  $\eta_{ex,tvcr}$ . This can be attributed to the fact that the augmented values of irreversibilities in the gascooler

and the evaporator lead to higher total irreversibility for TVTC than that for TVCR. Moreover, as  $T_{gc}$  increases, there is a corresponding increase in EF and a decrease in EP, resulting in a decline in exergetic efficiency.

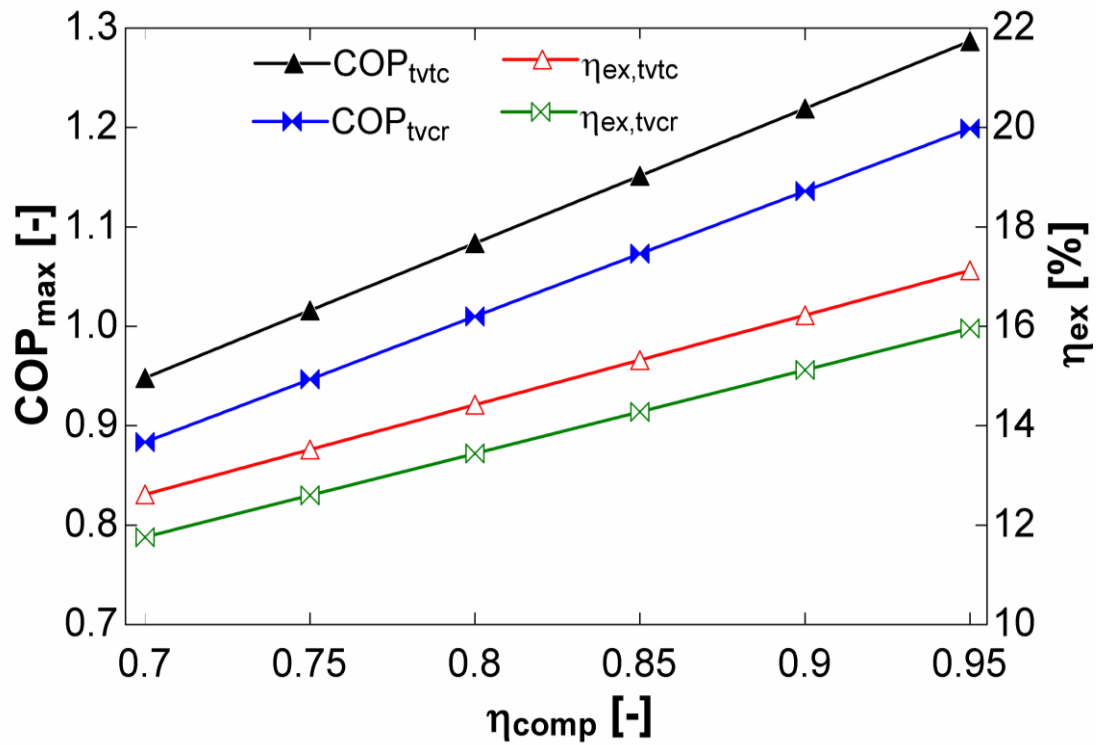


**Fig. 4.13** Effect of isentropic efficiency of compressor on COP and exergetic efficiency of TVCR and TVTC

Fig. 4.13 shows the variation of COP and exergetic efficiency for both cycles with isentropic efficiency of compressor ( $\eta_{comp}$ ). As  $\eta_{comp}$  increases, both COP and exergetic efficiency increase. For the studied range of  $\eta_{comp}$ , COP and exergetic efficiency of TVTC are 7.5% to 7.7% and 7.2% to 7.4%, respectively, higher than those of TVCR. This is due to the fact that as  $\eta_{comp}$  increases, compressor work decreases, and for the constant value of cooling capacity, COP increases for both TVCR and TVTC. Moreover, under ideal conditions when the isentropic efficiency of compressor ( $\eta_{comp}$ ) is 100%, the process in compressor is reversible adiabatic resulting in no change in specific entropy. As  $\eta_{comp}$  decreases due to frictional effects, the temperature at outlet of compressor rises which leads to increase in specific entropy at compressor's discharge. As a result, the entropy change during compression is no

longer zero, but rather positive. Hence, the irreversibility of compressor, as calculated using Eq. (4.31) increases. Moreover, this results in increase in the total irreversibility of cycle and hence decrease in the exergetic efficiency of the cycle, as  $\eta_{comp}$  decreases.

From a mathematical perspective, with an increase in  $\eta_{comp}$ , exergy of fuel (EF, represented by  $W_{tvtc}$ ) decreases while exergy of product (EP, represented by  $Q_{tvtc} \left( \frac{T_o}{T_r} - 1 \right)$ ) remains constant for a given value of  $T_r$ . As a result,  $\eta_{ex}$  increases, as depicted by Eq. (4.36). The reasoning behind the higher values of COP and exergetic efficiency of TVTC than those of TVCR is similar to that of Fig. 4.10.

### 4.5.3 Results of Environment Analysis

Table 4.10 demonstrates the yearly environmental penalty cost of CO<sub>2</sub> emissions per unit cooling capacity for both TVTC and TVCR. It is observed that the environmental penalty cost of TVTC ( $C_{env,tvtc}$ ) is 10.7% to 12.2% and 3.5% to 10.4% lower than that of TVCR ( $C_{env,tvcr}$ ) for the studied range of evaporator temperature and gascooler exit temperature, respectively. This shows that TVTC is more environmental-friendly than TVCR by saving the penalty cost of CO<sub>2</sub> emissions.

**Table 4.10** Yearly penalty cost of CO<sub>2</sub> emission for TVCR and TVTC

$T_e(^{\circ}C)$	$C_{env,tvcr}$ (\$/kW)	$C_{env,tvtc}$ (\$/kW)	$T_{gc}(^{\circ}C)$	$C_{env,tvcr}$ (\$/kW)	$C_{env,tvtc}$ (\$/kW)
-50	830	740	35	290	280
-40	685	620	40	340	330
-30	565	520	45	400	380
-20	465	430	50	460	430
-10	380	350	55	530	480
0	310	280			

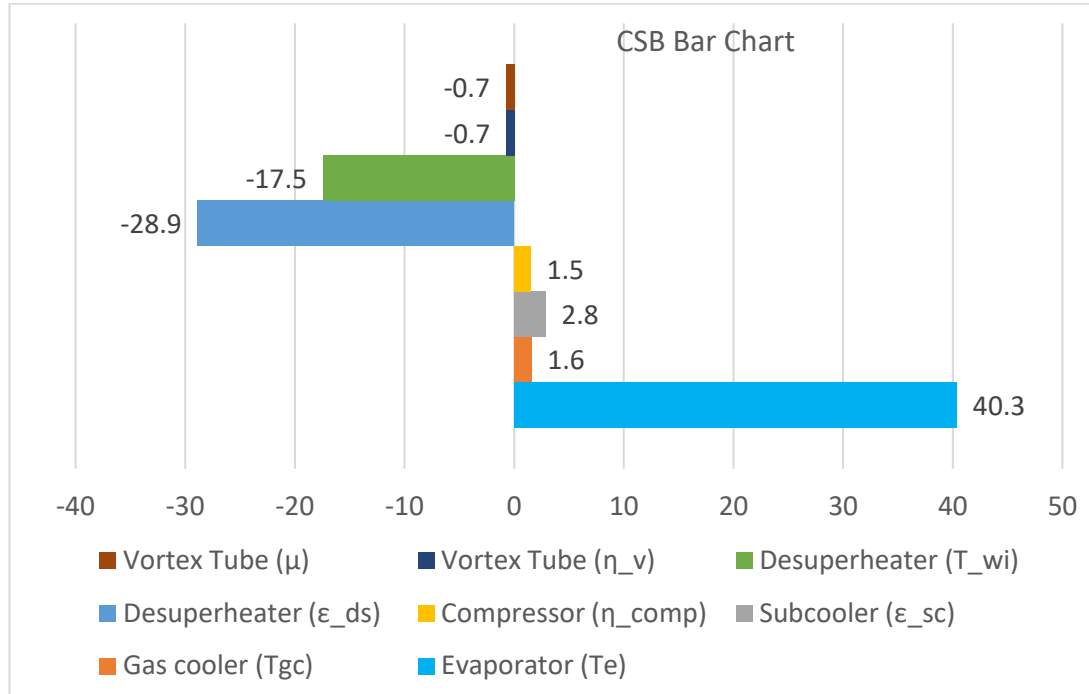
#### 4.5.4 Results of Structural Bond Method

Fig. 4.14 shows the values of the coefficient of structural bond (CSB) for various components of TVTC on the basis of Eq. (4.39) in section 3.5. These CSB values are calculated as written in the next few lines. When  $T_e$  is varied from  $-50^\circ\text{C}$  to  $0^\circ\text{C}$ , the irreversibility of evaporator varies from 8.4 kW to 5.1 kW results in change in total irreversibility from 210.3 kW to 77.2 kW, which gives a CSB value of 40.3. Similarly,  $T_{gc}$  is varied from  $35^\circ\text{C}$  to  $55^\circ\text{C}$ , the irreversibility of gascooler increases from 27.9 kW to 61.6 kW, affecting total irreversibility to increase from 79.1 kW to 132.2 kW, which gives its CSB value of 1.6. Moreover, when  $\eta_{comp}$  is varied from 0.6 to 1, irreversibility of the compressor decreases from 45.3 kW to 0 kW which decreases the total irreversibility from 154.3 kW to 85.2 kW and gives a CSB value of 1.5. Also, when  $\varepsilon_{sc}$  varies from 0.1 to 1, irreversibility of the subcooler increases from 0.6 kW to 3.1 kW which in turn increases the total irreversibility from 114.2 kW to 121.1 kW, which computes the CSB value to 2.8. Although the CSB value of the subcooler is higher than that of the compressor, however, increase in total irreversibility per unit increase in  $\varepsilon_{sc}$  is lower in subcooler than that of compressor. Therefore, the compressor is preferred over the subcooler to affect the overall performance of the system, and thus the parameter ‘isentropic efficiency of compressor’ is selected over the parameter ‘effectiveness of subcooler’.

The variation in irreversibility of VT is governed by two parameters, i.e., the cold mass fraction and isentropic efficiency of VT-nozzle, so is the CSB value. On a similar note, the CSB value of the desuperheater is influenced by two parameters, i.e., the effectiveness of desuperheater ( $\varepsilon_{ds}$ ) and water inlet temperature ( $T_{wi}$ ). Both the calculated CSB values of VT and desuperheater are negative, as depicted in Fig. 4.14, which shows that when the ‘system efficiency parameter’ i.e.,  $z_i$  is varied, then irreversibilities of these components decrease (or increase), which results in increase (or decrease) in the total irreversibility. Since the variation in irreversibility of VT and desuperheater per unit change in associated parameters for these components is not significant, these two components are excluded from the optimization study. Hence, evaporator temperature being the primary parameter, followed by gascooler exit



temperature, and finally, isentropic efficiency of the compressor being the design parameter are selected for optimization study.



**Fig. 4.14** Coefficient of structural bond (CSB) of various components of TVTC

#### 4.5.5 Multi-Objective Optimization

From the above parametric investigation and structural bond analysis, the most sensitive parameters influencing both the energy and exergy performances of TVTC are observed to be evaporator temperature ( $T_e$ ), gascooler exit temperature ( $T_{gc}$ ), and isentropic efficiency of the compressor ( $\eta_{comp}$ ). The performance parameters chosen for multi-objective optimization [149] (MOO) are exergetic efficiency ( $\eta_{ex,tvtc}$ ) and compressor work ( $W_{tvtc}$ ). The choice of these performance factors is based on the fact that  $W_{tvtc}$  indicates the operational cost, whereas  $\eta_{ex,tvtc}$  gives a thermodynamic viewpoint of the system. The input parameters should be optimized by minimising  $W_{tvtc}$  and maximising  $\eta_{ex,tvtc}$  since rise in  $W_{tvtc}$  is unwanted whereas rise in  $\eta_{ex,tvtc}$  is favourable.

Further, regression analysis is conducted by using quadratic model of 'Design Expert software' to obtain equations for performance parameters as a function of input parameters. For the regression analysis, the input parameters with their ranges, are

considered as:  $T_e$  ( $-50^{\circ}\text{C}$  to  $0^{\circ}\text{C}$ ),  $T_{gc}$  ( $35^{\circ}\text{C}$  to  $55^{\circ}\text{C}$ ), and  $\eta_{comp}$  (0.70 to 0.95). The equations obtained from the regression analysis which are to be utilised in the optimization process are as follows:

$$\begin{aligned} \eta_{ex,tvtc} = & 19.9490 - 0.2308 * T_e - 0.8986 * T_{gc} + 33.9512 * \eta_{comp} + 0.000717 \\ & * T_e * T_{gc} - 0.2260 * T_e * \eta_{comp} - 0.56 * T_{gc} * \eta_{comp} - 0.0040 * T_e^2 \\ & + 0.0105 * T_{gc}^2 + 3.752 * \eta_{comp}^2 \end{aligned} \quad (4.40)$$

$$\begin{aligned} W_{tvtc} = & 2.53949 + 0.0730 * T_e - 0.1260 * T_{gc} + 6.989 * \eta_{comp} - 0.001155 * T_e \\ & * T_{gc} + 0.030906 * T_e * \eta_{comp} - 0.036164 * T_{gc} * \eta_{comp} \\ & + 0.000381 * T_e^2 + 0.001001 * T_{gc}^2 - 1.84064 * \eta_{comp}^2 \end{aligned} \quad (4.41)$$

These two objective functions are optimized simultaneously and results are obtained using MATLAB software. In the current study, MOO has been conducted using genetic algorithm (GA)[150], which is a well-known technique to find the optimum solutions. A collection of optimal solutions resulting from trade-off between aforementioned objectives has been obtained and represented as ‘pareto optimal front’, as shown in

Fig. 4.15. These optimal solutions can be considered as several design points, for which system performance can be predicted. Among these points, three design points are arbitrarily selected i.e., ‘P’, ‘Q’ and ‘R’ to explain their significance from application point of view. Both ‘P’ and ‘R’ are the extreme points on the presented pareto front and ‘Q’ lies somewhere in the middle of ‘P’ and ‘R’. It is found that for all these points,  $T_{gc}$  is almost constant while  $T_e$  varies significantly, and  $\eta_{comp}$  is changing marginally. Also, as one moves from ‘P’ to ‘Q’, cooling capacity increases.

At ‘P’, both exergetic efficiency and compressor work have the highest values among all the points, and the evaporator temperature is in the vicinity of  $-40^{\circ}\text{C}$ . Since the exergy of product at this point is highest, which leads to maximum exergetic efficiency. Moreover, at ‘R’, both exergetic efficiency and compressor work have the lowest values among all the points, and the evaporator temperature is in the vicinity of  $0^{\circ}\text{C}$ . Also, at ‘Q’, both the objective functions have values between those of ‘P’ and

'R', and the evaporator temperature was found to be in the vicinity of -18 °C. The explanation for this is similar to that of 'P'. The abovementioned points (design points) on the pareto optimal front can be suitably utilised for various applications. Such as 'P', 'Q', and 'R' can be utilised for deep freezing applications, ice production, and water chilling plant applications, respectively. Moreover, the most optimised design points for the compressor have been obtained for  $\eta_{comp}$  of 0.905 and above. One of the purposes of this optimization study is to minimise compressor work; therefore, optimal solutions are obtained for higher values of compressor efficiency range (0.90 to 0.95).

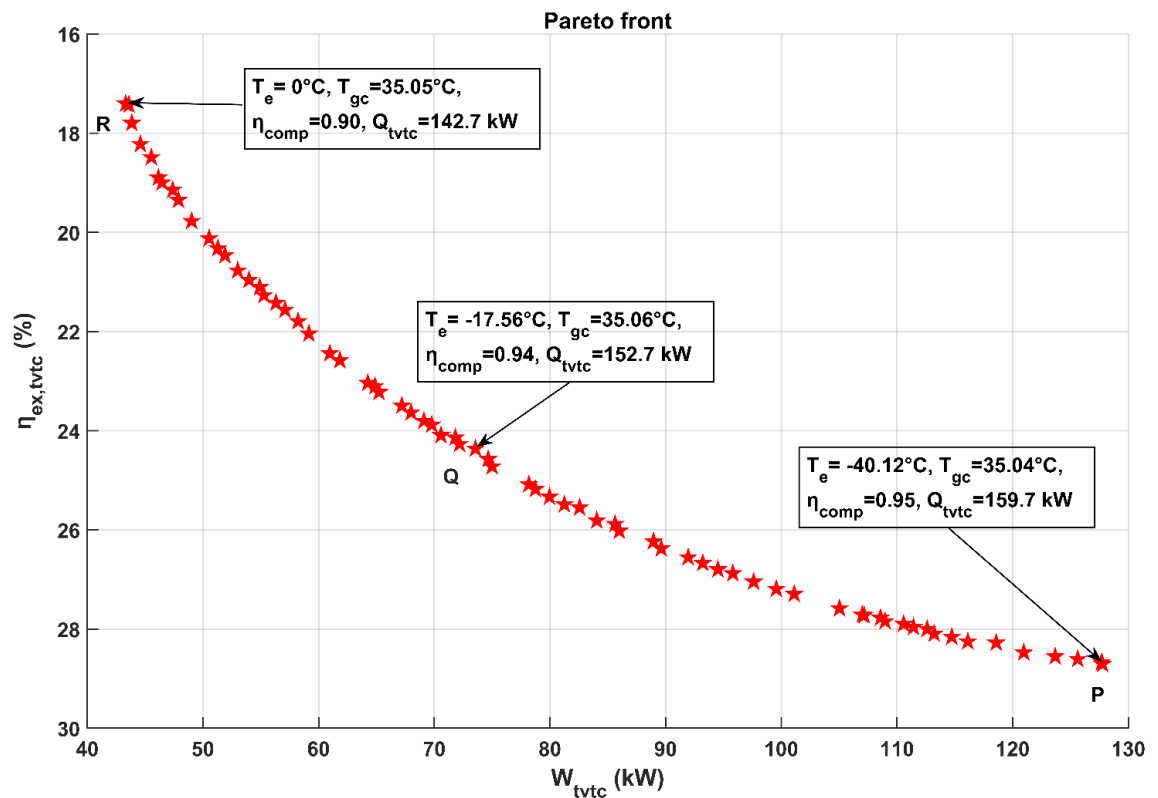


**Fig. 4.15** Pareto optimality obtained between compressor power and exergetic efficiency of TVTC

## CHAPTER 5: ECONOMIC ANALYSIS OF VORTEX TUBE COUPLED WITH TRANSCRITICAL AND SUBCRITICAL VAPOUR COMPRESSION REFRIGERATION SYSTEMS

### 5.1 INTRODUCTION

This chapter aims to conduct an economic analysis of the vortex tube integrated with the transcritical vapour compression refrigeration cycle (TVTC) and the subcritical vapour compression refrigeration cycle (VTC), and to compare the findings with those of the simple transcritical vapour compression cycle (TVCR). The cost rate of the plant system is primarily influenced by three factors: capital investment and maintenance costs, operational costs, and environmental penalty costs.

### 5.2 METHODOLOGY

#### 5.2.1 Assumptions

1. The cost functions of different components remain constant throughout the operational period of the system.
2. The system's performance is assumed to remain constant throughout the specified operational period.
3. Various conversion factors for this analysis are assumed to remain constant throughout the specified operational period of the system.
4. The expenses associated with the connection of pipelines and joints have been overlooked.

The heat transfer area for various heat exchangers can be calculated by the following equation.

$$A = \frac{Q}{U * LMTD} \quad (5.1)$$

Following the computation of the areas for different heat exchangers, their costs are determined using the cost functions presented in Table 5.1. The cost of the vortex tube is significantly lower than that of other components; consequently, the cost of the vortex tube has been disregarded[10].

**Table 5.1** Cost functions for various components of TVTC

S.No.	Components	Cost function (\$) [10, 151-154]
1.	Compressor (comp)	$C_{comp} = 9624.2 * W_{comp}^{0.46}$
2.	Throttle vale (th)	$C_{th} = 114.5 * \dot{m}_{th}$
3.	Evaporator (evap)	$C_{evap} = 1397 * A_{evap}^{0.89}$
4.	Gascooler (gc)	$C_{gc} = 2382.9 * A_{gc}^{0.68}$
5.	Separator (sep)	$C_{sep} = 280.3 * \dot{m}_{sep}$
6.	Subcooler (sub)	$C_{sub} = 383.5 * A_{sub}^{0.65}$
7.	Desuperheater (ds)	$C_{ds} = 2143 * A_{ds}^{0.514}$
8.	Vortex Tube (vt)	$C_{vt} = 0$

After calculating the cost for various components, total cost ( $C_k$ ) in dollars is calculated by Eq. (5.2)

$$C_k = C_{evap} + C_{gc} + C_{sub} + C_{sep} + C_{comp} + C_{th} + C_{vt} + C_{ds} \quad (5.2)$$

The plant cost rate (\$/year) can be calculated by the following expression:

$$\dot{C}_{plant} = \dot{C}_{CI\&OM} + \dot{C}_{OP} + \dot{C}_{env} \quad (5.3)$$

The above plant cost rate is composed of three components, first, capital investment and maintenance cost ( $\dot{C}_{CI\&OM}$ ), second, operational cost ( $\dot{C}_{OP}$ ) means cost associated with the electricity consumption, and third, environmental penalty cost ( $\dot{C}_{env}$ ).

The capital investment cost and maintenance cost in (\$/year) is given by Eq. (5.4)

$$\dot{C}_{CI\&M} = C_k * \Phi * CRF \quad (5.4)$$

Where,  $\Phi$  is the maintenance factor and CRF is the capital recovery factor, which is given below:

$$CRF = \frac{i(i+1)^n}{i(i+1)^n - 1} \quad (5.5)$$

where  $i$  is the interest rate in percentage and  $n$  is the plant lifetime in years.

The operational cost of system in \$/year is given by Eq. (5.6):

$$\dot{C}_{OP} = t_{op} * W_{comp} * \alpha_{elec} \quad (5.6)$$

Where,  $t_{op}$  is annual operation hour of the plant and  $\alpha_{elec}$  is cost of electrical power consumption in USD/kWh.

The environment penalty cost (\$/year) is given by Eq. (5.7) and Eq. (5.8):

$$\dot{C}_{env} = m_{CO_2} * C_{CO_2} \quad (5.7)$$

$$m_{CO_2} = \lambda_{CO_2} * W_{comp} * t_{op} \quad (5.8)$$

Where,  $m_{CO_2}$  is mass of  $CO_2$  emitted in the environment,  $C_{CO_2}$  is the cost of capturing the  $CO_2$  emitted and  $\lambda_{CO_2}$  is the emission factor.

By substituting values of Eqs (5.4), (5.6) and (5.7) in Eq (5.3), the total plant cost rate (\$/year) of the system can be calculated.

### 5.3 RESULTS AND DISCUSSION

In this section, economic analysis of TVTC and VTC has been shown. The effect of operating and performance parameters on various costs per year of the system has been demonstrated for both the systems. Table 5.2 shows the input data for various parameters for economic analysis of TVTC and VTC.

**Table 5.2** Input data for various parameters for economic analysis of TVTC and VTC

S.No.	Parameters	Values [151, 155, 156]
1.	Overall heat transfer coefficient of evaporator ( $U_e$ )	0.03 kW m <sup>-2</sup> K <sup>-1</sup>
2.	Overall heat transfer coefficient of gascooler ( $U_{gc}$ )	0.03 kW m <sup>-2</sup> K <sup>-1</sup>
	Overall heat transfer coefficient of condenser ( $U_c$ )	0.03 kW m <sup>-2</sup> K <sup>-1</sup>
3.	Overall heat transfer coefficient of subcooler ( $U_{sub}$ )	0.01 kW m <sup>-2</sup> K <sup>-1</sup>
4.	Overall heat transfer coefficient of desuperheater ( $U_{ds}$ )	0.15 kW m <sup>-2</sup> K <sup>-1</sup>
5.	Temperature difference between air and refrigerant in evaporator and gascooler/ condenser	10 K
6.	Maintenance factor ( $\Phi$ )	1.06
7.	Interest rate ( $i$ )	15%
8.	Plant lifetime ( $n$ )	10 years
9.	Annual operational hour ( $t_{op}$ )	5000 h
10.	Electrical power cost ( $\alpha_{elec}$ )	0.075 USD/kWh
11.	Emission factor ( $\lambda_{CO_2}$ )	0.968 kg/kWh
12.	Cost of CO <sub>2</sub> avoided ( $C_{CO_2}$ )	0.09 USD/kg of CO <sub>2</sub> emission
13.	Cooling Capacity or plant cooling load (Q)	100 kW
14.	Evaporator temperature ( $T_e$ )	0° C
15.	Condenser temperature( $T_c$ ), Gascooler exit temperature ( $T_{gc}$ )	50° C
16.	Isentropic efficiency of compressor ( $\eta_{comp}$ )	0.85 ( in TVTC), 0.75 ( in VTC)
17.	Effectiveness of various heat exchangers	0.9

### 5.3.1 Economic Analysis of TVTC

In this section, effect of evaporator temperature, condenser temperature and cooling capacity has been observed on capital investment and maintenance cost, operation cost, environmental penalty cost and plant cost per year of TVTC.

#### 5.3.1.1 Effect of evaporator temperature on costs of TVTC

Fig. 5.1 illustrates the impact of evaporator temperature on total plant cost, capital investment, maintenance cost, and environmental penalty cost of TVTC. In this scenario, the evaporator temperature is the sole variable, while all other parameters remain constant. As the evaporator temperature increases, both the environmental penalty cost and operational cost decrease. Since both these costs are dependent on the compressor power and as the evaporator temperature increases, compressor power decreases for the given value of cooling capacity or plant cooling load.

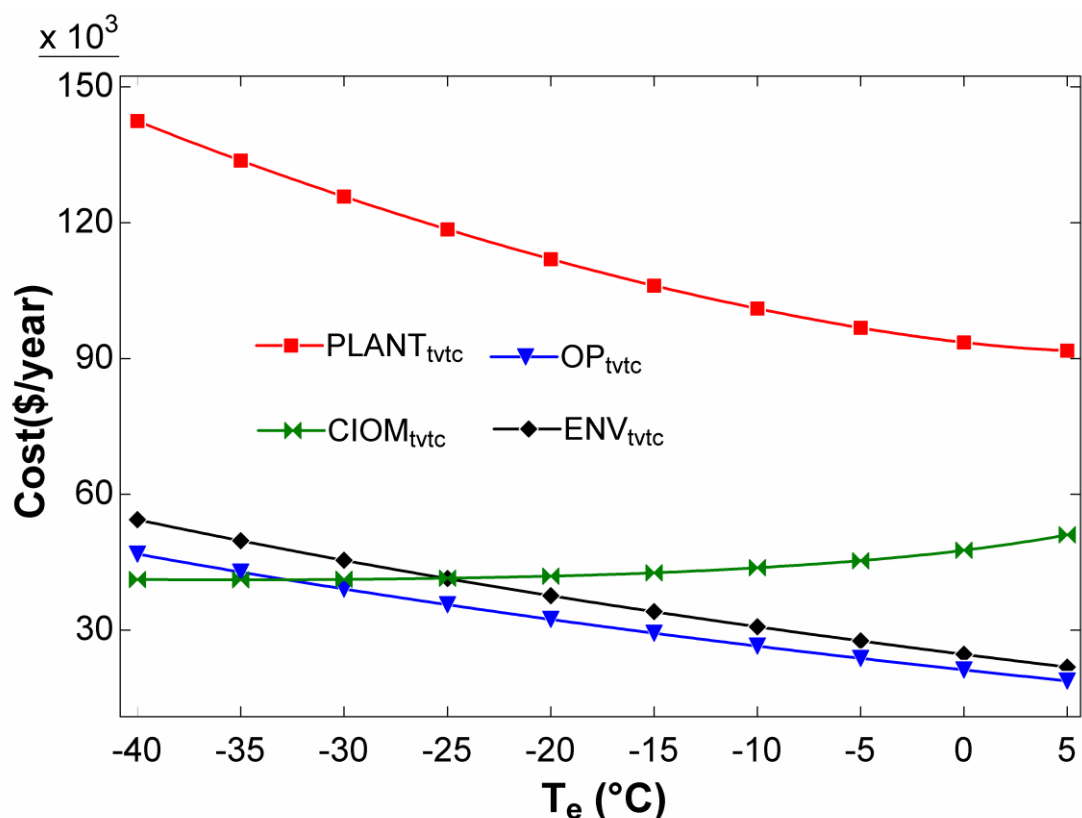


**Fig. 5.1** Effect of evaporator temperature on various costs of TVTC

Furthermore, an increase in evaporator temperature results in a decrease in total plant cost. Total plant cost is determined by three factors: operational cost, environmental



penalty cost, and capital investment & maintenance cost. The initial two costs decline, whereas the third cost experiences a slight increase as the evaporator temperature rises. Consequently, the reduction in operational costs and environmental penalty costs outweighed the third factor. Therefore, the total cost of the plant decreases as the evaporator temperature increases.

### 5.3.1.2 Effect of gascooler exit temperature on costs of TVTC

Fig. 5.2 illustrates the impact of gas cooler exit temperature on total plant cost, capital investment & maintenance cost, and environmental penalty cost of the TVTC system. As gascooler temperature rises, operational costs and environmental penalty costs increase, whereas capital investment and maintenance costs decrease. Furthermore, an increase in the gascooler exit temperature correlates with an increase in total plant load. The same reasoning applies here as outlined in the preceding paragraph.

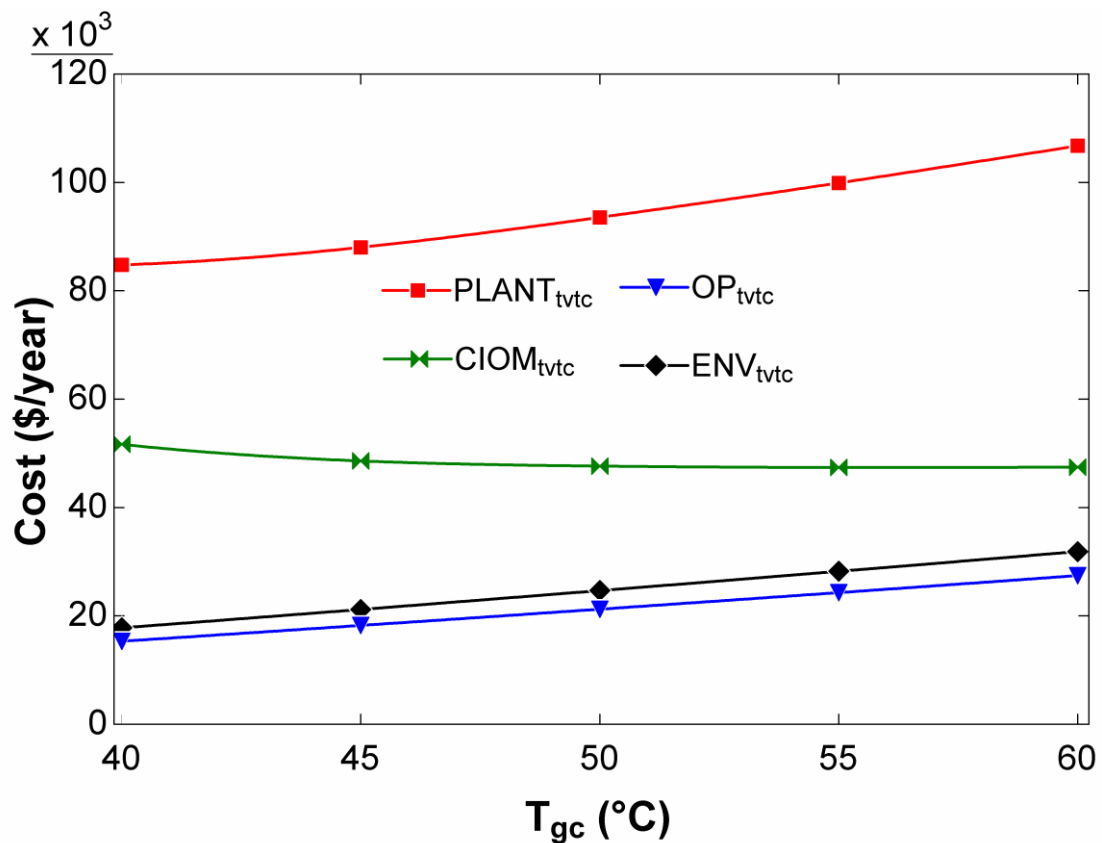
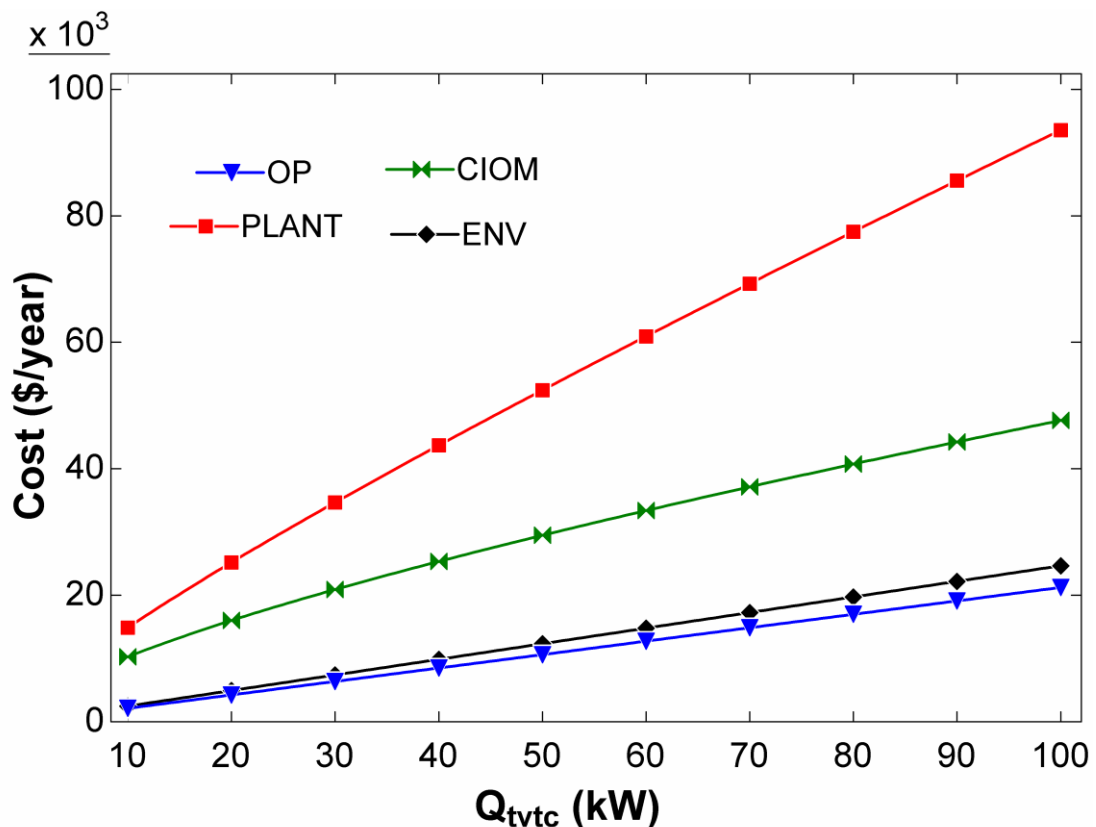


Fig. 5.2 Effect of gascooler exit temperature on various costs of TVTC

### 5.3.1.3 Effect of cooling capacity on costs of TVTC

Fig. 5.3 illustrates the relationship between cooling capacity and the total costs associated with the plant, including capital investment & maintenance expenses, and environmental penalty costs of the TVTC. In this case, the temperatures at the exit of both the evaporator and the gas cooler are considered. With an increase in cooling load, there is a corresponding rise in all cost parameters. This phenomenon can be articulated as an increase in cooling load correlating with a larger heat exchange area and elevated compressor work or electricity consumption. This will result in an increase in all three costs, thereby raising the overall plant cost.



**Fig. 5.3** Effect of cooling capacity on various costs of TVTC

### 5.3.1.4 Comparison of plant cost between TVTC and TVCR

Table 5.3 illustrates the impact of evaporator and gas cooler exit temperatures on the total plant costs of TVTC and TVCR. The plant cost of TVCR is observed to be 6.8% to 0.8% and 1% to 7.3% higher than that of TVTC, corresponding to the specified

range of evaporator temperature and gas cooler exit temperature, respectively. This supports the application of vortex tubes in transcritical vapour compression cycles from an economic standpoint. Furthermore, TVTC is cost effective at lower and higher values of evaporator and gas cooler exit temperatures, respectively.

**Table 5.3** Comparison of plant cost of TVTC and TVCR with variation of evaporator and gascooler temperature

$T_e$ (°C)	$\dot{C}_{plant,tvtc}$ (\$/year)	$\dot{C}_{plant,tvcr}$ (\$/year)	$T_{gc}$ (°C)	$\dot{C}_{plant,tvtc}$ (\$/year)	$\dot{C}_{plant,tvcr}$ (\$/year)
-40	142400	152100	40	84000	84800
-30	125700	132300	45	88000	90100
-20	111900	116400	50	93500	96000
-10	101000	104100	55	99900	104400
0	93100	93800	60	106700	114500

### 5.3.2 Economic Analysis of VTC

In this section, effect of evaporator temperature, condenser temperature and cooling capacity has been observed on capital investment and maintenance cost, operation cost, environmental penalty cost and plant cost per year of VTC.

#### 5.3.2.1 Effect of evaporator temperature on various costs of VTC

Fig. 5.4 illustrates the impact of evaporator temperature on total plant cost, capital investment, maintenance cost, and environmental penalty cost of TVTC. In this case, the evaporator temperature is the sole variable, while all other parameters remain constant. As the evaporator temperature increases, both the environmental penalty cost and operational cost decrease. Since both these costs are dependent on the compressor power and as the evaporator temperature increases, compressor power decreases for the given value of cooling capacity or plant cooling load. Furthermore, an increase in evaporator temperature results in a decrease in total plant cost. Total plant cost is determined by three factors: operational cost, environmental penalty cost, and capital investment & maintenance cost. The initial two costs decrease, whereas the third cost experiences a slight increase as the evaporator temperature rises. Consequently, the reduction in operational costs and environmental penalty costs dominate the capital

investment & maintenance cost. Therefore, the total cost of the plant decreases as the evaporator temperature increases.

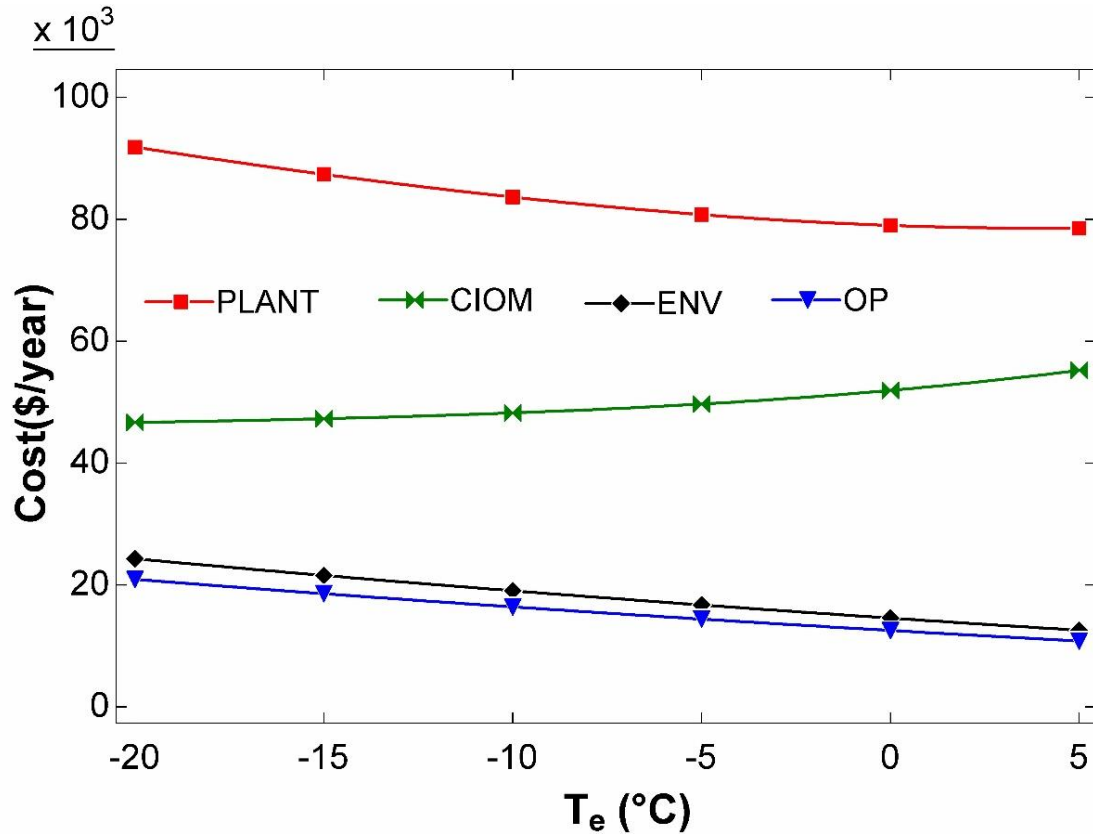


**Fig. 5.4** Effect of evaporator temperature on various costs of VTC

### 5.3.2.2 Effect of condenser temperature on various costs of VTC

Fig. 5.5 illustrates the impact of condenser temperature on total plant cost, capital investment & maintenance cost, and environmental penalty cost of the VTC system. As gascooler temperature rises, operational costs and environmental penalty costs increase, whereas capital investment and maintenance costs slightly increases. Furthermore, an increase in the condenser temperature correlates with an increase in total plant load. The same reasoning applies here as outlined in the preceding paragraph.

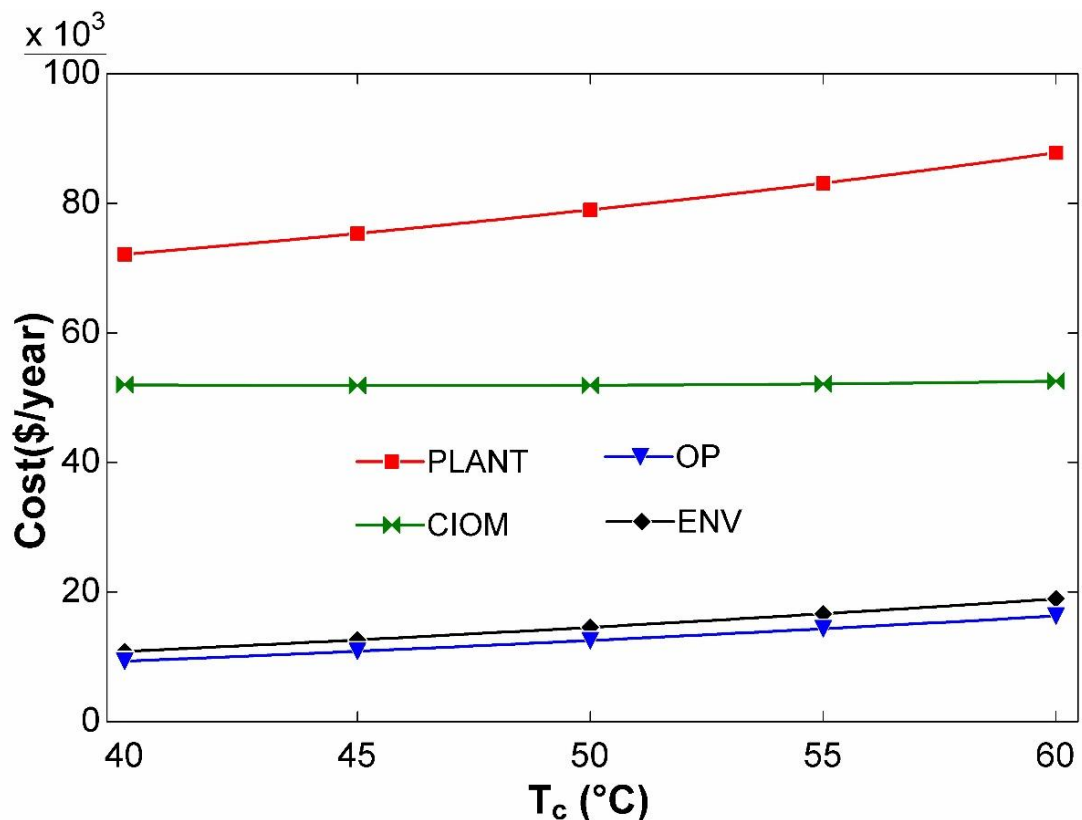


**Fig. 5.5** Effect of condenser temperature on various costs of VTC

### 5.3.2.3 Effect of cooling capacity on various costs of VTC

Fig. 5.6 illustrates the relationship between cooling capacity and various costs of VTC. With an increase in cooling load, there is a corresponding rise in all cost parameters. This phenomenon can be articulated as an increase in cooling load correlating with a larger heat exchange area and elevated compressor work or electricity consumption. This will result in an increase in all three costs, thereby raising the overall plant cost.

### 5.3.2.4 Comparison of plant cost between VTC and VCR

Table 5.4 illustrates the impact of evaporator and gas cooler exit temperatures on the total plant costs of VTC and VCR. The plant cost of VCR is observed to be 16.7% to 10.4% and 7.5% to 17% higher than that of VTC, corresponding to the specified range of evaporator temperature and condenser temperature, respectively. This supports the application of vortex tubes in subcritical vapour compression cycles from an economic standpoint. Furthermore, VTC is cost effective at lower and higher values of evaporator and gas cooler exit temperatures, respectively.

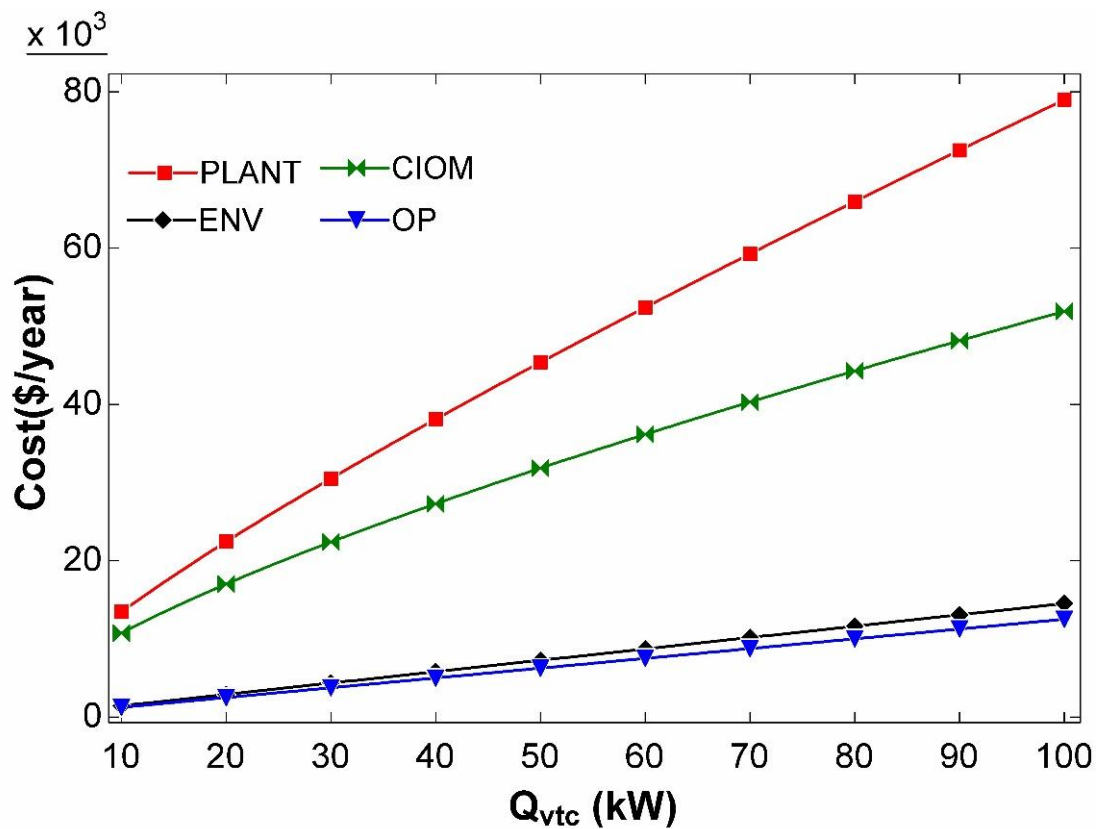


**Fig. 5.6** Effect of cooling capacity on various costs of VTC

**Table 5.4** Comparison of plant cost of VTC and VCR with variation of evaporator and gascooler temperature

$T_e$ (°C)	$\dot{C}_{plant,vtc}$ (\$/year)	$\dot{C}_{plant,vcr}$ (\$/year)	$T_c$ (°C)	$\dot{C}_{plant,vtc}$ (\$/year)	$\dot{C}_{plant,vcr}$ (\$/year)
-20	91846	107174	40	72145	77585
-15	87385	100929	45	75351	82666
-10	83651	95689	50	79002	88402
-5	80768	91473	55	83120	94997
0	79002	88402	60	87816	102760
5	78558	86774			

## CHAPTER 6: COMPUTATIONAL FLUID DYNAMICS (CFD) STUDY OF VORTEX TUBE

### 6.1 INTRODUCTION

This chapter deals with computational fluid dynamics study of vortex tube using compressed air as a working fluid. The objectives of this chapters are as follows:

- To improve the thermal performance or energy separation phenomenon of vortex tube by suitable geometrical modification.
- To see the effect of air entry angle on cold exit of vortex tube.
- To find the optimum air entry angle for maximum temperature drop at cold exit.

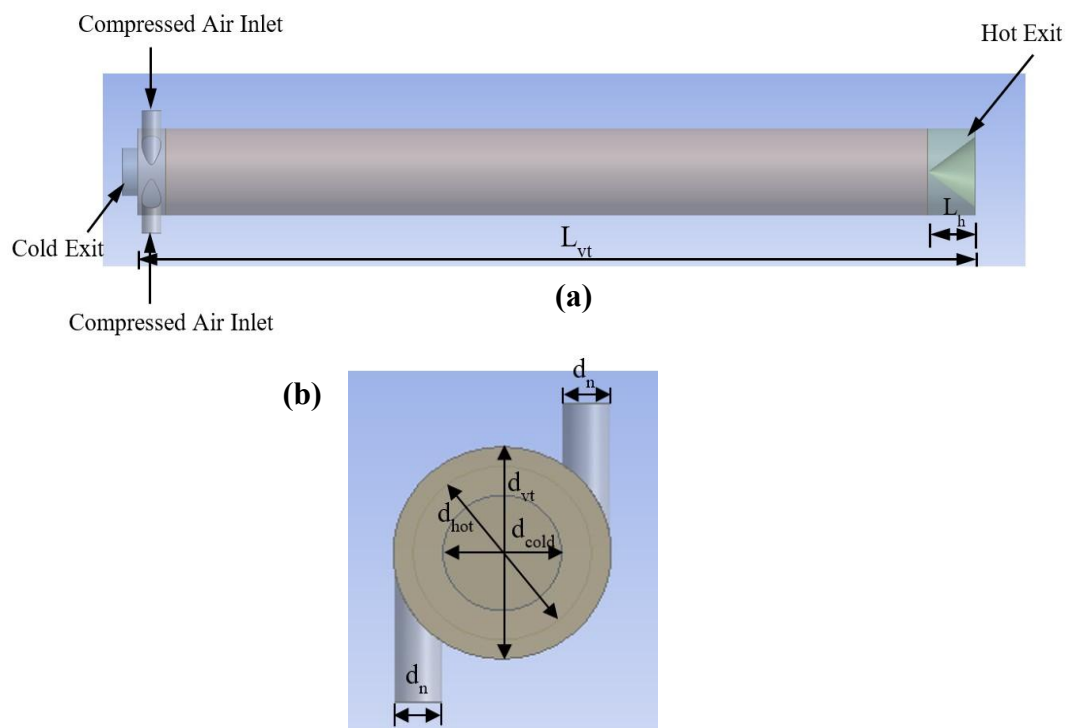
### 6.2 GEOMETRICAL DESCRIPTION

Fig. 6.1 illustrates the geometrical configuration of the counter flow vortex tube. The identical geometry is utilised for the study of computational fluid dynamics (CFD). The vortex tube consists of several components, including a cold orifice, a hot conical valve, a vortex generator with two openings for air entry, and the main vortex body where the energy separation phenomenon occurs. Table 6.1 presents the dimensions of the vortex tube[157].

This study examines the impact of geometrical modification on thermal performance of vortex tube by examining the impact of air entry angles on the temperature drop at cold exit. Fig. 6.2 depicts the different nozzle entry angles ranging from 0° to 5°, illustrating the entry of compressed air through two openings. All other dimensions remain constant while only the entry angle is varied.

**Table 6.1** Dimensions of vortex tube

S. No.	Geometrical Features	Dimensions (mm)
1.	Diameter of nozzle ( $d_n$ )	2.4
2.	Diameter of cold orifice ( $d_{cold}$ )	6.2
3.	Diameter of vortex tube ( $d_{vt}$ )	11.4
4.	Diameter of hot control valve ( $d_{hot}$ )	9.3
5.	Length of vortex tube ( $L_{vt}$ )	106
6.	Length of cold orifice ( $L_{cold}$ )	3
7.	Length of hot control valve ( $L_{hot}$ )	9.3
8.	Half cone angle of hot control valve ( $\theta_{hot}$ )	37.8°



**Fig. 6.1** Geometrical configuration of counter flow vortex tube (a) Front view (b) side view



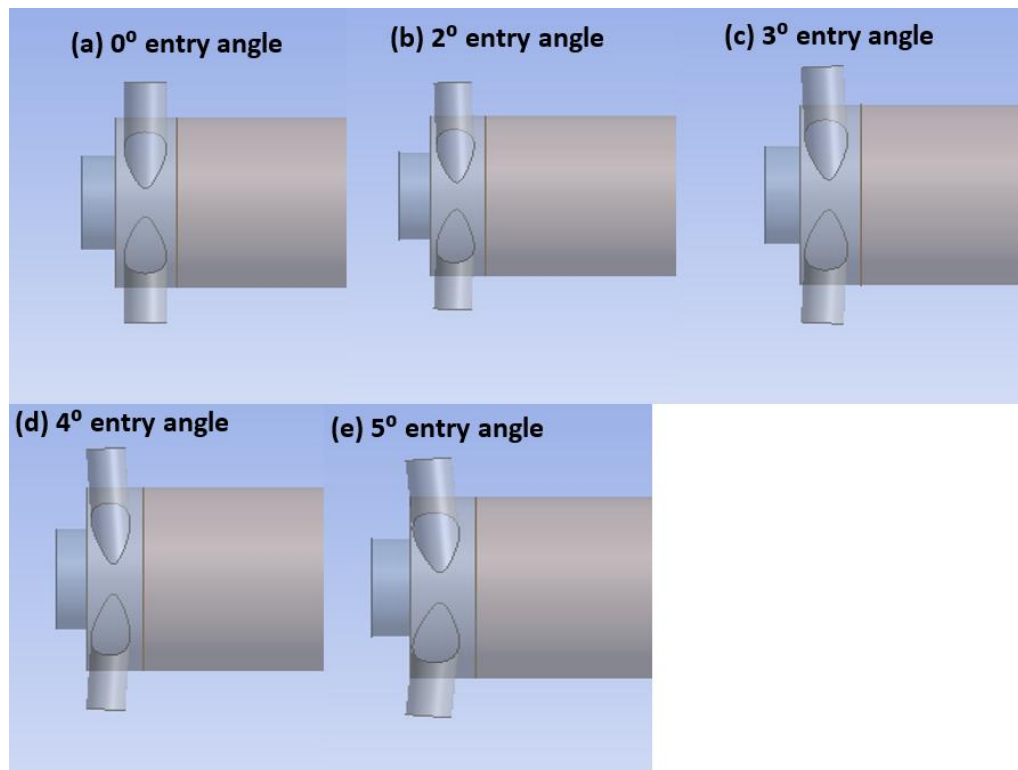


**Fig. 6.2** Various nozzle entry angles (a) 0° (b) 2° (c) 3° (d) 4° (e) 5°

### 6.3 NUMERICAL MODELLING

Numerical modelling is performed using the computational fluid dynamics study using ANSYS Fluent 2022R1 software. The configuration of the system is 12<sup>th</sup> Gen Intel(R) Core (TM) i7-12700 2.10 GHz, 16 GB RAM, 12 cores. The geometrical model of the VT is designed by the design modeller of the ANSYS Fluent 2022R1 workbench. The computational cost and time optimisation in the simulation process is done by performing Grid Independence (GI) test. The

#### 6.3.1 Governing Equations

The compressible turbulent and highly rotating flow inside the vortex tube is assumed to be three-dimensional, steady state and employs the standard  $k - \varepsilon$  turbulence model on basis of finite volume method. Rafiee et al. [158] showed that the  $k - \varepsilon$  model can be selected to simulate the effect of turbulence inside the computational domain of vortex tube. Consequently, the governing equations are arranged by the conservation

of mass, momentum and energy equations. The turbulence kinetic energy ( $k$ ) and the rate of dissipation ( $\varepsilon$ ) are obtained from the following equations:

$$\frac{\partial}{\partial t}(\rho k) + \frac{\partial}{\partial x_i}(\rho k u_i) = \frac{\partial}{\partial x_j} \left[ \left( \mu + \frac{\mu_t}{\sigma_k} \right) \frac{\partial k}{\partial x_j} \right] + G_k + G_b - \rho \varepsilon - Y_M \quad (6.1)$$

$$\frac{\partial}{\partial t}(\rho \varepsilon) + \frac{\partial}{\partial x_i}(\rho \varepsilon u_i) = \frac{\partial}{\partial x_j} \left[ \left( \mu + \frac{\mu_t}{\sigma_\varepsilon} \right) \frac{\partial \varepsilon}{\partial x_j} \right] + C_{1\varepsilon} \frac{\varepsilon}{k} (G_k + C_{3\varepsilon} G_b) - C_{2\varepsilon} \rho \frac{\varepsilon^2}{k} \quad (6.2)$$

In these equations,  $G_k$ ,  $G_b$ , and  $Y_M$  represent the generation of turbulence kinetic energy due to the mean velocity gradients, the generation of turbulence kinetic energy due to buoyancy and the contribution of the fluctuating dilatation in compressible turbulence to the overall dissipation rate, respectively.  $C_{1\varepsilon}$  and  $C_{3\varepsilon}$  are constant.  $\sigma_k$  and  $\sigma_\varepsilon$  are the turbulent Prandtl numbers. The turbulent (or eddy) viscosity,  $\mu_t$ , is computed as follows:

$$\mu_t = \rho C_\mu \frac{k^2}{\varepsilon} \quad (6.3)$$

Where,  $C_\mu$  is a constant. The model constants  $C_{1\varepsilon}$ ,  $C_{2\varepsilon}$ ,  $C_\mu$ ,  $\sigma_k$  and  $\sigma_\varepsilon$  have the following default values:  $C_{1\varepsilon} = 1.44$ ,  $C_{2\varepsilon} = 1.92$ ,  $C_\mu = 0.09$ ,  $\sigma_k = 1.0$ ,  $\sigma_\varepsilon = 1.3$  and both energy and wall Prandtl numbers are 0.85.

### 6.3.2 Mesh Information

The 3D CFD mesh grid of vortex tube is shown in Fig. 6.3. Various meshing methods have been used for the generation of 3D CFD mesh. The vortex tube geometry has been partitioned in four sections for separate meshing method in particular section of vortex tube. Those sections of vortex tube are, cold end, hot end, vortex generator and main vortex body. The mesh methods used for main vortex body and cold end are sweep method followed by inflation. The meshing method used for hot end is path confirming method which in turn gives tetrahedron mesh elements. The mesh method used for vortex generator is automatic method. The total number of elements in the mesh grid are 1870916 and total numbers of nodes are 1861408 in the mesh grid as shown in Fig. 6.3.

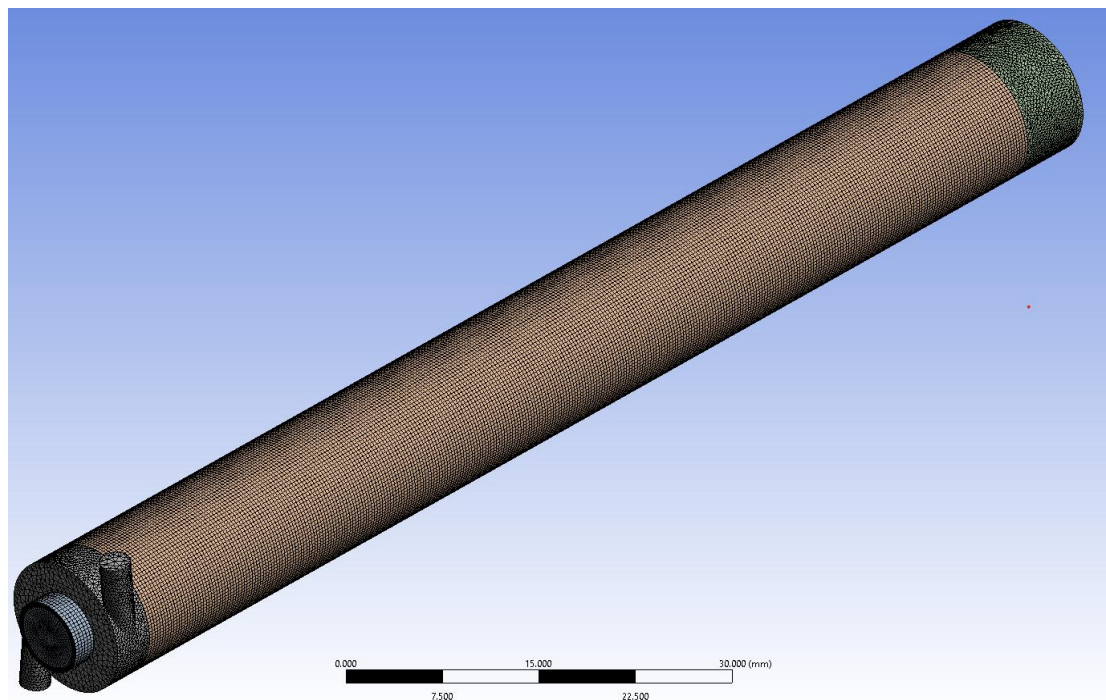


**Fig. 6.3** 3D CFD Mesh Grid of Vortex Tube with 1870916 elements

### 6.3.3 Boundary Conditions

The boundary condition for the present study has been illustrated in Table 6.2. The inlet to VT is modeled as 'pressure inlet' and both the outlets i.e., cold exit and hot exit are modeled as 'pressure outlet'. The boundary condition at inlet are 4.84 bar of pressure and 294 K temperature, kept fixed according the previous experimental study. For the outlet boundary condition, pressure at cold exit is ambient while pressure at hot exit is slightly higher than ambient i.e. 0.7 bar gauge pressure. A no-slip boundary condition is used on all walls of the system. The standard  $k - \varepsilon$  turbulence model has been selected with standard wall function for 3D CFD study. In the solution method, SIMPLE is taken under consideration for Pressure-velocity coupling. Moreover, in spatial discretization, second order upwind is used for density, momentum, turbulent kinetic energy, turbulent dissipation rate and energy in order to simulate the phenomenon of flow pattern and temperature separation in a vortex tube with the variation of air entry angle by using the FLUENT software package of ANSYS 2022 R1. The gradient method is considered as 'Least square cell based' and second order is used for pressure. The under-relaxation factors for various term are as

follows; pressure= 0.3, density =1, body force = 1, momentum= 0.7, turbulent kinetic energy = 0.8, turbulent dissipation rate = 0.8, turbulent viscosity and energy =1.

**Table 6.2** Boundary condition of the vortex tube

	Gauge Pressure (bar)	Temperature (K)
Inlet	4.84 bar	294
Cold outlet	0	---
Hot outlet	0.7 bar	---

### 6.3.4 Grid Independence

In Computational Fluid Dynamics (CFD), a grid independence test, or mesh independence test, is an essential procedure to verify that the numerical outcomes are not influenced by the mesh size. It ensures that the selected mesh is sufficiently refined to capture critical flow characteristics while avoiding excessive refinement that would elevate computational costs without enhancing accuracy. A grid independence test entails executing the same simulation repeatedly with progressively finer meshes and analysing the results. The goal is to identify the point at which additional mesh refinement yields minimal alterations in results. The procedure for the grid independence test is outlined as follows:

- Choose various mesh sizes and initiate computation with a coarse mesh, subsequently refining it progressively.
- Execute the identical simulation on each mesh utilizing the same boundary conditions and solver configurations.
- When the variation in outcomes between consecutive mesh refinements becomes insignificant, the solution is said to be grid independent.

Fig. 6.4 illustrates the temperature differentials at the cold end for various element or mesh sizes. Initially, for the specified boundary conditions and computational model, a mesh size of 2 mm is employed, resulting in a temperature differential of less than 5 K at the cold exit. Furthermore, as the element size increases, the temperature differential begins to rise. Beyond a specific element size, the temperature differential at the cold end remains relatively stable. Figure 6.4 illustrates that the temperature

differences at the cold end are 31.27 K (at point A), 31.31 K (at point B), and 31.41 K (at point C) for element sizes of 0.3 mm, 0.25 mm, and 0.2 mm, respectively. The temperature differences are nearly identical, indicating that the results are independent of mesh size. Point C provides a more accurate solution at an element size of 0.2 mm; however, this significantly increases the computational time compared to Point A. Consequently, point A has been selected, with an element size of 0.3 mm, which conserves computational time relative to the 0.2 mm element size at point C, while yielding nearly identical results.

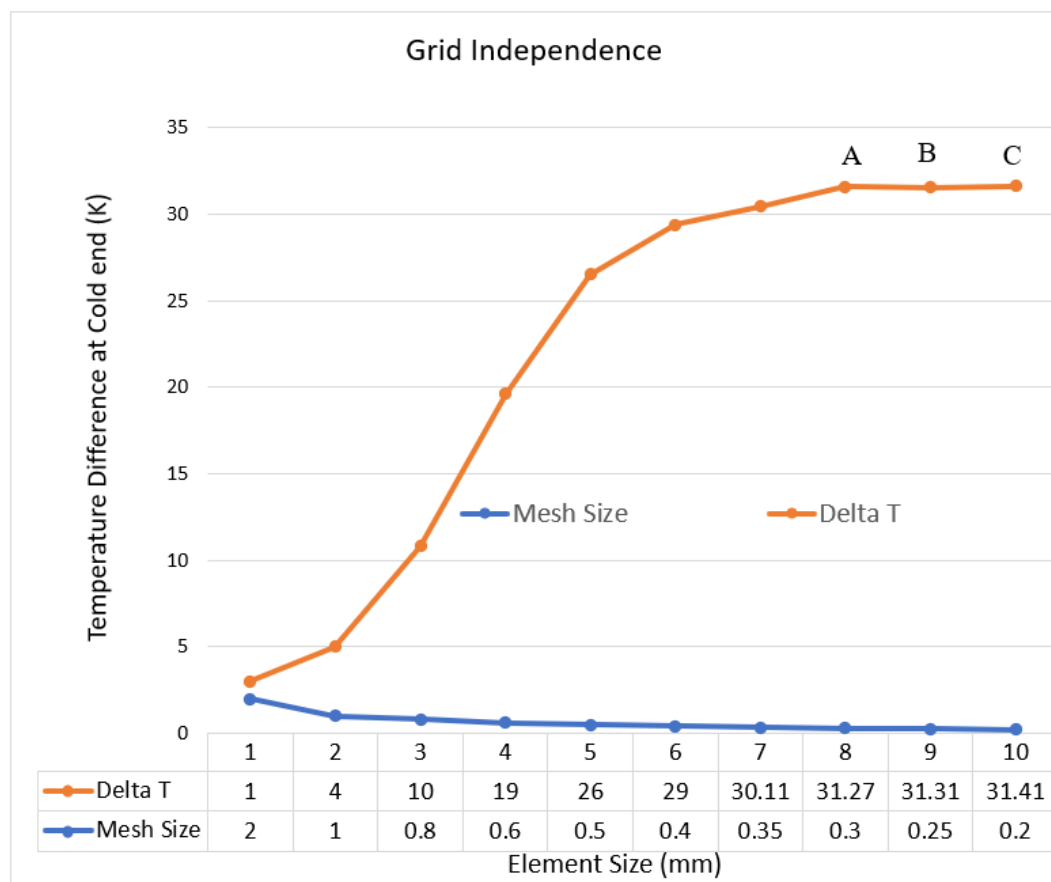
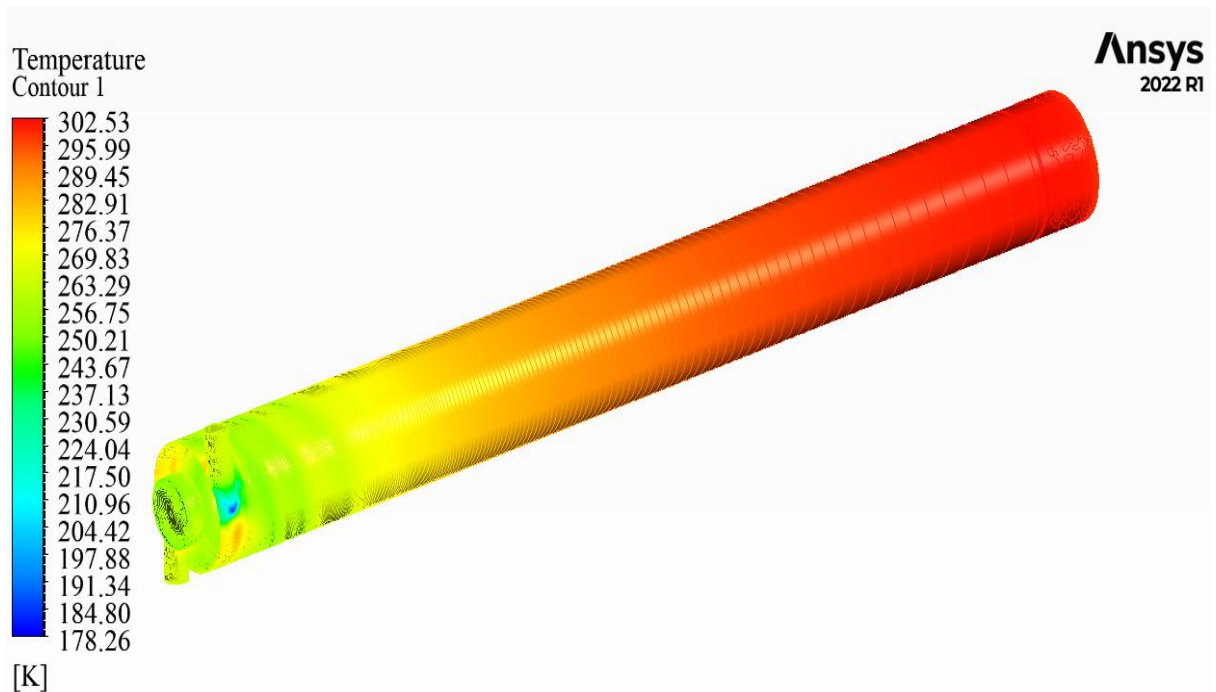


**Fig. 6.4** Grid Independence study for vortex tube

## 6.4 RESULTS AND DISCUSSION

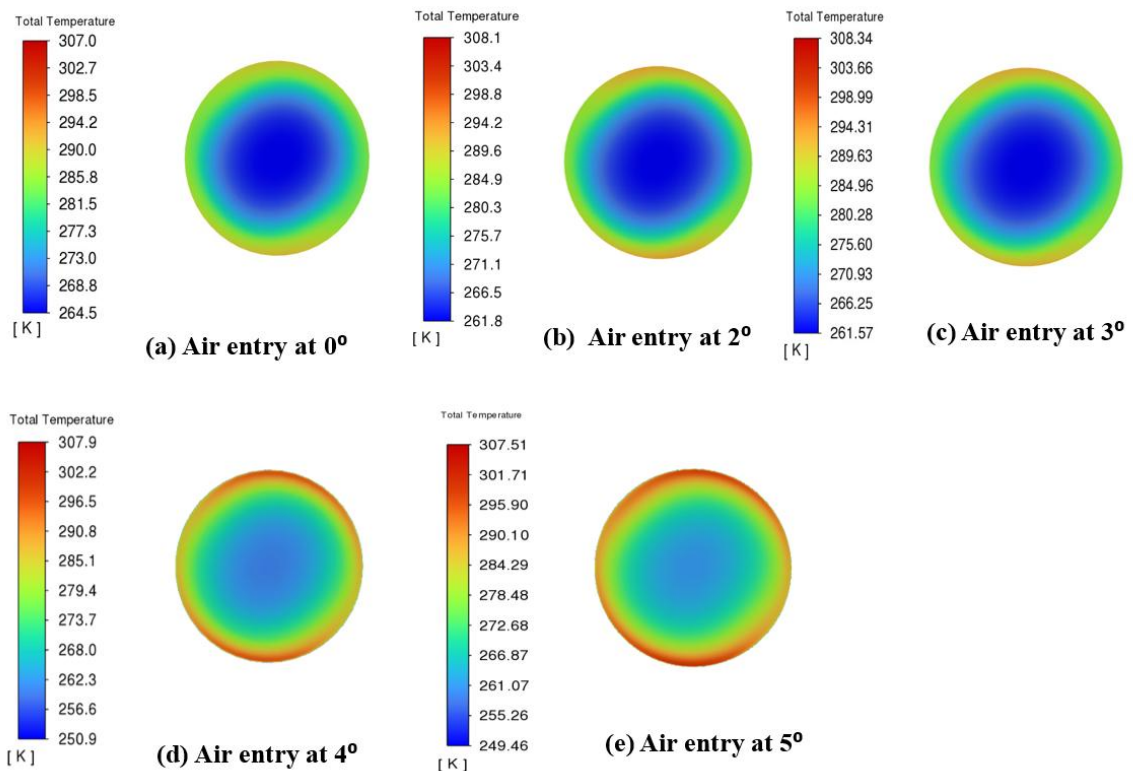
This section deals with the effect of nozzle entry angle on thermodynamic performance of vortex tube. An effort is made to find the optimum air entry angle for maximum cold exit temperature drop. Fig. 6.5 shows the temperature contour in the vortex tube.

Fig. 6.6 illustrate the various temperature contour at cold exit for various air entry angles.



**Fig. 6.5** Temperature contour in vortex tube

Fig. 6.5 shows the temperature contour in the vortex tube. It is clearly visible that at hot exit temperature is higher than the cold end. The temperature of the air gradually decreasing when the air comes back towards the cold exit after releasing its energy to the peripheral stream. This can be explained by the concept of inner friction and turbulence effect [68]. According to this, the tangential velocity of the peripheral layer is lower than that of the inner layer at the entrance of the tube, meaning that a free vortex is being formed. Because of the shear stress between different layers, the slow peripheral flow was accelerated by the inner flow, while the inner flow is decelerated. In this process, kinetic energy was transferred from the inner layer to the outer layer by inner friction. Temperature rise occurred because the energy transferred to the peripheral flow, and additional energy transported by turbulence between the two layers helped the formation of temperature gradient in the vortex tube. The concept of the inner friction and turbulence effect is supported by numerous experimental, theoretical and numerical studies conducted by other researchers[69-74].



**Fig. 6.6** Temperature contour at the cold exit for various air entry angles in VT (a)  $0^\circ$  (b)  $2^\circ$  (c)  $3^\circ$  (d)  $4^\circ$  (e)  $5^\circ$

Fig. 6.6 shows the temperature contour at the cold exit for various entry angle in Vortex Tube. The air entry angle for the base case is  $0^\circ$ . The results of base case have been compared with that of all other air entry angles i.e.,  $2^\circ$ ,  $3^\circ$ ,  $4^\circ$ ,  $5^\circ$ . As one moves from air entry angle  $0^\circ$  towards the  $5^\circ$ , the cold end temperature decreases, get minimum value and then increases. The maximum temperature drop has been obtained at cold exit when air enters the VT at an angle of  $2^\circ$  and  $3^\circ$ . The minimum cold end temperature obtained is near about 262 K, giving improvement from 2 K to 3 K with respect to the base case (i.e. air entry angle at  $0^\circ$ ). As per the explanation given in the preceding paragraph (for Fig. 6.5), the maximum transfer of kinetic energy could be the possible reason for maximum temperature drop at cold end for geometry given in Fig 6.6 (b) and (c) i.e., at  $2^\circ$  and  $3^\circ$  air entry angle of vortex tube.



## CHAPTER 7: CONCLUSION

### 7.1 Vortex Tube Coupled with Subcritical Vapour Compression Refrigeration Cycle (VTC)

In the current study, comprehensive energy, exergy and multi-objective optimization of VTC for refrigerant R1234yf have been performed, and the results are compared with those of VCR. The following points have been inferred from this study:

1. VTC has an optimum intermediate temperature ( $T_{int,opt}$ ) and pressure ( $P_{int,opt}$ ) that correspond to the maximum COP. Both  $T_{int,opt}$  and  $P_{int,opt}$  reduce with a decrease in the evaporator temperature, and vice versa.
2. Cooling capacity increases as the evaporator temperature increases and decreases as the condenser temperature rises for both VTC and VCR. For the considered range of condenser temperature, cooling capacity is 14.53% to 49.73% greater for VTC than VCR. Also, for the considered range of evaporator temperature, cooling capacity is 13.19% to 30.53% greater for VTC than VCR.
3. As the evaporator temperature increases,  $COP_{vtc,m}$  increases, and it is 5.30% to 14.87% higher than  $COP_{vcr}$ . Similarly, as the condenser temperature increases,  $COP_{vtc,m}$  decreases, and it is 5.59% to 27.32% higher than  $COP_{vcr}$ .
4. The foremost contributors to efficiency defect in VTC are the condenser and compressor. Also, the total efficiency defect of all expansion devices (VT and two throttle valves) in VTC is significantly lower than that of a single throttle device in VCR which makes VTC an attractive option.
5. For the studied range of evaporator and condenser temperatures, the exergetic efficiency of VTC is superior to that of VCR. In both cycles, the exergetic efficiency increases as the evaporator and condenser temperatures decrease and the isentropic efficiency of the compressor increases.
6. The most influential parameters affecting the thermodynamic performance of VTC are evaporator temperature, condenser temperature, and isentropic efficiency of the compressor.
7. In the multi-objective optimization using GA, the evaporator temperature is found to be the major decisive factor setting the optimized solutions, which can direct the design of the system based on VTC for various applications.



## 7.2 Vortex Tube coupled with Transcritical Vapour Compression Refrigeration Cycle (TVTC)

The present study deals with energy, exergy, environmental, and structural bond analysis followed by multi-objective optimization of a vortex tube coupled with trans-critical vapour compression refrigeration cycle (TVTC) using CO<sub>2</sub>. The following main points build the conclusion of this study:

1. For the studied range of evaporator ( $T_e$ ) and gascooler temperatures ( $T_{gc}$ ), optimum gascooler pressure of TVCR is 2.1% to 11.7% higher than that of TVTC.
2. With an increase in  $T_e$ , cooling capacity slightly decreases while COP increases for both the cycles. The cooling capacity and COP of TVTC are 20.3% to 21.1% and 7.8% to 11.3%, respectively, higher than that of TVCR.
3. With an increase in  $T_{gc}$ , both cooling capacity and COP decrease for both cycles. However, the cooling capacity and COP of TVTC are 10.1% to 20.6% and 2.3% to 9.7%, respectively, higher than those of TVCR.
4. The effect of various design parameters such as  $\mu$ ,  $\eta_v$ , and  $\varepsilon_{ds}$  on thermodynamic performance of TVTC is insignificant; however, the effectiveness of subcooler ( $\varepsilon_{sc}$ ) has a greater impact on the performance than other design parameters.
5. The gascooler has the highest irreversibility among all the components of TVTC and TVCR. Moreover, the total irreversibility of both cycles decreases with evaporator temperature and increases with gascooler exit temperature. The total irreversibility of TVTC is higher than that of TVCR; however, exergetic efficiency of TVTC is higher than that of TVCR. The exergetic efficiency of TVTC is 7.9% to 11.3% (with variation of  $T_e$ ) and 2.3% to 9.7% (with variation of  $T_{gc}$ ) higher than that of TVCR.

6. The environmental penalty cost per unit cooling capacity of TVTC is found to be 3.5% to 12.2% lower than that of TVCR for the studied range of evaporator and gascooler temperatures.
7. The results of multi-objective optimization utilising GA indicate that the evaporator temperature is the most important determinant in determining the optimal solutions, which can direct the design of TVTC-based systems for a variety of applications.

### **7.3 Economic Analysis of Vortex Tube coupled with Transcritical and Subcritical Vapour Compression Refrigeration Systems**

This study also performs the economic or cost analysis of TVTC and VTC and compares results of these systems with those of base cases i.e., TVCR and VCR, respectively. For the economic analysis, three cost terms have been considered, which are capital & maintenance cost, operational cost and environmental penalty cost. All three cost when added it becomes plant cost. The effect of various parameters such as evaporator temperature, gascooler exit temperature, condenser temperature and cooling load has been observed on all three components of cost and plant cost rate. It is found that plant cost rate of TVCR is 6.8% to 7.3% higher than that of TVTC and plant cost rate of VCR is 7.5% to 17% higher than that of VTC. This justifies the use of vortex tube in transcritical and subcritical vapour compression refrigeration system from the economic or cost perspective.

### **7.4 Computational Fluid Dynamic (CFD) Analysis of Vortex Tube**

A 3D solid model of vortex tube has been developed and the effect of geometrical parameter i.e. air entry angle has been observed on the temperature separation inside the vortex tube. The CFD analysis is conducted using ANSYS FLUENT 2022 R1 and standard k-epsilon model is used for computation of results. The maximum temperature drop has been obtained at cold exit when air enters the VT at 2° and 3°. The minimum cold end temperature obtained is near about 262 K, giving improvement of 2 K to 3 K with respect to the base case (i.e. at 0° entry angle).

## 7.5 Future Scope

The findings of this study have the potential to inform the development of vortex tube integrated with vapour compression refrigeration systems. These results may provide designers with guidance on how to integrate more energy-efficient systems. The thermodynamic and economic analyses followed by multi-objective optimization of TVTC and VTC systems featuring parametric investigation and CFD study of vortex tube were the focus of this research. As outlined in the following section, the findings derived from this thesis research also indicate a number of potential avenues for future investigation:

1. To use advanced exergy analysis to understand the effect of the avoidable and unavoidable parts of exergy destruction in each component and optimize based on minimization of the avoidable exergy destruction in each component.
2. To perform experimental research with the purpose of augmenting the corpus of knowledge.
3. To integrate the VTC and TVTC with several thermal systems like Organic Rankine cycles in order to develop a combined cycle and running compressor from turbine power.
4. To utilize a waste heat-powered double-effect absorption refrigeration system instead of a mechanical refrigeration system and single effect absorption systems to cool the warm ambient air.
5. In order to achieve trade-offs, it is necessary to employ further optimisation techniques such as particle swarm optimisation and ant colony approaches, followed by a comparison.
6. To perform exergo-economic analysis and emergy analysis on the TVTC and VTC and compare these results with the base case.
7. To see effect of the same geometrical parameters on thermal performance of converging-diverging vortex tube, diverging vortex tube and curved vortex tube.
8. To perform the same CFD analysis of vortex tube with some real gas instead of air.

## REFERENCES

1. Xue, Y., M. Arjomandi, and R. Kelso, *The working principle of a vortex tube*. international journal of refrigeration, 2013. **36**(6): p. 1730-1740.
2. Cebeci, I., V. Kirmaci, and U. Topcuoglu, *The effects of orifice nozzle number and nozzle made of polyamide plastic and aluminum with different inlet pressures on heating and cooling performance of counter flow Ranque–Hilsch vortex tubes: An experimental investigation*. International Journal of Refrigeration, 2016. **72**: p. 140-146.
3. Kandil, H.A. and S.T. Abdelghany, *Computational investigation of different effects on the performance of the Ranque–Hilsch vortex tube*. Energy, 2015. **84**: p. 207-218.
4. Bovand, M., et al., *Application of Response Surface Methodology to optimization of a standard Ranque–Hilsch vortex tube refrigerator*. Applied Thermal Engineering, 2014. **67**(1-2): p. 545-553.
5. Li, N., et al., *Experimental study of the energy separation in a vortex tube*. International journal of refrigeration, 2015. **55**: p. 93-101.
6. Xue, Y., M. Arjomandi, and R. Kelso, *Energy analysis within a vortex tube*. Experimental thermal and fluid science, 2014. **52**: p. 139-145.
7. Takahama, H. and H. Yokosawa, *Energy separation in vortex tubes with a divergent chamber*. 1981.
8. Escudier, M. and J. Keller, *Recirculation in swirling flow-a manifestation of vortex breakdown*. AIAA journal, 1985. **23**(1): p. 111-116.
9. Keller, J. and M. Göbel, *Die thermodrossel: eine anlage zur entspannung komprimierter flüssigkeiten unter wärmeabgabe*. KI. Luft-und Kältetechnik, 1997. **33**(2): p. 57-60.
10. Wan, Y., et al., *A novel self-condensing transcritical CO<sub>2</sub> power cycle with a vortex tube: Thermoeconomic assessment study and comparison*. Energy Conversion and Management, 2023. **286**: p. 117026.
11. Maurer, T., *Patent DE 197 48 083 A1*. Entspannungseinrichtung, 1999.
12. Zhu, J., *Experimental investigation of vortex tube and vortex nozzle for applications in air-conditioning, refrigeration, and heat pump systems*. 2015.
13. Bruno, T.J., *Laboratory applications of the vortex tube*. Journal of Chemical Education, 1987. **64**(11): p. 987.
14. Selek, M., et al., *Experimental examination of the cooling performance of Ranque–Hilsch vortex tube on the cutting tool nose point of the turret lathe through infrared thermography method*. International Journal of Refrigeration, 2011. **34**(3): p. 807-815.
15. Mugdadi, B. and M. Al-Nimr, *A novel hybrid cooling system combining vortex tube with absorption cooler*. International Journal of Energy Research, 2022. **46**(7): p. 8793-8802.
16. Wang, J., et al., *Thermodynamic, Economic Analysis, and Multiobjective Optimization of a Novel Transcritical CO<sub>2</sub> Rankine Cycle with a Vortex Tube*. Journal of Energy Engineering, 2022. **148**(1): p. 04021061.
17. Hodnebrog, Ø., et al., *Global warming potentials and radiative efficiencies of halocarbons and related compounds: A comprehensive review*. Reviews of Geophysics, 2013. **51**(2): p. 300-378.
18. Schuster, P., et al., *Biotransformation of 2, 3, 3, 3-tetrafluoropropene (HFO-1234yf)*. Toxicology and Applied Pharmacology, 2008. **233**(2): p. 323-332.
19. Takizawa, K., K. Tokuhashi, and S. Kondo, *Flammability assessment of CH<sub>2</sub>CF<sub>3</sub>CF<sub>3</sub>: comparison with fluoroalkenes and fluoroalkanes*. Journal of Hazardous Materials, 2009. **172**(2-3): p. 1329-1338.

20. Minor, B.H., D. Herrmann, and R. Gravell, *Flammability characteristics of HFO-1234yf*. Process Safety Progress, 2010. **29**(2): p. 150-154.
21. Minor, B. and M. Spatz, *HFO-1234yf low GWP refrigerant update*. 2008.
22. Fujitaka, A., et al. *Application of low global warming potential refrigerants for room air conditioner*. in *2010 International Symposium on Next-generation Air Conditioning and Refrigeration Technology*, Tokyo, Japan. 2010.
23. Zilio, C., R. Brignoli, and J. Brown. *Experimental analysis of a minichannel air cooled condenser operating with R1234yf*. in *The 23rd IIR International Congress of Refrigeration*. Prague, Czech Republic. 2011.
24. Lee, H., et al., *Transient thermal model of passenger car's cabin and implementation to saturation cycle with alternative working fluids*. Energy, 2015. **90**: p. 1859-1868.
25. Bansal, P. and B. Shen, *Analysis of environmentally friendly refrigerant options for window air conditioners*. Science and Technology for the Built Environment, 2015. **21**(5): p. 483-490.
26. Devotta, S., A.S. Padalkar, and K.V. Mali, *Low GWP refrigerants as alternatives to HCFC-22 in room air conditioners*. Science and Technology for the Built Environment, 2016. **22**(8): p. 1128-1135.
27. Sethi, A., E.V. Becerra, and S.Y. Motta, *Low GWP R134a replacements for small refrigeration (plug-in) applications*. International Journal of Refrigeration, 2016. **66**: p. 64-72.
28. Bellos, E. and C. Tzivanidis, *Multi-objective optimization of a solar assisted heat pump-driven by hybrid PV*. Applied Thermal Engineering, 2019. **149**: p. 528-535.
29. Nawaz, K., et al., *R1234yf and R1234ze (E) as low-GWP refrigerants for residential heat pump water heaters*. International Journal of Refrigeration, 2017. **82**: p. 348-365.
30. Richter, M., M.O. McLinden, and E.W. Lemmon, *Thermodynamic Properties of 2, 3, 3-Tetrafluoroprop-1-ene (R1234yf): Vapor Pressure and p–p–T Measurements and an Equation of State*. Journal of Chemical & Engineering Data, 2011. **56**(7): p. 3254-3264.
31. Yadav, S., J. Liu, and S.C. Kim, *A comprehensive study on 21st-century refrigerants-R290 and R1234yf: A review*. International Journal of Heat and Mass Transfer, 2022. **182**: p. 121947.
32. Fang, W., et al., *A critical review of synthetic chemicals in surface waters of the US, the EU and China*. Environment international, 2019. **131**: p. 104994.
33. Bamigbetan, O., et al., *Review of vapour compression heat pumps for high temperature heating using natural working fluids*. International journal of refrigeration, 2017. **80**: p. 197-211.
34. Abas, N., et al., *Natural and synthetic refrigerants, global warming: A review*. Renewable and Sustainable Energy Reviews, 2018. **90**: p. 557-569.
35. Lorentzen, G., *Revival of carbon dioxide as a refrigerant*. H AND V ENGINEER, 1993. **66**: p. 9-9.
36. Bruno, F., M. Belusko, and E. Halawa, *CO2 refrigeration and heat pump systems—a comprehensive review*. Energies, 2019. **12**(15): p. 2959.
37. Bellos, E. and C. Tzivanidis, *A comparative study of CO2 refrigeration systems*. Energy Conversion and Management: X, 2019. **1**: p. 100002.
38. Barta, R.B., E.A. Groll, and D. Ziviani, *Review of stationary and transport CO2 refrigeration and air conditioning technologies*. Applied Thermal Engineering, 2021. **185**: p. 116422.
39. Shao, L.-L. and C.-L. Zhang, *Thermodynamic transition from subcritical to transcritical CO2 cycle*. International Journal of Refrigeration, 2016. **64**: p. 123-129.

40. Ranque, G., *Expériences sur la détente giratoire avec productions simultanées d'un échappement d'air chaud et d'un échappement d'air froid*. J. phys. Radium, 1933: p. 112-114.
41. Joseph, R.G., *Method and apparatus for obtaining from alpha fluid under pressure two currents of fluids at different temperatures*. 1934, US patent p. 1:952, 281.
42. Hilsch, R., *The use of the expansion of gases in a centrifugal field as cooling process*. Review of Scientific Instruments, 1947. **18**(2): p. 108-113.
43. Westley, R., *A bibliography and survey of the vortex tube*. 1954.
44. Curley, W. and R. McGree Jr, *Bibliography of vortex tubes*. Refrig Eng, 1951. **59**(2): p. 191-193.
45. Kalvinskas, L., *Vortex tubes (an extension of Wesley's bibliography)*. Jet Propulsion Laboratory, California Inst of Technology Literature Search, 1956. **56**.
46. Dobratz, B.M., *Vortex tubes: a bibliography*. Vol. 7829. 1964: University of California, Lawrence Radiation Laboratory.
47. Nash, J.M., *The Ranque-Hilsch vortex tube and its application to spacecraft environmental control systems*. Dev Theor Appl Mech, 1972. **6**(6).
48. Finko, V., *Cooling and condensation of gas in a vortex flow*. Soviet Physics Technical Physics, 1983. **28**: p. 1089-1093.
49. Bruno, T.J., *Applications of the vortex tube in chemical analysis*. Process Control Qual, 1992. **3**: p. 195-207.
50. Bruno, T., *APPLICATIONS OF THE VORTEX TUBE IN CHEMICAL ANALYSIS. II: APPLICATIONS*. American laboratory, 1993. **25**(14): p. 16-16.
51. Baz, A., R. Johnston, and D. Uhler, *The dynamic characteristics of vortex tube-assisted hyperbaric chambers*. Ocean engineering, 1986. **13**(4): p. 387-408.
52. Baz, A. and D. Uhler, *A compressed gas-powered heating system for underwater divers*. Ocean Engineering, 1986. **13**(3): p. 273-290.
53. Baz, A., J. Gilheany, and A. Kalvaitis, *Feasibility of vortex tube-assisted environmental control of a manned underwater research habitat*. Ocean engineering, 1988. **15**(1): p. 33-54.
54. Riu, K.-J., J.-s. Kim, and I.-S. Choi, *Experimental investigation on dust separation characteristics of a vortex tube*. JSME International Journal Series B Fluids and Thermal Engineering, 2004. **47**(1): p. 29-36.
55. Martin, R.W. and K.W. Zilm, *Variable temperature system using vortex tube cooling and fiber optic temperature measurement for low temperature magic angle spinning NMR*. Journal of Magnetic Resonance, 2004. **168**(2): p. 202-209.
56. Colgate, S.A. and J.R. Buchler, *Coherent Transport of Angular Momentum: The Ranque-Hilsch Tube as a Paradigm*. Annals of the New York Academy of Sciences, 2000. **898**(1): p. 105-112.
57. Eiamsa-ard, S. and P. Promvonge, *Review of Ranque-Hilsch effects in vortex tubes*. Renewable and sustainable energy reviews, 2008. **12**(7): p. 1822-1842.
58. Lewins, J. and A. Bejan, *Vortex tube optimization theory*. Energy, 1999. **24**(11): p. 931-943.
59. Eiamsa-Ard, S., K. Wongcharee, and P. Promvonge, *Experimental investigation on energy separation in a counter-flow Ranque-Hilsch vortex tube: Effect of cooling a hot tube*. International communications in heat and mass transfer, 2010. **37**(2): p. 156-162.
60. Behera, U., et al., *Numerical investigations on flow behaviour and energy separation in Ranque-Hilsch vortex tube*. International Journal of Heat and mass transfer, 2008. **51**(25-26): p. 6077-6089.
61. Parulekar, B., *The short vortex tube*. J Refrig, 1961. **4**(4): p. 74-80.



62. Kalashnik, M. and K. Visheratin, *Cyclostrophic adjustment in swirling gas flows and the Ranque-Hilsch vortex tube effect*. Journal of Experimental and Theoretical Physics, 2008. **106**(4): p. 819-829.
63. Eiamsa-ard, S. and P. Promvonge, *Numerical investigation of the thermal separation in a Ranque-Hilsch vortex tube*. International journal of heat and mass transfer, 2007. **50**(5-6): p. 821-832.
64. Fröhlingsdorf, W. and H. Unger, *Numerical investigations of the compressible flow and the energy separation in the Ranque-Hilsch vortex tube*. International Journal of Heat and Mass Transfer, 1999. **42**(3): p. 415-422.
65. Farouk, T. and B. Farouk, *Large eddy simulations of the flow field and temperature separation in the Ranque-Hilsch vortex tube*. International Journal of Heat and Mass Transfer, 2007. **50**(23-24): p. 4724-4735.
66. Behera, U., et al., *CFD analysis and experimental investigations towards optimizing the parameters of Ranque-Hilsch vortex tube*. International Journal of Heat and Mass Transfer, 2005. **48**(10): p. 1961-1973.
67. Gao, C., et al., *Experimental study on a simple Ranque-Hilsch vortex tube*. Cryogenics, 2005. **45**(3): p. 173-183.
68. Fulton, C., *Ranque's tube*. Refrigerating Engineering, 1950. **5**: p. 473-479.
69. Kazantseva, O., S.A. Piralishvili, and A. Fuzeeva, *Numerical simulation of swirling flows in vortex tubes*. High Temperature, 2005. **43**(4): p. 608-613.
70. Trofimov, V., *Physical effect in Ranque vortex tubes*. Journal of Experimental and Theoretical Physics Letters, 2000. **72**: p. 249-252.
71. Lay, J., *An experimental and analytical study of vortex-flow temperature separation by superposition of spiral and axial flow: part 2*. Journal of heat transfer, 1959. **81**(3): p. 213-221.
72. Alimov, R., *Flow friction and heat and mass transfer in a swirled flow*. Journal of engineering physics, 1966. **10**(4): p. 251-257.
73. Reynolds, A.J., *Energy flows in a vortex tube*. Zeitschrift für angewandte Mathematik und Physik ZAMP, 1961. **12**: p. 343-357.
74. Hartnett, J. and E. Eckert, *Experimental study of the velocity and temperature distribution in a high-velocity vortex-type flow*. Transactions of the American Society of Mechanical Engineers, 1957. **79**(4): p. 751-758.
75. Shannak, B.A., *Temperature separation and friction losses in vortex tube*. Heat and mass transfer, 2004. **40**(10): p. 779-785.
76. Ahlborn, B. and S. Groves, *Secondary flow in a vortex tube*. Fluid Dynamics Research, 1997. **21**(2): p. 73.
77. Farouk, T., B. Farouk, and A. Gutsol, *Simulation of gas species and temperature separation in the counter-flow Ranque-Hilsch vortex tube using the large eddy simulation technique*. International Journal of Heat and Mass Transfer, 2009. **52**(13-14): p. 3320-3333.
78. Aljuwayhel, N., G. Nellis, and S. Klein, *Parametric and internal study of the vortex tube using a CFD model*. International journal of refrigeration, 2005. **28**(3): p. 442-450.
79. Ahlborn, B., J. Keller, and E. Rebhan, *The heat pump in a vortex tube*. 1998.
80. Ahlborn, B.K. and J.M. Gordon, *The vortex tube as a classic thermodynamic refrigeration cycle*. Journal of applied physics, 2000. **88**(6): p. 3645-3653.
81. Nimbalkar, S.U. and M.R. Muller, *An experimental investigation of the optimum geometry for the cold end orifice of a vortex tube*. Applied Thermal Engineering, 2009. **29**(2-3): p. 509-514.
82. Kurosaka, M., *Acoustic streaming in swirling flow and the Ranque-Hilsch (vortex-tube) effect*. Journal of Fluid Mechanics, 1982. **124**: p. 139-172.

83. Chu, J.Q., *Acoustic streaming as a mechanism of the Ranque-Hilsch effect*. 1982: The University of Tennessee.
84. Kuroda, H., *An experimental study of temperature separation in swirling flow*. 1983: The University of Tennessee.
85. Li, D., et al., *Thermodynamic analysis of vortex tube and expansion work output devices for the transcritical carbon dioxide cycle*. Refrigeration Science and Technology, 2000: p. 463-470.
86. Sarkar, J., *Cycle parameter optimization of vortex tube expansion transcritical CO<sub>2</sub> system*. International Journal of Thermal Sciences, 2009. **48**(9): p. 1823-1828.
87. Sarkar, J., *Exergy analysis of vortex tube expansion vapour compression refrigeration system*. International Journal of Exergy, 2013. **13**(4): p. 431-446.
88. Jain, G., A. Arora, and S. Gupta, *Performance analysis of a transcritical N<sub>2</sub>O refrigeration cycle with vortex tube*. International Journal of Ambient Energy, 2019. **40**(4): p. 350-356.
89. Jain, G., A. Arora, and S.N. Gupta, *Exergy analysis of the transcritical N<sub>2</sub>O refrigeration cycle with a vortex tube*. International Journal of Green Energy, 2018. **15**(9): p. 507-516.
90. Jain, G., A. Arora, and S. Gupta, *Performance characteristics of a two-stage transcritical N<sub>2</sub>O refrigeration cycle with vortex tube*. International Journal of Ambient Energy, 2020. **41**(5): p. 491-499.
91. Shet, S., O. Patil, and N. Agrawal, *Energetic and exergetic studies of modified CO<sub>2</sub> transcritical refrigeration cycles*. Gas, 2016. **3**: p. 2.
92. Xie, Y.B., et al., *CO<sub>2</sub> trans-critical two stage compression refrigeration cycle with vortex tube*. Applied Mechanics and Materials, 2011. **52**: p. 255-260.
93. Liu, Y.F., C.J. Geng, and G.Y. Jin, *Vortex tube expansion transcritical CO<sub>2</sub> heat pump cycle*. Applied Mechanics and Materials, 2012. **190**: p. 1340-1344.
94. Liu, Y.F. and G.Y. Jin, *Vortex tube expansion two-stage transcritical CO<sub>2</sub> refrigeration cycle*. Advanced Materials Research, 2012. **516**: p. 1219-1223.
95. Liu, Y., Y. Sun, and D. Tang, *Analysis of a CO<sub>2</sub> transcritical refrigeration cycle with a vortex tube expansion*. Sustainability, 2019. **11**(7): p. 2021.
96. Dubey, A.M., G. Das Agrawal, and S. Kumar, *Performance evaluation and optimal configuration analysis of a transcritical carbon dioxide/propylene cascade system with vortex tube expander in high-temperature cycle*. Clean Technologies and Environmental Policy, 2016. **18**: p. 105-122.
97. Luo, Z., et al., *Performance improvement of transcritical CO<sub>2</sub> refrigeration cycle by integrating vortex tube expansion: Simulation and optimization*. Thermal Science and Engineering Progress, 2023. **45**: p. 102078.
98. Singh, P., *Study of vortex tube integrated alternative refrigeration and air conditioning options for energy conservation (PhD Thesis)*, in Centre for Energy Studies. 2009, Indian Institute of Technology, Delhi (IITD).
99. Christensen, K., et al., *Energy savings in refrigeration by means of a new expansion device. Report of Energy research programme*. Journal, 2001(1223/99): p. 0006.
100. Liu, Y., et al., *Effect of initial pressure on explosion characteristics of 2, 3, 3, 3-tetrafluoropropene*. Journal of Loss Prevention in the Process Industries, 2021. **69**: p. 104320.
101. Bolaji, B. and Z. Huan, *Ozone depletion and global warming: Case for the use of natural refrigerant—a review*. Renewable and Sustainable Energy Reviews, 2013. **18**: p. 49-54.
102. Mansour, A., J. Lagrandeur, and S. Poncet, *Analysis of transcritical CO<sub>2</sub> vortex tube performance using a real gas thermodynamic model*. International Journal of Thermal Sciences, 2022. **177**: p. 107555.



103. Mohiuddin, M. and S. Elbel, *A fresh look at vortex tubes used as expansion device in vapor compression systems*. 2014.
104. Zhu, J. and S. Elbel, *Vortex tube heat booster to improve performance of heat driven cooling cycles for automotive applications*. 2016, SAE Technical Paper.
105. Şentürk Acar, M., E. Oğuzhan, and O. Arslan, *The performance of vapor compression cooling system aided Ranque-Hilsch vortex tube*. Thermal Science, 2019.
106. Puangcharoenchai, P., et al., *Experimental investigation of performance enhancement of a vapor compression refrigeration system by vortex tube cooling*. International Journal of Air-Conditioning and Refrigeration, 2020. **28**(02): p. 2050018.
107. Mansour, A., et al., *Thermodynamic analysis of a transcritical CO<sub>2</sub> heat pump integrating a vortex tube*. Applied Thermal Engineering, 2023. **224**: p. 120076.
108. Majidi, D., H. Alighardashi, and F. Farhadi, *Best vortex tube cascade for highest thermal separation*. International journal of refrigeration, 2018. **85**: p. 282-291.
109. Zhao, P., et al., *Performance analysis of a self-condensation compressed carbon dioxide energy storage system with vortex tube*. Journal of Energy Storage, 2021. **41**: p. 102995.
110. Cetin, T.H. and J. Zhu, *Thermodynamic assessment of a novel self-condensing sCO<sub>2</sub> recompression system with vortex tube*. Energy Conversion and Management, 2022. **269**: p. 116110.
111. Xu, W., et al., *Study of an integrated vortex tube used in hydrogen pre-cooling system*. International Journal of Hydrogen Energy, 2024. **54**: p. 971-978.
112. Chen, J., et al., *Numerical investigation of the vortex tube performance in novel precooling methods in the hydrogen fueling station*. International journal of hydrogen energy, 2021. **46**(7): p. 5548-5555.
113. Lagrandeur, J., et al., *On the benefit of integrating vortex tubes in PEMFC system for preheating hydrogen in FCEV technologies*. International Journal of Hydrogen Energy, 2024. **52**: p. 1141-1152.
114. Celik, A., M. Yilmaz, and O.F. Yildiz, *Improvement of diesel engine startability under low temperatures by vortex tubes*. Energy reports, 2020. **6**: p. 17-27.
115. Celik, A., M. Yilmaz, and O.F. Yildiz, *Effects of vortex tube on exhaust emissions during cold start of diesel engines*. Applications in Energy and Combustion Science, 2021. **6**: p. 100027.
116. Qyyum, M.A., et al., *An innovative vortex-tube turbo-expander refrigeration cycle for performance enhancement of nitrogen-based natural-gas liquefaction process*. Applied Thermal Engineering, 2018. **144**: p. 117-125.
117. Qyyum, M.A., et al. *A novel vortex tube-based N<sub>2</sub>-expander liquefaction process for enhancing the energy efficiency of natural gas liquefaction*. in *E3S Web of Conferences*. 2017. EDP Sciences.
118. Markal, B., O. Aydın, and M. Avci, *Exergy analysis of a counter-flow Ranque-Hilsch vortex tube having different helical vortex generators*. International Journal of Exergy, 2012. **10**(2): p. 228-238.
119. Dincer, K., *Experimental investigation of the effects of threefold type Ranque-Hilsch vortex tube and six cascade type Ranque-Hilsch vortex tube on the performance of counter flow Ranque-Hilsch vortex tubes*. International Journal of Refrigeration, 2011. **34**(6): p. 1366-1371.
120. Bej, N. and K. Sinhamahapatra, *Numerical analysis on the heat and work transfer due to shear in a hot cascade Ranque-Hilsch vortex tube*. International Journal of Refrigeration, 2016. **68**: p. 161-176.
121. Bej, N. and K. Sinhamahapatra, *Exergy analysis of a hot cascade type Ranque-Hilsch vortex tube using turbulence model*. International Journal of Refrigeration, 2014. **45**: p. 13-24.

122. Dutta, T., K. Sinhamahapatra, and S. Bandyopadhyay, *Experimental and numerical investigation of energy separation in counterflow and uniflow vortex tubes*. International Journal of Refrigeration, 2021. **123**: p. 9-22.
123. Manimaran, R., *Computational analysis of energy separation in a counter-flow vortex tube based on inlet shape and aspect ratio*. Energy, 2016. **107**: p. 17-28.
124. Manimaran, R., *Computational analysis of flow features and energy separation in a counter-flow vortex tube based on number of inlets*. Energy, 2017. **123**: p. 564-578.
125. Avci, M., *The effects of nozzle aspect ratio and nozzle number on the performance of the Ranque–Hilsch vortex tube*. Applied thermal engineering, 2013. **50**(1): p. 302-308.
126. Xue, Y. and M. Arjomandi, *The effect of vortex angle on the efficiency of the Ranque–Hilsch vortex tube*. Experimental Thermal and Fluid Science, 2008. **33**(1): p. 54-57.
127. Hamdan, M.O., B. Alsayyed, and E. Elnajjar, *Nozzle parameters affecting vortex tube energy separation performance*. Heat and Mass Transfer, 2013. **49**: p. 533-541.
128. Acar, M.S. and O. Arslan, *Exergo-economic Evaluation of a new drying system Boosted by Ranque-Hilsch vortex tube*. Applied Thermal Engineering, 2017. **124**: p. 1-16.
129. Villalón-López, L.F., et al., *Energy, exergy, exergoeconomic analysis, and optimization in a natural gas decompression station with a vortex tube and geothermal preheating*. Sustainability, 2024. **16**(4): p. 1669.
130. Shahsavari, A., A. Jahangiri, and G. Ahmadi, *Energy and exergy analysis and multi-objective optimization of using combined vortex tube-photovoltaic/thermal system in city gate stations*. Renewable Energy, 2022. **196**: p. 1017-1028.
131. Cho, H., H. Lee, and C. Park, *Performance characteristics of an automobile air conditioning system with internal heat exchanger using refrigerant R1234yf*. Applied Thermal Engineering, 2013. **61**(2): p. 563-569.
132. Arora, A. and S. Kaushik, *Theoretical analysis of a vapour compression refrigeration system with R502, R404A and R507A*. International Journal of Refrigeration, 2008. **31**(6): p. 998-1005.
133. Klein, S. and F. Alvarado, *Engineering Equation Solver, version 9.237, F-Chart Software*. 2012, Middleton.
134. Bagheri, B.S., et al., *Optimization and comprehensive exergy-based analyses of a parallel flow double-effect water-lithium bromide absorption refrigeration system*. Applied Thermal Engineering, 2019. **152**: p. 643-653.
135. Sarkar, J. *Use of vortex tube as expansion device in isobutane-based refrigeration system*. in *Proc. Int. Conf. Recent Dev. Mech. Eng. (ICRDME- 2008)* 2008. SUS Coll. Eng. Technol. Punjab, India.
136. Agarwal, S., A. Arora, and B. Arora, *Energy and exergy analysis of vapor compression–triple effect absorption cascade refrigeration system*. Engineering Science and Technology, an International Journal, 2020. **23**(3): p. 625-641.
137. Hamdan, M.O., S.-A. Al-Omari, and A.S. Oweimer, *Experimental study of vortex tube energy separation under different tube design*. Experimental Thermal and Fluid Science, 2018. **91**: p. 306-311.
138. Zendejboudi, A., et al., *Modeling and multi-objective optimization of an R450A vapor compression refrigeration system*. International Journal of Refrigeration, 2019. **100**: p. 141-155.
139. Konak, A., D.W. Coit, and A.E. Smith, *Multi-objective optimization using genetic algorithms: A tutorial*. Reliability Engineering and System Safety, 2006. **91**(9): p. 992-1007.
140. Holland, J.H., *Genetic Algorithms*. Scientific American, 1992. **267**(1): p. 66-73.
141. Mishra, A., B. Arora, and A. Arora, *Exergy-based sustainability analysis of combined cycle gas turbine plant integrated with double-effect vapor absorption refrigeration*

- system. Journal of the Brazilian Society of Mechanical Sciences and Engineering, 2024. **46**(1): p. 20.
142. Aminyavari, M., et al., *Exergetic, economic and environmental (3E) analyses, and multi-objective optimization of a CO<sub>2</sub>/NH<sub>3</sub> cascade refrigeration system*. Applied Thermal Engineering, 2014. **65**(1-2): p. 42-50.
143. Misra, R., P.K. Sahoo, and A. Gupta, *Thermoeconomic optimization of a LiBr/H<sub>2</sub>O absorption chiller using structural method*. J. Energy Resour. Technol., 2005. **127**(2): p. 119-124.
144. Solanki, N., A. Arora, and R.K. Singh, *Advance exergy and coefficient of structural bond analysis of dedicated mechanical subcooled vapor compression refrigeration system*. International Journal of Refrigeration, 2023. **153**: p. 266-280.
145. Jones, D.R. and J.R. Martins, *The DIRECT algorithm: 25 years Later*. Journal of global optimization, 2021. **79**(3): p. 521-566.
146. Kırmacı, V. and O. Uluer, *An experimental investigation of the cold mass fraction, nozzle number, and inlet pressure effects on performance of counter flow vortex tube*. 2009.
147. Saidi, M. and M. Valipour, *Experimental modeling of vortex tube refrigerator*. Applied thermal engineering, 2003. **23**(15): p. 1971-1980.
148. Kaya, M., et al., *The experimental investigation and thermo-dynamic analysis of vortex tube*. Heat and Mass Transfer, 2017. **53**(2): p. 395-405.
149. Mishra, A., B. Arora, and A. Arora, *Multi-objective optimization of an inlet air-cooled combined cycle power plant*. Journal of Thermal Science and Engineering Applications, 2023. **15**(7): p. 071005.
150. Konak, A., D.W. Coit, and A.E. Smith, *Multi-objective optimization using genetic algorithms: A tutorial*. Reliability engineering & system safety, 2006. **91**(9): p. 992-1007.
151. Aminyavari, M., et al., *Exergetic, economic and environmental (3E) analyses, and multi-objective optimization of a CO<sub>2</sub>/NH<sub>3</sub> cascade refrigeration system*. Applied Thermal Engineering, 2014. **65**(1): p. 42-50.
152. Mosaffa, A.H., et al., *Exergoeconomic and environmental analyses of CO<sub>2</sub>/NH<sub>3</sub> cascade refrigeration systems equipped with different types of flash tank intercoolers*. Energy Conversion and Management, 2016. **117**: p. 442-453.
153. Nabil, M.H., et al., *Thermo-Economic Assessment of Advanced Triple Cascade Refrigeration System Incorporating a Flash Tank and Suction Line Heat Exchanger*. Energy Conversion and Management, 2023. **295**: p. 117630.
154. Zare, V., S. Mahmoudi, and M. Yari, *An exergoeconomic investigation of waste heat recovery from the Gas Turbine-Modular Helium Reactor (GT-MHR) employing an ammonia–water power/cooling cycle*. Energy, 2013. **61**: p. 397-409.
155. Roy, R. and B.K. Mandal, *Energy, exergy and economic optimization of a two-stage refrigeration system using low-GWP alternative refrigerants for high-temperature lift applications*. Journal of the Brazilian Society of Mechanical Sciences and Engineering, 2023. **45**(8): p. 403.
156. Dimian, A.C. and C.S. Bildea, *Chemical process design: Computer-aided case studies*. 2008: John Wiley & Sons.
157. Skye, H., G. Nellis, and S. Klein, *Comparison of CFD analysis to empirical data in a commercial vortex tube*. International journal of refrigeration, 2006. **29**(1): p. 71-80.
158. Rafiee, S.E. and M. Rahimi, *Experimental study and three-dimensional (3D) computational fluid dynamics (CFD) analysis on the effect of the convergence ratio, pressure inlet and number of nozzle intake on vortex tube performance–Validation and CFD optimization*. Energy, 2013. **63**: p. 195-204.

## LIST OF PUBLICATIONS

The above work presented in the thesis has partially appeared in the form of following publications/ communications in international journals and conferences.

### International Journals

1. Khera, R., Arora, A. and Arora, B.B., 2023. Performance analysis and multi-objective optimization of a vortex tube integrated single-stage vapour compression refrigeration cycle. *International Journal of Refrigeration*, 154, pp.335-348.
2. Khera, R., Arora, A. and Arora, B.B., 2024. Energy, exergy, environmental (3E) analyses and multi-objective optimization of vortex tube coupled with transcritical refrigeration cycle. *International Journal of Refrigeration*, 167, pp.137-151.
3. Khera, R., Arora, A., Arora, B.B. (2024). Energy and Exergy Analyses of Vortex Tube Coupled Vapour Compression Refrigeration Cycle. Recent Advances in Mechanical Engineering, Volume 2. ICMech-REC 2023. Lecture Notes in Mechanical Engineering. Springer, Singapore. [https://doi.org/10.1007/978-981-97-2249-5\\_13](https://doi.org/10.1007/978-981-97-2249-5_13).

### International Conferences

1. Khera, R., Arora, A. and Arora, B.B., 2023, June. Energy and Exergy Analyses of Vortex Tube Coupled Vapour Compression Refrigeration Cycle. In *International Conference on Mechanical Engineering: Researches and Evolutionary Challenges* at NIT Warangal (pp. 151-161). Singapore: Springer Nature Singapore.
2. Khera, R., Arora, A. and Arora, B.B., 2024, June. Performance Enhancement of Transcritical vapour compression refrigeration cycle using vortex Tube. In 2<sup>nd</sup> International conference on optimisation Technique in Engineering and Technology at Dronacharya Group of Institutions.